1-1-2018

Techno-Economic Analysis and Optimization of Distributed Energy Systems

Jian Zhang

Techno-economic analysis and optimization of distributed energy systems

By

Jian Zhang

A Dissertation
Submitted to the Faculty of
Mississippi State University
in Partial Fulfillment of the Requirements
for the Degree of Doctor of Philosophy
in Mechanical Engineering
in the Department of Mechanical Engineering

Mississippi State, Mississippi

August 2018

Techno-economic analysis and optimization of distributed energy systems

By

Jian Zhang

Approved:

Heejin Cho
(Major Professor)

Pedro J. Mago
(Committee Member)

Rogelio Luck
(Committee Member)

Alta A. Knizley
(Committee Member)

Yucheng Liu
(Graduate Coordinator)

Jason Keith
Dean
Bagley College of Engineering

Name: Jian Zhang

Date of Degree: August 10, 2018

Institution: Mississippi State University

Major Field: Mechanical Engineering

Major Professor: Dr. Heejin Cho

Title of Study: Techno-economic analysis and optimization of distributed energy systems

Pages in Study 134

Candidate for Degree of Doctor of Philosophy

As a promising approach for sustainable development, distributed energy systems have received increasing attention worldwide and have become a key topic explored by researchers in the areas of building energy systems and smart grid. In line with this research trend, this dissertation presents a techno-economic analysis and optimization of distributed energy systems including combined heat and power (CHP), photovoltaics (PV), battery energy storage (BES), and thermal energy storage (TES) for commercial buildings.

First, the techno-economic performance of the CHP system is analyzed and evaluated for four building types including hospital, large office, large hotel, and secondary school, located in different U.S. regions. The energy consumption of each building is obtained by EnergyPlus simulation software. The simulation models of CHP system are established for each building type. From the simulation results, the payback period (PBP) of the CHP system in different locations is calculated. The parameters that have an influence on the PBP of the CHP system are also analyzed.

Second, PV system and integrated PV and BES (PV-BES) system are investigated for several commercial building types, respectively. The effects of the variation in key parameters, such as PV system capacity, capital cost of PV, sell back ratio, battery capacity, and capital cost of battery, on the performance of PV and/or PV-BES system are explored.

Finally, subsystems in previous chapters (CHP, PV, and BES) along with TES system are integrated together based on a proposed control strategy to meet the electric and thermal energy demand of commercial buildings (i.e., hospital and large hotel). A multi-objective particle swarm optimization (PSO) is conducted to determine the optimal size of each subsystem with the objective to minimize the payback period and maximize the reduction of carbon dioxide emissions. Results reveal how the key factors affect the performance of distributed energy system and demonstrate the proposed optimization can be effectively utilized to obtain an optimized design of distributed energy systems that can get a tradeoff between the environmental and economic impacts for different buildings.

ACKNOWLEDGEMENTS

I would like to extend my deepest gratitude to my advisor, Dr. Heejin Cho, who has provided invaluable support, encourage, and guidance during these four years which contribute to completing this work. I am also grateful to my committee members Dr. Pedro Mago, Dr. Rogelio Luck, and Dr. Alta Knizley for all of their guidance and help throughout my graduate education. Additionally, I would like to thank the Mechanical Engineering (ME) Department as well as my colleagues in ME. Finally, I would like to thank my family and my parents, for their patience, understanding, and support.

TABLE OF CONTENTS

LIST OF TABLES

LIST OF FIGURES

NOMENCLATURE

AD	hourly absolute difference
AS	annual savings
A_{surf}	net surface area of PV modules
BES	battery energy storage
CHP	combined heat and power
C_E	specific capacity cost of BES
C_f	fixed cost of BES
C_{inv}	inverter cost
C_m	operating and maintenance cost of PV
C_P	specific power cost of BES
C_{pgu}	specific capacity cost of PGU
C_{PV}	PV module cost
C_v	variable operating and maintenance cost of BES
Cap_{PV}	capacity of the PV system
CF	cash flow
CHP	combined heat and power
RCDE	carbon dioxide emission
$Cost_{C,BES}$	capital cost of BES
$Cost_{C,inv}$	capital cost of inverter
$Cost_{C,pgu}$	capital cost of PGU
$Cost_{C,PV}$	capital cost of PV modules
$Cost_{C,total}$	total capital cost of PV-BES system
$Cost_e$	cost of electricity from the grid
$Cost_f$	fuel cost

$Cost_{OM,BES}$	operating and maintenance cost of BES
$Cost_{OM,PV}$	operating and maintenance cost of PV
d_{PV}	degradation rate
D	daily positive difference
DPBP	discounted payback period
e_{con}	the hourly electricity consumption
e_{gen}	the hourly electricity generation
E_{ave}	average hourly building electric load
$Ebat$	battery capacity
$E_{building}$	electric energy consumption of the building
E_{gen}	electric energy generation
E_{grid}	electricity purchased from the grid
$E_{grid,DES}$	electricity purchased from the grid with the distributed energy system applied
$E_{grid,PV-BES}$	electricity purchased from the grid with the PV-BES system applied
E_{load}	building electric load
E_{max}	maximum hourly building electric load
E_{pgu}	electricity generated by the PGU
E_{PV}	annual usable electricity energy generated by the PV system
$Etes$	capacity of TES system
EF_e	grid emission factor
EF_f	natural gas emission factor
f_{activ}	fraction of surface area with active solar cells
F_{boiler}	fuel energy consumption by the boiler
F_{boiler}	fuel consumption of the building
F_l	original fuel purchased
$F_{l,DES}$	fuel purchased with the distributed energy system applied
F_m	total fuel energy consumption

F_{pgu}	fuel energy required to operate the PGU
FEL	following the electricity load
G_b	direct solar radiation
$G_{b,s}$	direct solar radiation on array
G_d	diffuse solar radiation
$G_{d,s}$	diffuse solar radiation on array
G_r	ground reflected solar radiation
$G_{r,s}$	ground reflected solar radiation on array
G_T	total solar radiation on array
i	discount rate
In	amount of money that the PV owner can get from the incentive policies
j	inflation rate
n	the day of the year
N	quantity of the PV modules
ND	annual negative difference
$\overline{ND}$	normalized negative difference
$Pbat$	rated power of BES
PBP	payback period
PBP_w	payback period with incentives
PD	annual positive difference
$\overline{PD}$	normalized positive difference
P_C	charging power
P_{DC}	discharging power
P_{load}	building electric power
P_{gen}	electric generation power
PGU	power generation unit
P_{pgu}	rated power of PGU
P_{PV}	total power levels of the PV array

PV	photovoltaic
Q_{boiler}	auxiliary heat provided by boiler
Q_h	building heating load
Q_{hc}	heat required to satisfy the heating load
Q_R	recovered thermal energy
r_b	battery ratio
r_e	electricity ratio
SOC	state of charge of BES system
SOC_T	state of charge of TES system
t	time expressed in years
TES	thermal energy storage
TMY	Typical Meteorological Year
α_s	solar altitude angle
β	surface tilt of the modules
γ	surface azimuth angle
γ_s	solar azimuth angle
δ_s	solar declination
Δe	the hourly difference between electricity consumption and generation
Δt	time step
η_C	battery charging efficiency
η_{boiler}	boiler thermal efficiency
η_{cell}	module conversion efficiency
η_{DC}	battery discharging efficiency
η_{hc}	heating coil efficiency
η_{invert}	DC to AC conversion efficiency
η_{pgu}	PGU thermal efficiency
η_{rec}	efficiency of the heat recovery system
η_{tC}	TES charging efficiency
η_{tDC}	TES discharging efficiency

θ	solar angle of incidence
θ_Z	solar zenith angle
ρ	ground reflectance
φ	latitude
∅	percentage of payback period reduction
Ψ	solar zenith angle
ω_s	hour angle

CHAPTER I

INTRODUCTION

1.1 Background

Fossil-fuel based central power plants and distribution systems have low overall efficiency due to the low fuel energy conversion efficiency (about 30%) and energy losses that occur during the transmission and distribution process of electric power to individual users [1]. Therefore, the generation and distribution of electric energy in more efficient and effective ways have become a popular focus of recent research work.

Distributed energy systems consist of a series of generation, storage, and energy monitoring and control solutions, which can be tailored to many specific applications [2]. Figure 1.1 shows categories of distributed energy systems. Due to the merits of increasing the resource energy efficiency and reducing the pollution, distributed energy systems have received an increased interest lately. Many Studies on certain technologies have been conducted by different researchers [3–9]. Also, a large number of incentive policies have been proposed by the government as well as utility companies all over the world to promote the installation of distributed energy systems [10–12]. Moreover, an increasing number of investigations on the integration of different distributed energy technologies have been performed. Some researchers focused on combining multiple distributed generation systems including CHP, wind power, geothermal, solar power, etc [13–15]. Some scholars have performed research to improve the integration of on-site

generation with energy storage to increase the overall system efficiency and economic benefits [16–19].

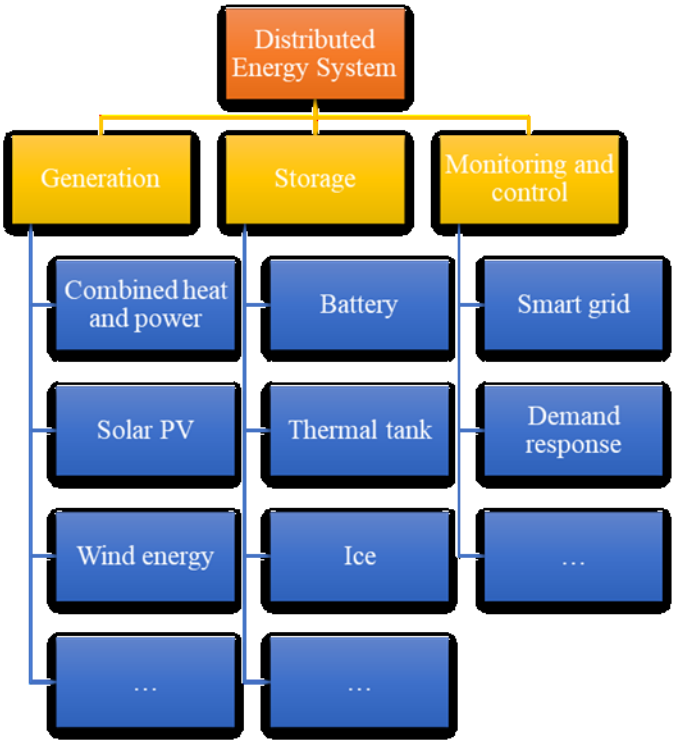

Figure 1.1 Categories of distributed energy systems

1.2 Research objectives

In line with the current research trend, the objective of this dissertation is to perform a techno-economic analysis and design optimization of distributed energy systems including combined heat and power (CHP), solar photovoltaics (PV), and battery and thermal energy storage (BES and TES) for commercial buildings located in several U.S. regions. In order to achieve this objective, the following topics have been investigated in each chapter:

- Chapter II focuses on investigating the techno-economic performance of CHP systems for different building types located in 11 U.S. states. The payback period (PBP) of each CHP system is chosen as the indicator and compared across the selected building types and locations. In this way, it is possible to qualitatively identify parameters that have an influence on the PBP.
- Chapter III develops a PV model for different building types in five U.S. states and conducts payback period and parameter analysis to determine the influence of the variation in key parameters on the performance of the PV system.
- Chapter IV provides an analysis of the integrated photovoltaic and battery energy storage (PV-BES) system for four building types located in four different states.
- Chapter V presents an integrated distributed energy system consists of CHP, PV, BES, and TES based on the proposed control strategy. Furthermore, this chapter provides a multi-objective particle swarm optimization (PSO) to determine the optimal size of each subsystem with the objective to minimize the PBP and maximize the reduction of carbon dioxide emissions (RCDE).

1.3 Literature review

1.3.1 Combined heat and power

Combined heat and power (CHP) systems, as one type of distribution energy system, offer an effective way to make use of the waste heat energy from an on-site electric power generation unit (PGU) to contribute to satisfying the thermal load of a building [20–24]. Additionally, CHP systems can significantly reduce electricity grid

dependence and save operational costs [25–27]. Thus, it is widely used all around the world. According to an investigation conducted by the International Energy Agency (IEA) [28], the G8+5 countries had the potential to raise their CHP systems capacity almost 430 GWe in 2015, and over 830 GWe in 2030. In the U.S., the total CHP systems capacity in 2012 was estimated 82 GWe [29]. European CHP systems potential studies indicated that the total capacity in Europe can be raised to within the range of 150–250 GWe by 2025 [30]. Moreover, many researchers have conducted studies on the performance of CHP systems. Bernotat et al. [31] studied the performance of CHP systems for clustered dwellings. The results showed that small-scale CHP has high prospects, especially for the areas that have high heat demands. Konstantakos et al. [32] proposed a CHP investment model to evaluate the economic viability and the investment risk of the CHP system. The results indicated that small fluctuations of natural gas price do not affect the investment to a crucial degree. Knizley et al. [33][34] developed a CHP system with two power generation units (PGUs) working together. One PGU delivered power at a constant base load, and the other PGU operated following the electricity load. The results showed that CHP systems provide a potential for cost, primary energy consumption (PEC), and emissions savings over a traditional separate heating and power system. Cho et al. [35] examined combined cooling, heating, and power (CCHP) systems with respect to operating cost, PEC, and carbon dioxide emissions (CDE), using minimization functions to optimize the system operation based on each parameter. The results indicated that optimizing the CCHP system on the basis of cost minimization does not imply that PEC or CDE will also be minimized. Hu and Cho [36] proposed a probability constrained multi-objective optimization model to optimize the operation

strategy of CCHP systems for different climate conditions based on operational cost, primary energy consumption, and carbon dioxide emissions. Yun et al. [37] proposed a power generation and heat recovery model for reciprocation internal combustion engines and their model can provide reliable estimates of performance maps for power and thermal output for engines with various capacities.

1.3.2 Solar Photovoltaic

As a renewable energy, solar photovoltaics have drawn more and more attention all over the world. According to the report of the International Energy Agency (IEA) [38], the world had increased more solar photovoltaic (PV) capacity in the four years since 2010 (2014 study) than in the previous four decades before 2010, and in early 2014 the total global capacity overtook 150 gigawatts (GW). In this report, PV's share of global electricity will reach 16% by 2050, which increases significantly from the 11% goal in the 2010 report.

Despite the fast development of photovoltaic technology, the growth speed of renewable energy capacity, including solar energy, still cannot defeat that of fossil fuel [39][40]. Thus, many scholars focused on improving photovoltaic technology in order to reduce the fossil fuel dependency and to meet a large fraction of increasing electricity demand [41–43]. Renno et al. [44] introduced a new method to provide a more accurate evaluation of the electric and thermal production of a point-focus concentration photovoltaic and thermal system. Bianchini et al. [6] carried out 18 months of experiments with 8 different photovoltaic plants. The performance of photovoltaic plants were measured on-site and compared in different environmental conditions. Based on the experimental data, the economic performance was assessed for each photovoltaic plant.

Armendariz-Lopez et al. [45] estimated the energy production of photovoltaic technologies on TRNSYS based on a Typical Meteorological Year (TMY). In their research, the energy generation and the cost of the photovoltaic array with different orientations and inclinations were compared. In this comparative analysis, the authors determined the geometric orientations which provide the best life-cycle cost. Adam and Adam [46] analyzed the performance of a 500 kWp solar photovoltaic system and explored the contribution of the PV system in reducing the greenhouse gas emission. The result showed that the PV system could reduce the CO_2 emission significantly. Thus, the PV system could be one of the major ways to reduce the CO_2 emission. Kulworawanichpong and Mwambeleko [47] conducted the design and cost analysis of a stand-alone solar photovoltaic system for a rural household as well as identified some common mistakes appearing in the process of sizing, installing and maintaining a solar system. Quesada et al. [48] proposed a tracking strategy for photovoltaic solar system located in high latitude regions and evaluated the performance of the solar tracking photovoltaic panel hourly and seasonally. The result showed that a zenith-set sun tracking strategy was not beneficial for overcast or mostly cloudy days in summer.

1.3.3 Energy storage

With renewable energy receiving increasing attention, battery energy storage (BES) systems are now a key technology necessary to increase the renewable energy source penetration and improve the overall system efficiency by load shifting and peak shaving [49]. There has been an increased emphasis in improving photovoltaic system integration with energy storage to increase the overall system efficiency and economic benefits [17][50]. As integration of PVs and energy storage systems is becoming an

important issue, significant work has been done in developing methods to properly size PV and battery energy storage systems. Oliveira and Hendrick [51] evaluated the PV capacity based on the ratio of the yearly PV generation to the yearly energy consumption and the storage capacity based on the ratio of useful storage energy to the yearly energy consumption. In their study, the PV capacity varied from 0 to 300% and the storage capacity changed from 0 to 100% to evaluate different levels of self-sufficiency (i.e., ratio of PV-generated energy that is locally consumed to the total consumption). Their results showed that the most economical way to reach self-sufficiency values up to 40% was to install a PV only, while for self-sufficiency beyond 40%, a PV coupled with energy storage seemed to be the best option. In another study, Venu et al. [52] proposed a methodology to size a battery energy storage system aiming at shaving the peak load of a residential building. In their work, the power rating of the battery was decided based on the desired amount of peak-shaving, that is, the percentage of the peak load. The energy rating of the battery was determined by the daily energy demand, at which the battery energy storage system could achieve the goal of desired peak-shaving. In addition, there are extensive studies that focus on developing new materials and technologies for battery storage as well as PV system [6][53][54].

1.3.4 Incentive policies for distributed energy systems

In order to promote the installation of various distributed energy systems, the governments and utility companies of many countries have proposed many incentive polies. Soares et al. [10] assessed the influence of alternative depreciation policies on the promoting of CHP systems in Brazil. The results showed that fiscal incentives could promote the popularization of CHP plants and improve the feasibility of such ventures,

though it reduced the fiscal revenues of government. Hawkes et al. [55] investigated different policy approaches regarding the energy use in the residential sector. The authors found that simultaneous support for energy efficiency measures and micro-CHP could be justified, as long as the heat-to-power ratio and capacity of the micro-CHP system were appropriate. Pellegrino et al. [56] analyzed the effect of different support schemes on the retail price of micro-CHP systems. The results indicated that a retail price that is several times higher than the case without any incentive could be achieved with the Feed-in Tariff (FIT) scheme. Pade et al. [57] examined different promotion schemes and assessed necessary incentive levels for fuel cell based micro-CHP in Denmark, France, and Portugal. The authors found that the necessary support levels were not extremely high compared to the initial support level. Athawale et al. [58] analyzed the impact of capital cost and low and volatile CHP capacity factors on the economics of CHP systems. The results showed that an incentive which is more likely to help resist against the risk of unfavorable outcomes was better than a one-time upfront capital incentive.

Chou et al. [59] presented a method to evaluate the benefit of installing a PV system with the government financial subsidies, especially feed-in-tariff (FIT) and tax abatement policies. Their results showed how a government could promote the development of the PV industry by increasing the FIT prices. Yuan et al. [11] built a feedback model of China's photovoltaic industry to estimate the influence of investment policy on the developing of PV industry and found that the investment policy only had a small influence on the price fluctuation and industry overcapacity. Hassan et al. [12] investigated the influence of FIT incentives on the optimal operation of battery storage for PV system in the UK. Their results provided an insight on how to optimize the battery

storage operation strategy to maximize the benefit from FIT for PV users. Simpson and Clifton [60] evaluated the impacts of incentive policies on the adoption of residential PV system in Australia using Diffusion of Innovations Theory. They reported that the incentive policies could promote the adoption of PV due to the contribution of reducing the payback period of systems. Bertsch et al. [61] presented a techno-economic analysis to explore the factors that affect the profitability of residential solar PV in Germany and Ireland and found that the FIT policy was one of the crucial drivers to make PV-storage system profitable.

1.3.5 Optimization of distributed energy systems

As the integration of different distributed energy resources is becoming a popular topic, significant work has been done in developing methods to properly size each part of the distributed energy systems. Fossati et al. [62] proposed an approach to optimize the size of energy storage system for microgrids on the basis of the genetic algorithm. The goal of their study was to determine the power rate and energy capacity for the energy storage system properly with an objective to minimize the operating cost of the microgrid. Also, some researchers applied mathematical models to optimize the distributed energy systems. Mehleri et al. [63] proposed a mixed-integer linear programming (MILP) model to optimize the design of distributed energy systems at the neighborhood level. Their objectives were to obtain the minimum investment and annual operating cost by selecting the subsystem components among several different technologies including combined heat and power units, photovoltaic systems, boilers, central power grid. Their results showed that special constraints are necessary to ensure that correct designs are produced. In another study, Venu et al. [52] presented a method

to size the battery energy storage system in order to shave the peak load for a residential building. In their study, the rated power of the battery was determined according to the desired amount of peak-shaving, i.e., the percentage of the peak load. The energy capacity of the battery was decided by the daily energy demand at which the goal of desired peak-shaving could be achieved. Khaki et al. [64] applied the genetic algorithm to optimize the energetic and the exergetic performances of an integrated photovoltaic/ thermal system. First and second law efficiencies of the integrated system were the performance evaluation criteria used in their study. Results indicated that a first law efficiency of 39.27% and a second law efficiency of 10.75% could be achieved for the optimized system. Mariaud et al.[65] proposed a mathematical model to optimize the capacity and operation of the distributed energy system (PV and battery system). Results revealed that the optimal configuration is an integration of mono-crystalline silicon PVs and lithium-ion batteries with an investment cost of 1.72 million pounds.

CHAPTER II

DESIGN AND TECHNO-ECONOMIC ANALYSIS FOR COMBINED HEAT AND POWER (CHP) SYSTEM

This chapter presents a techno-economic analysis for combined heat and power (CHP) systems and evaluates the effectiveness of existing incentive policies in several different U.S. states. In this chapter, four types of buildings, i.e., hospital, large office, large hotel, and secondary school, are selected and examined in 11 different locations in United State. Using the EnergyPlus simulation software, the energy consumption of each building was obtained. Then the simulation models of the CHP system were established for each reference building with the Mathcad software. For each reference building, the CHP system was operated in two different modes, the base-loaded mode and the following the electricity load (FEL) mode. Then for each operating mode, the payback period of the CHP systems in different locations was calculated according to local incentive policies. This payback period was compared to the one without considering incentive policies. There are several issues that have an influence on the payback period of CHP system: capacity of the PGU, the operational strategy of CHP system, location (climate), and the ratio of electricity cost to fuel (natural gas) cost, $Cost_e/Cost_f$. The effects of these factors were also discussed in this chapter.

2.1 Commercial reference building models

The U.S. Department of Energy (DOE) [66] [67] has developed 16 commercial reference building models, which represent nearly 70% of the commercial buildings in the U.S. These reference buildings provide complete descriptions for whole building energy analysis using EnergyPlus simulation software. In this paper, four types of buildings are selected: hospital, large office, large hotel, and secondary school. These four building types were chosen because the power and thermal energy consumptions in those buildings are relatively larger compared to other DOE commercial reference building models, so that the existing CHP incentives can be effectively evaluated with the consideration of its capacity limit in some states' incentive policies. In addition, the feasibility of CHP systems in different types of buildings can be effectively demonstrated using those four building types because each building has unique power and thermal load profiles. Types and characteristics of the chosen reference buildings are listed in Table 2.1.

Table 2.1 Types and characteristics of the chosen reference buildings [66]

Building Type	Floor Area (ft^2)	No. of floors	Heating Type	Cooling Type
Hospital	241,351	5	Natural gas boiler	Water cooled electric chiller
Large Office	498,588	12	Natural gas boiler	Water cooled electric chiller
Large Hotel	122,120	6	Natural gas boiler	Air cooled electric chiller
Secondary School	210,887	2	Natural gas boiler	Air cooled electric chiller

For the four types of reference buildings, 11 locations are chosen to evaluate the existing CHP incentive policies in different states. The selected locations and their corresponding climate zones and weather conditions are presented in Table 2. In the reference models, lights and equipment in the buildings are powered by the electricity imported from the grid. The heating energy to the buildings is supplied by natural gas. In this paper, electric and heating energy demands for each building in different locations are obtained by simulating those reference building models in EnergyPlus software. Then, based on the energy demands, CHP models were run in the Mathcad software, and the CHP performance was compared with that of the reference buildings.

Table 2.2 Selected locations for reference buildings

Selected City Name	Climate Zone	Condition
Phoenix, AZ	2B	Hot – Dry
San Francisco, CA	3C	Warm – Marine
Hartford, CT	5A	Cool – Humid
Chicago, IL	5A	Cool – Humid
Boston, MA	5A	Cool – Humid
Atlantic City, NJ	4A	Mixed – Humid
Albuquerque, NM	4B	Mixed – Dry
Kennedy, NY	5A	Cool – Humid
Houston, TX	2A	Hot – Humid
Baltimore, MD	4A	Mixed – Humid
Madison, WI	6A	Cold – Humid

Figure 2.1 shows the daily electric and thermal load demands, obtained using EnergyPlus software, for the selected reference buildings located in Baltimore, MD. Figures marked with (a), (b), (c) and (d) represent the daily load trend of hospital, large office, large hotel and secondary school, respectively, while those marked (1), and (2) represent the daily electric and thermal loads on January 1st and July 1st, respectively. As expected, Figure 2.1 illustrates that the electric load on a summer day is higher than that on a winter day for all building types, while the thermal load on a winter day is larger than that on a summer day for all building types. It illustrates that the large hotel has the relatively high thermal energy demand on both winter and summer days compared to electric energy demand, while the large office and secondary school buildings have almost no thermal energy demand during a winter day. The hospital building has a good amount of thermal load in a winter day, but it looks relatively small in the figure because of a large electric load in a winter day.

Figure 2.2 shows the monthly electric and thermal load for the selected reference buildings in Baltimore, MD. As shown in Figure 2.2, the monthly electric and thermal load trends are similar for all building types (i.e., high electric load and low thermal load during summer months and an opposite trend during winter months). The hospital building in the figure tends to have relatively high monthly electric load and relatively small monthly thermal load throughout the year in all climate locations, although it has a good amount of monthly thermal load compared to all other building types.

The annual electric and thermal load for the four kinds of reference buildings in all locations are shown in Table 2.3. The ratios of annual electric to thermal load for those reference buildings in all locations are provided in Table 2.4. The ratios of annual

electric to thermal load, shown in Table 2.4, can be a good indicator to show the balance between the electric to thermal load demand from a building: the ratio close to 1 indicates that the building has a well-balanced electric and thermal energy demand while the ratio greater than 1 indicates that it has the relatively high electric energy demand compared to the thermal energy demand. Table 2.4 shows that, based on the building type, the large hotel building has a better balance of the electric and thermal energy load among all building types and that, based on the location, colder climate cities (e.g., Hartford, CT, Chicago, IL Boston, MA, and Madison, WI) tend to have a better balance compared to the cities in hot climates (e.g., Albuquerque, NM and Houston, TX).

2.2 CHP model description

Figure 2.3 shows a schematic of a CHP system. As shown in the figure, the PGU is used to produce electricity on-site, and the waste heat from the PGU is recovered to provide the heating energy for the building.

In this chapter, the CHP system was operated in two different strategies, base-loaded and following the electricity load (FEL). These two strategies are introduced in the following sections.

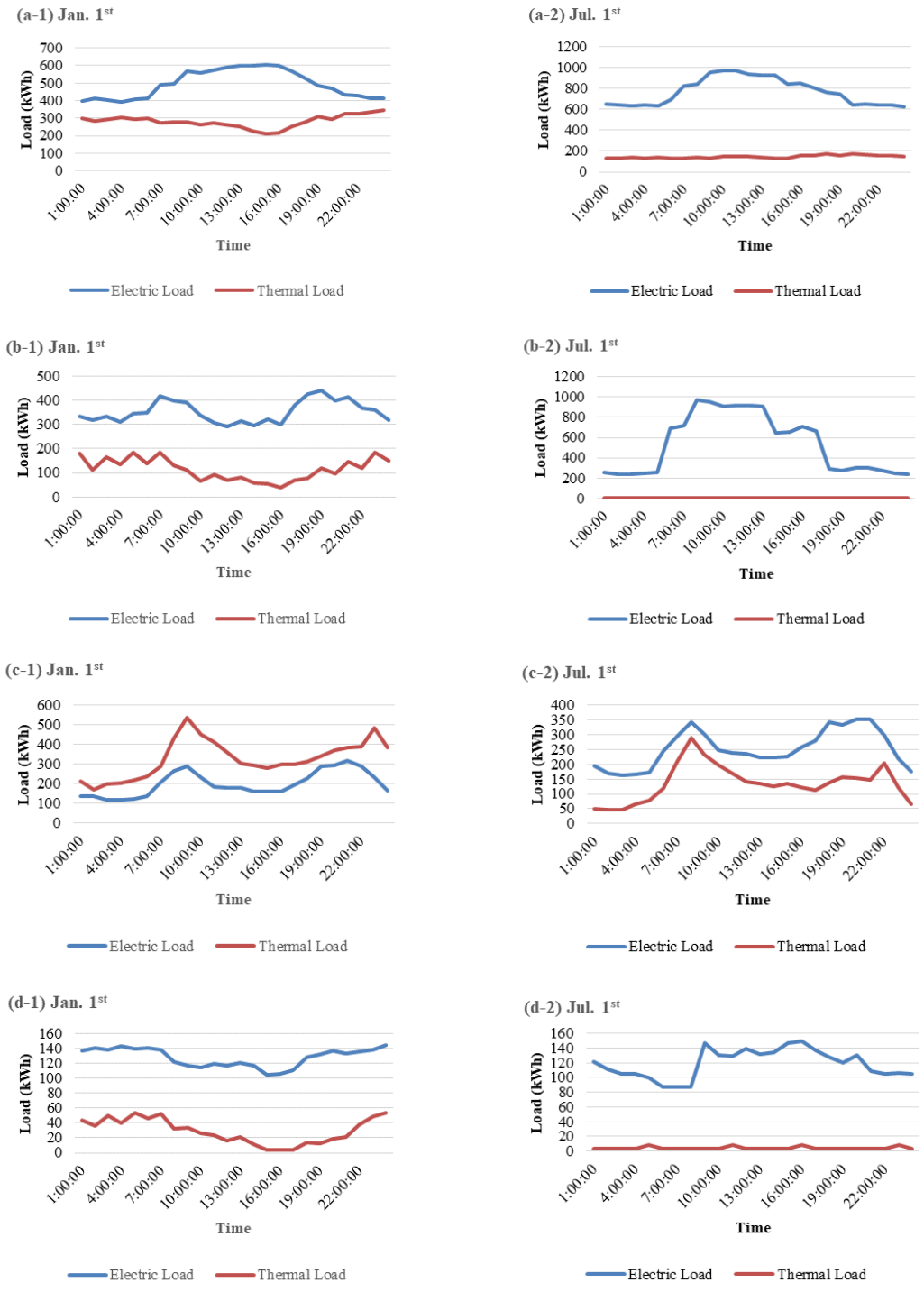

Figure 2.1 Daily electric and thermal load in Baltimore, MD on (1) Jan 1st and (2) Jul 1st for four kinds of buildings: (a) Hospital building; (b) Large office building; (c) Large hotel building; (d) Secondary school building

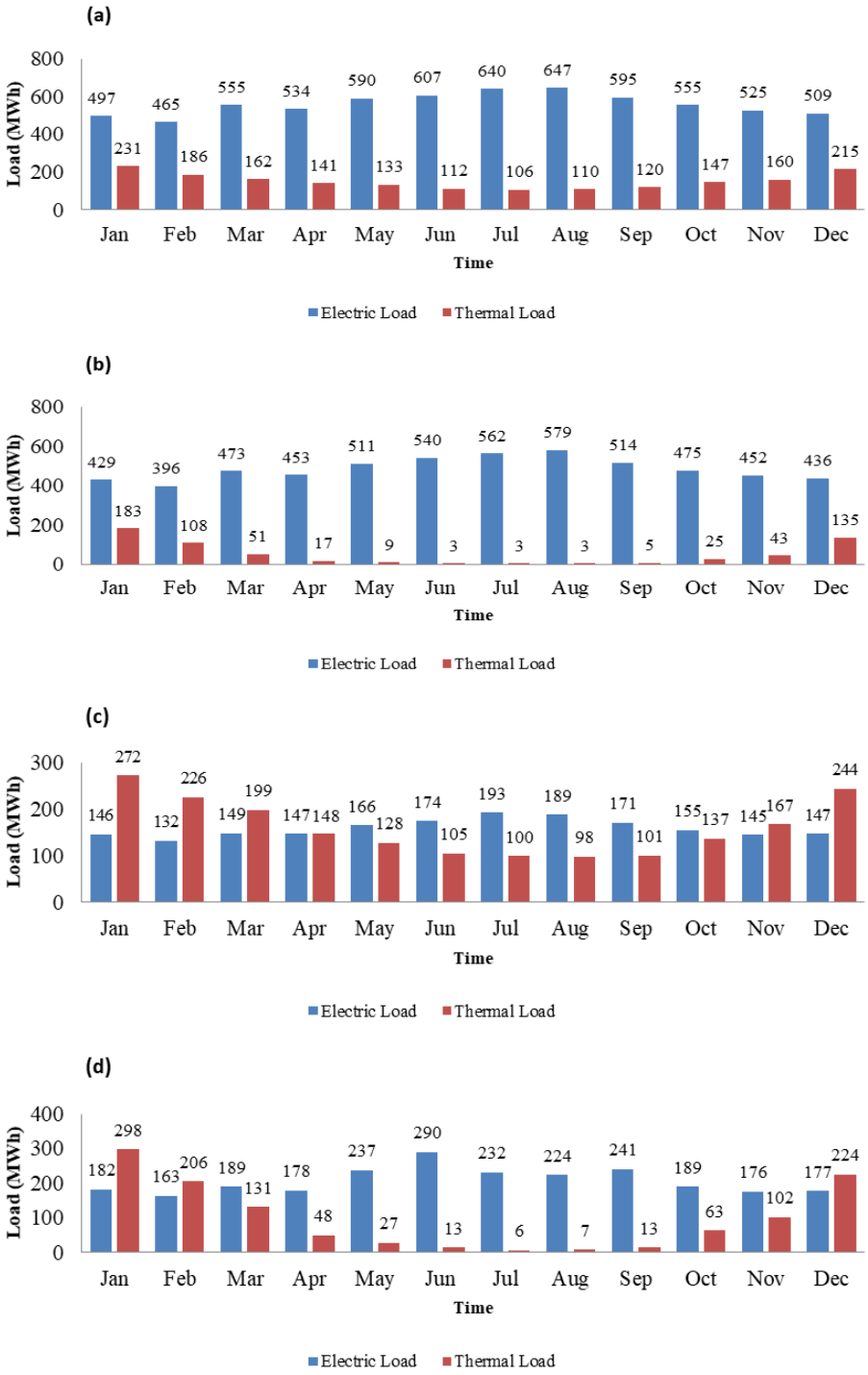

Figure 2.2 Monthly electric and thermal load for four kinds of buildings in Baltimore, MD; (a) Hospital building: (b) Large office building; (c) Large hotel building; (d) Secondary school building

Table 2.3 Annual electric and thermal load for the reference buildings in different locations (Unit: MWh)

City	Hospital		Large Office		Large Hotel		Secondary School	
	E_{Load}	T_{Load}	E_{Load}	T_{Load}	E_{Load}	T_{Load}	E_{Load}	T_{Load}
Phoenix, AZ	6926	1424	6168	236	2091	1118	3101	343
San Francisco, CA	6162	1620	5262	367	1807	1571	2110	590
Hartford, CT	6313	1951	5365	745	1813	2128	2249	1363
Chicago, IL	6423	2322	5455	984	1857	2296	2339	1596
Boston, MA	6302	1942	5329	795	1834	2197	2235	1508
Atlantic City, NJ	6553	1935	5499	595	1877	2099	2340	1184
Albuquerque, NM	6182	1284	5356	294	1856	1783	2354	799
Kennedy, NY	6547	1820	5500	597	1884	2079	2365	1194
Houston, TX	7551	1831	6544	253	2159	1251	3175	374
Baltimore, MD	6718	1823	5820	586	1913	1922	2477	1139
Madison, WI	6269	2536	5375	1302	1839	2482	2291	1973

Table 2.4 Ratio of annual electric to thermal load for the reference buildings in different locations

City	Hospital	Large Office	Large Hotel	Secondary School
Phoenix, AZ	4.86	26.14	1.87	9.04
San Francisco, CA	3.80	14.34	1.15	3.58
Hartford, CT	3.24	7.20	0.85	1.65
Chicago, IL	2.77	5.54	0.81	1.47

Table 2.4 (Continued)

Boston, MA	3.25	6.70	0.83	1.48
Atlantic City, NJ	3.39	9.24	0.89	1.98
Albuquerque, NM	4.81	18.22	1.04	2.95
Kennedy, NY	3.60	9.21	0.91	1.98
Houston, TX	4.12	25.87	1.73	8.49
Baltimore, MD	3.69	9.93	1.00	2.17
Madison, WI	2.47	4.13	0.74	1.16

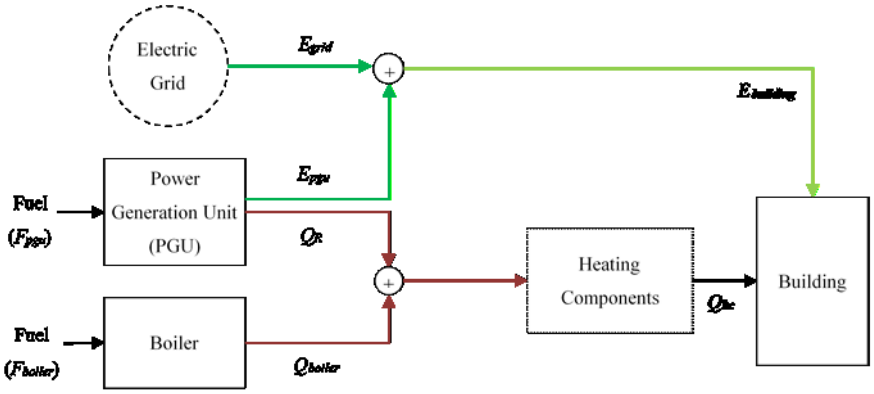

Figure 2.3 Schematic of a CHP system

2.2.1 The base-loaded operation strategy

For the base-loaded operation strategy, the PGU is operated at base load conditions, supplying a constant electrical demand to meet a portion of the electrical load. In this case, the PGU is sized to output the minimum electric requirement for each

building type in each location. Therefore, the fuel energy required to operate the PGU is calculated as:

$$F_{pgu} = E_{pgu}/\eta_{pgu} \tag{2.1}$$

where E_{pgu} is the electricity generated by the PGU and η_{pgu} is the PGU thermal efficiency, which is assumed to be constant and independent of the electric demand.

The electricity purchased from the grid is:

$$E_{grid} = E_{building} - E_{pgu} \tag{2.2}$$

where $E_{building}$ is the electric energy consumption of the building including lights, electric equipment, etc.

Then the waste heat recovered from the PGU can be estimated as:

$$Q_R = (F_{pgu} - E_{pgu})\eta_{rec} = F_{pgu}(1 - \eta_{pgu})\eta_{rec} \tag{2.3}$$

where Q_R is the recovered thermal energy and η_{rec} is the efficiency of the heat recovery system.

The heat required to satisfy the heating load is calculated as:

$$Q_{hc} = Q_h/\eta_{hc} \tag{2.4}$$

where Q_h is the building heating load and η_{hc} is the heating coil efficiency.

The CHP system is used to supply heating to the building at any specific hour when it is running. Therefore, if the thermal energy recovered from the PGU is not enough to balance the thermal load of the building, the boiler of the CHP system will be used to provide the additional heat. So if

$$Q_R > Q_{hc} \tag{2.5}$$

then

$$Q_{boiler} = 0 \tag{2.6}$$

If

$$Q_R < Q_{hc} \tag{2.7}$$

then

$$Q_{boiler} = Q_{hc} - Q_R \tag{2.8}$$

The fuel energy consumption by the boiler is calculated as:

$$F_{boiler} = Q_{boiler}/\eta_{boiler} \tag{2.9}$$

where η_{boiler} is the boiler thermal efficiency.

The total fuel energy consumption is expressed as:

$$F_m = F_{pgu} + F_{boiler} \tag{2.10}$$

2.2.2 The FEL operation strategy

For the FEL operation strategy, the total electricity required by the building is supplied by the PGU:

$$E_{pgu} = E_{building} \tag{2.11}$$

In the hour time step simulation, the electrical energy supplied by the PGU is set to be equal to the energy consumption for the specific hour.

The fuel consumption of the PGU is expressed as:

$$F_{pgu} = E_{pgu}/\eta_{pgu} \tag{2.12}$$

Then the waste heat recovered from the PGU can be estimated as:

$$Q_R = (F_{pgu} - E_{pgu})\eta_{rec} = F_{pgu}(1 - \eta_{pgu})\eta_{rec} \tag{2.13}$$

The heat required to satisfy the heating load is calculated as:

$$Q_{hc} = Q_h/\eta_{hc} \tag{2.14}$$

The CHP system also is used to supply heat to the building at any specific hour when it is running. Therefore, if the thermal energy recovered from the PGU is not enough to balance the thermal load of the building, the boiler of the CHP system will be used to provide the additional heat. So if

$$Q_R > Q_{hc} \tag{2.15}$$

then

$$Q_{boiler} = 0 \tag{2.16}$$

If

$$Q_R < Q_{hc} \tag{2.17}$$

then

$$Q_{boiler} = Q_{hc} - Q_R \tag{2.18}$$

The fuel energy consumption by the boiler is calculated as:

$$F_{boiler} = Q_{boiler}/\eta_{boiler} \tag{2.19}$$

The total fuel energy consumption is expressed as:

$$F_m = F_{pgu} + F_{boiler} \tag{2.20}$$

2.2.3 CHP efficiency

Table 2.5 Efficiency assumptions for CHP system

Symbol	Name	Value
η_{pgu}	Rated PGU electric efficiency (for base-load case)	0.3
η_{rec}	Efficiency of the heat recovery system	0.8
η_{hc}	Heating coil efficiency	0.8
η_{boiler}	Boiler thermal efficiency	0.8

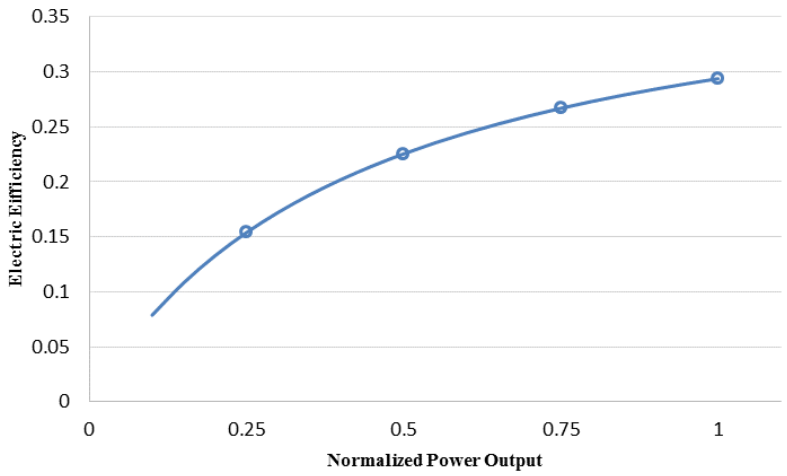

Figure 2.4 Variation of the PGU thermal efficiency with the normalized power output (for FEL)

Efficiency values of CHP components that are typically found in the field and used in this analysis are provided in Table 2.5 and Figure 2.4. The same efficiency values are used in the analysis for different building types and locations. For the base-loaded operation strategy, a fixed PGU electric generation efficiency of 0.3 is used, as shown in Table 2.5, because of its constant power output requirement. For the FEL operation strategy, the PGU electric generation efficiency varies with its power output as shown in Figure 2.4. Note that a typical normalized efficiency curve, shown in Figure 2.4 and derived from the method introduced in Ref. [68], is used in this analysis, and this curve is de-normalized using maximum electric demand values for each building in each location.

2.3 Incentive analysis

Typically, the cost of a CHP system consists of capital cost and maintenance cost. Since the capital cost is a large part of the total cost of the CHP system, only the capital

cost is considered in this chapter. The capital cost varies with different kinds of PGU. In this chapter, a reciprocating internal combustion engine is selected as the PGU. According to literature [69–71], the specific capacity cost of the PGU (C_{pgu}) is assumed as 1500$/kW. So the capital cost of the CHP system is calculated as:

$$Cost_{c,pgu} = C_{pgu} \cdot P_{pgu} \tag{2.21}$$

where P_{pgu} is the rated power of the PGU, in this case is the capacity of the reciprocating internal combustion engine.

In order to get the payback period of the CHP system, the amount of annual savings that can be obtained during the usage of the CHP system must be known.

The annual savings is calculated as:

$$AS = E_{building}Cost_e + F_{building}Cost_f - E_{grid}Cost_e - F_mCost_f \tag{2.22}$$

where $Cost_e$ is the cost of electricity (from the grid), $Cost_f$ is the cost of fuel and $F_{building}$ is the fuel consumption of the building which is estimated as:

$$F_{building} = Q_h/\eta_h \tag{2.23}$$

The fuel adopted in this study is the natural gas. Table 2.6 shows the electricity and natural gas prices used in the simulation for each location.

With the capital cost and annual savings known, the payback period can be calculated as:

$$PBP = Cost_{c,pgu}/AS \tag{2.24}$$

As mentioned before, both the federal government and the state government have proposed many incentive policies to promote the CHP systems. Table 2.7 shows the part of the incentive policies for different locations. These incentives include capital grants,

rebate and utility credits, etc. With these incentives, the payback period could be estimated as:

$$PBP_w = \frac{Cost_{c,pgu}}{AS-In} \tag{2.25}$$

where PBP_w is the payback period when taking the incentives into consideration. In is the amount of money that the CHP owner can get from the government due to incentive policies.

The percentage of the payback period reduction is:

$$\emptyset = \frac{PBP-PBP_w}{PBP} \times 100\% \tag{2.26}$$

Table 2.6 Electricity and natural gas prices used in the simulation for each location

City	$Cost_e$ * ($/kWh)	$Cost_f$ ** ($/kWh)	Cost Ratio ($Cost_e/Cost_f$)
Phoenix, AZ	0.0953	0.031	3.074
San Francisco, CA	0.1341	0.023	5.83
Hartford, CT	0.1465	0.028	5.232
Chicago, IL	0.0799	0.026	3.073
Boston, MA	0.1384	0.036	3.844
Atlantic City, NJ	0.1278	0.028	4.564
Albuquerque, NM	0.0932	0.021	4.438
Kennedy, NY	0.1506	0.026	5.792
Houston, TX	0.0816	0.026	3.709
Baltimore, MD	0.1043	0.033	3.161
Madison, WI	0.1051	0.024	4.379

* Obtained from Ref. [72]; ** Obtained from Ref. [73].

Table 2.7 Incentive policy for each location [74]

City	Incentive policy
Phoenix, AZ	*Rebate:* obtain funding ranging from $400/kW to $500/kW and up to a maximum of 50% of the installed cost of any project
San Francisco, CA	*Rebate:* Obtain funding up to $95,000 for hardware projects *Grant* for Internal Combustion Engine (CHP): $0.46/W
Hartford, CT	A capital *grant* of $200/kW
Chicago, IL	Design Incentive *Grant* of $75/kW; Constructive Incentive *Grant* of $175/kW capacity; Production Incentive *Grant* of $0.08/kWh
Boston, MA (1)	The maximum *grant* available is $200,000
Boston, MA (2)	*Grant* of $750/kW, not to exceed 50% of total project costs
Atlantic City, NJ	*Grant* for CHP systems greater than 1.0 MW and up to 3.0 MW: $0.55/W
Albuquerque, NM	*Rebate:* Custom rebates are worth up to $400/kW saved and efficiency studies for large commercial and industrial customers can cover up to 75% of the study cost
Kennedy, NY	*Grant* for designs 3% to 9% above designated baseline: $0.11/kWh saved, capped at 75% for CHP system cost
Houston, TX	*Grant* incentives to offset 20% of the upfront implementation costs
Baltimore, MD	Payment of $250/kW of net system capacity payment; Production payment of $0.07/kWh for net electricity produced during the 18 months, capped at $2,000,000 per project and 50% of total cost

Table 2.7 (Continued)

Madison, WI	Incentive *grants* for installing recommended energy efficiency improvements: $0.1/kwh savings; $300/kw savings. The maximum incentive is $40,000 or 20% of project costs

2.4 Results and discussion

The results obtained from the incentive analysis using the CHP model are presented in this section. Figure 2.5 shows the annual savings in the energy consumption cost of different CHP operational strategies for hospital buildings. As can be seen, when the CHP system operates under the base-loaded mode, the annual savings in the energy consumption cost are all positive values for all locations. When the CHP system operates under the FEL mode, the annual savings for Phoenix, Chicago, Houston, and Baltimore are negative values, and the others remain positive. A negative annual savings means that the capital cost of the CHP system can never be paid back. Note that since there are two different kinds of incentive policies for Boston, we list Boston (1) and Boston (2) in the figures below in order to compare the two incentive policies.

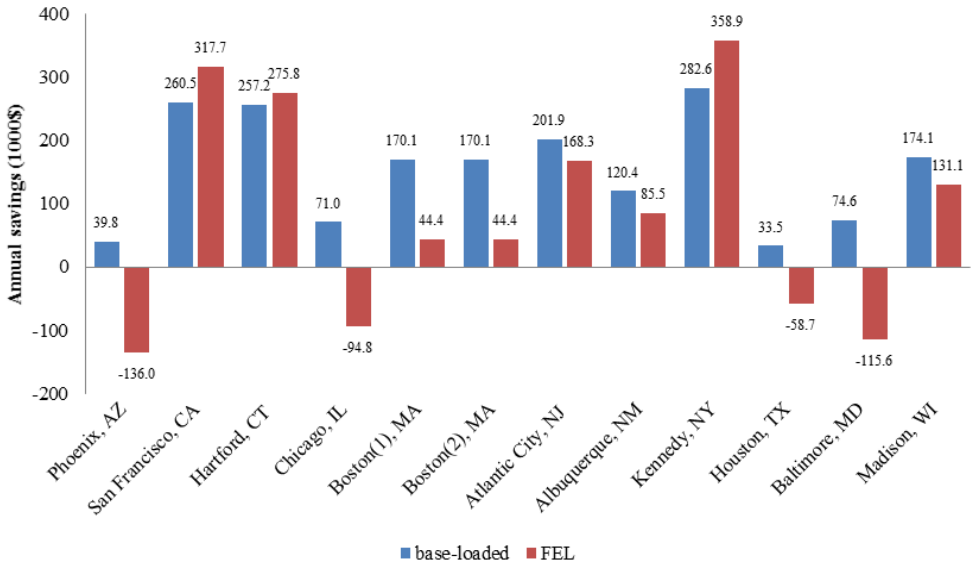

Figure 2.5 Annual savings in the energy consumption cost of different CHP operational strategies for hospital buildings

Figure 2.6 shows the results of the payback period analysis for hospital buildings in different locations. Figure 2.6 (a) indicates the capital cost payback period of CHP systems without incentives for hospital buildings. In the figure, the lack of a bar and marked as N/A means that it is impossible to recover the cost of investment for implementing CHP in that situation. As can be seen in Figure 2.6 (a), for the same location, the payback period of based-loaded operation strategy is shorter than that of FEL situation. For the base-loaded situation, the payback periods in the locations of San Francisco, Hartford, Boston, Atlantic City, Albuquerque, Kennedy and Madison are all under 5 years, which is very desirable. For the FEL situation, the payback periods are longer than that of the base-loaded situation and even more than 10 years in some locations, such as Boston, Atlantic City, Albuquerque and Madison. So for these

locations, FEL strategy is not a good choice. For San Francisco, Hartford and Kennedy, the payback period difference between the two strategies is not that big.

Figure 2.6 (b) shows the capital cost payback period of CHP systems with incentives for hospital buildings, and Figure 2.6 (c) indicates the payback period percentage reduction due to incentives. The reduction of the payback period demonstrates the incentive level in each location. The larger the reduction is, the higher the incentive level is. However, in some locations, though the reduction is large, the payback period is still too long. For example, the payback period reduction for Phoenix can reach up to 33.3%, but the payback period will be still more than 10 years.

There are several issues that have an influence on the payback period of CHP systems: capacity of the PGU, the operational strategy of CHP system, climate location, building electric and thermal load characteristics, and the value of cost ratio, which is defined in Table 2.6.

As a comparison, though the value of cost ratio in Chicago is similar to that in Phoenix, the payback period for Chicago is shorter than the case in Phoenix. This is mainly due to the difference of the climate in two locations. As shown in Table 2.2, Phoenix is in 2B climate zone, and the climate there is hotter than in Chicago, which is located in 5A climate zone. That means the CHP system in Phoenix will consume more fuel to provide the electrical energy for cooling during the summer period.

As shown in Table 2.2, both Hartford and Boston are located in 5A climate zones, but there is still some difference between their payback periods. This is because the value of cost ratio in Hartford is larger than that in Boston, which means using the electricity

generated by the CHP system instead of purchasing electricity from the grid can save more money in Hartford than the same case in Boston.

As can be seen in Table 2.6 (a), in some locations such as Boston, MA, Atlantic City, NJ, Albuquerque, NM and Madison, WI, the capacity of the PGU and the operational strategy have a significant influence on the payback period. When the CHP system is operated with a small capacity PGU under base-loaded strategy, the payback period is really short. However, the payback period increases significantly when the CHP system is operated with a large capacity PGU under FEL strategy. So for these locations, it is important to choose a proper capacity and operational strategy.

Figure 2.7 shows the annual savings in the energy consumption cost of different CHP operational strategies for large office buildings. As can be seen, the annual savings in the energy consumption cost of the base-loaded CHP systems are all positive values for all locations except for Phoenix, AZ. When the CHP system operates under the FEL mode, the annual savings for Phoenix, AZ, Chicago, IL, Boston, MA, Houston, TX, and Baltimore, MD are negative values and the others remain positive.

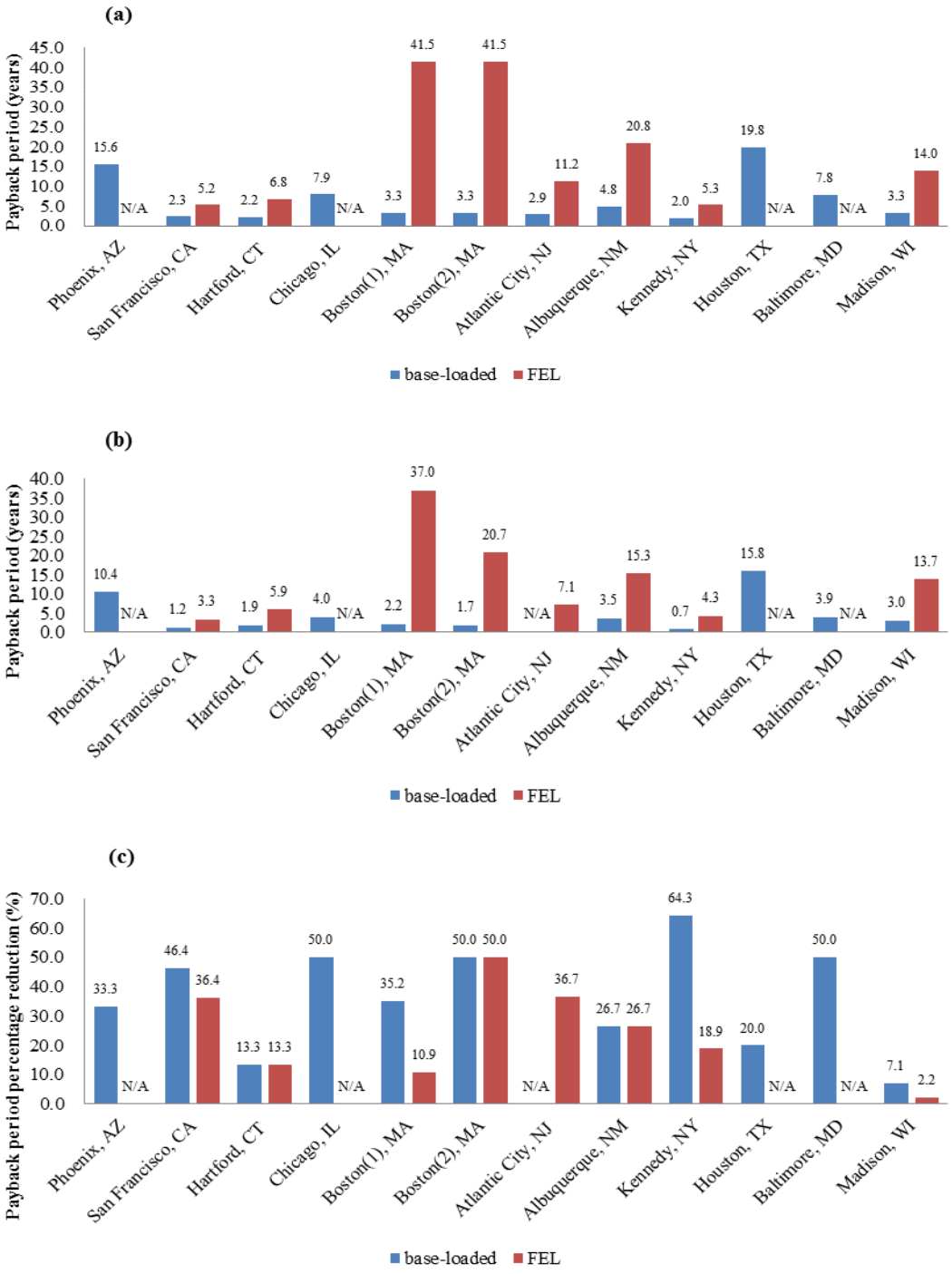

Figure 2.6 Results of payback period analysis for hospital buildings: (a) Capital cost payback period of CHP systems without incentives; (b) Capital cost payback period of CHP systems with incentives; (c) Capital cost payback period percentage reduction

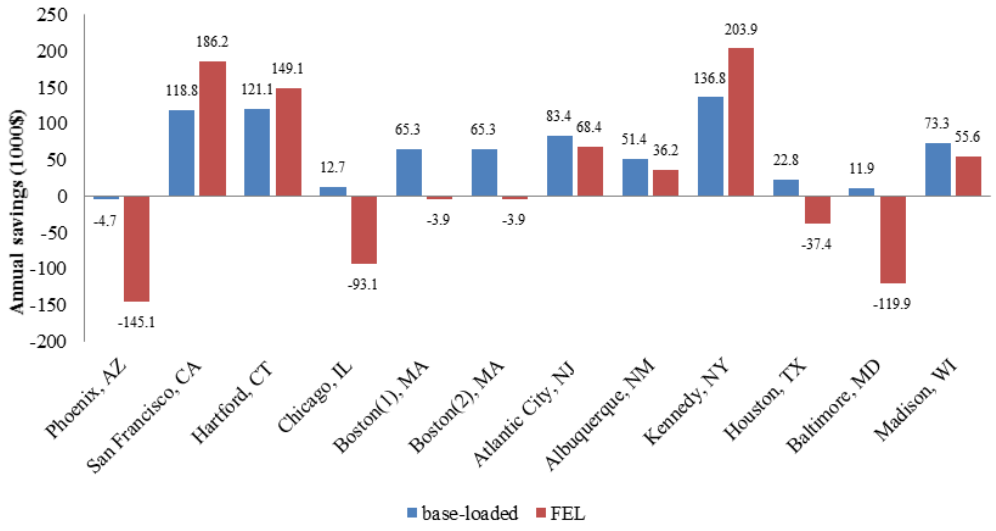

Figure 2.7 Annual savings in the energy consumption cost of different CHP operational strategies for large office buildings

Figure 2.8 shows the results of the payback period analysis for large office buildings in different locations. The capital cost payback period of CHP systems without incentives for large office buildings is shown in Figure 2.8 (a). Similar to the hospital buildings, the payback period of the based-loaded operational strategy is much shorter than that of FEL situation (if existing) for a specified location. For the base-loaded situation, the payback periods in the locations of San Francisco, CA, Hartford, CT, Boston, MA, Atlantic City, NJ, Kennedy, NY and Madison, WI are all within 5 years, which is very desirable. While for the FEL situation, the payback periods in these locations (if existing) are more than 10 years.

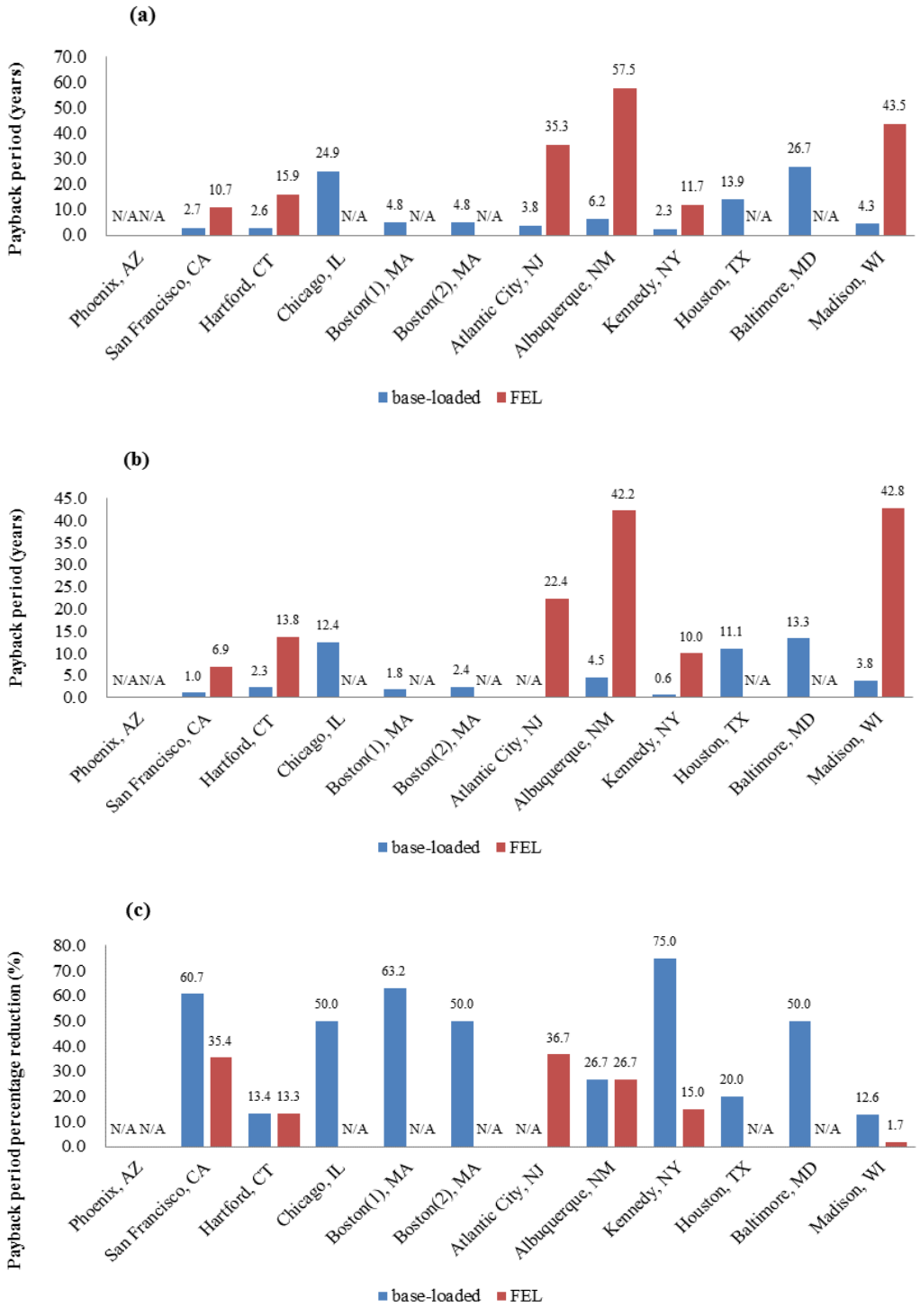

Figure 2.8 Results of payback period analysis for large office buildings: (a) Capital cost payback period of CHP systems without incentives; (b) Capital cost payback period of CHP systems with incentives; (c) Capital cost payback period percentage reduction

Figure 2.8 (b) and (c) show the capital cost payback period with incentives and the payback period percentage reduction due to incentives for large office buildings, respectively. The largest reduction of the payback period occurs at Kennedy, NY, which can reach up to 75% when the CHP system is operated in base-loaded strategy. For the base-loaded CHP system in Albuquerque, NM, the payback period reduction is 26.7%. The payback period can be reduced from 6.2 years to 4.5 years, which is an acceptable value. However, for the FEL situation, the payback period in each location (if existing) is still too long even taking the reduction into consideration.

Figure 2.9 shows the annual savings in the energy consumption cost of different CHP operational strategies for large hotel buildings. As can be seen, the annual savings in the energy consumption cost of the base-loaded CHP system are all positive values for all locations. While the CHP system is operated under the FEL mode, the annual savings for Phoenix, AZ is a negative value, and the other locations remain positive.

Figure 2.10 (a) shows the capital cost payback period of CHP systems without incentives for large hotel buildings in different locations. It can be seen that base-loaded CHP systems are very attractive choices for a large hotel in many locations, such as San Francisco, CA, Hartford, CT, Boston, MA, Atlantic City, NJ, Albuquerque, NM, Kennedy, NY, Baltimore, MD and Madison, WI. In these areas, the payback periods are all less than 3 years. For FEL CHP systems, the payback periods in some locations are less than 5 years and are acceptable, such as San Francisco, CA, Hartford, CT, and Kennedy, NY.

Figure 2.10 (b) and (c) show the capital cost payback period with incentives and the payback period percentage reduction due to incentives for large hotel buildings,

respectively. It is important to mention here that the payback period reduction for the base-loaded CHP system in Boston (1), MD can reach up to 100%. This is because, in this case, the capital cost is less than the maximum grant in Boston, which is $200,000. In addition, the payback period reduction in Atlantic City, NJ is 0% due to the restriction of the PGU capacity. The eligible project size should be greater than 1MW.

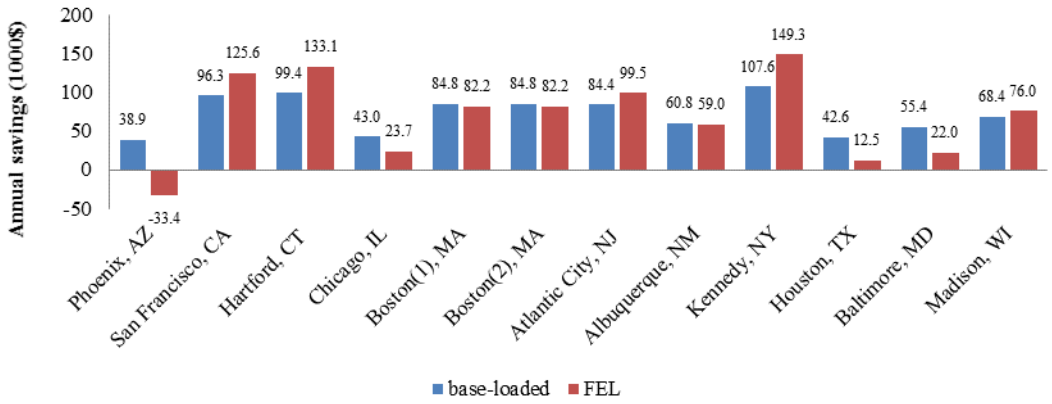

Figure 2.9 Annual savings in the energy consumption cost of different CHP operational strategies for large hotel buildings

Figure 2.11 shows the annual savings in the energy consumption cost of different CHP operational strategies for secondary school buildings. Similar to the hospital buildings, for base-loaded CHP systems, the annual savings in the energy consumption cost are all positive values for all locations. While as for the FEL CHP systems, the annual savings for Phoenix, AZ, Chicago, IL, Houston, TX and Baltimore, MD are negative values and the others remain positive.

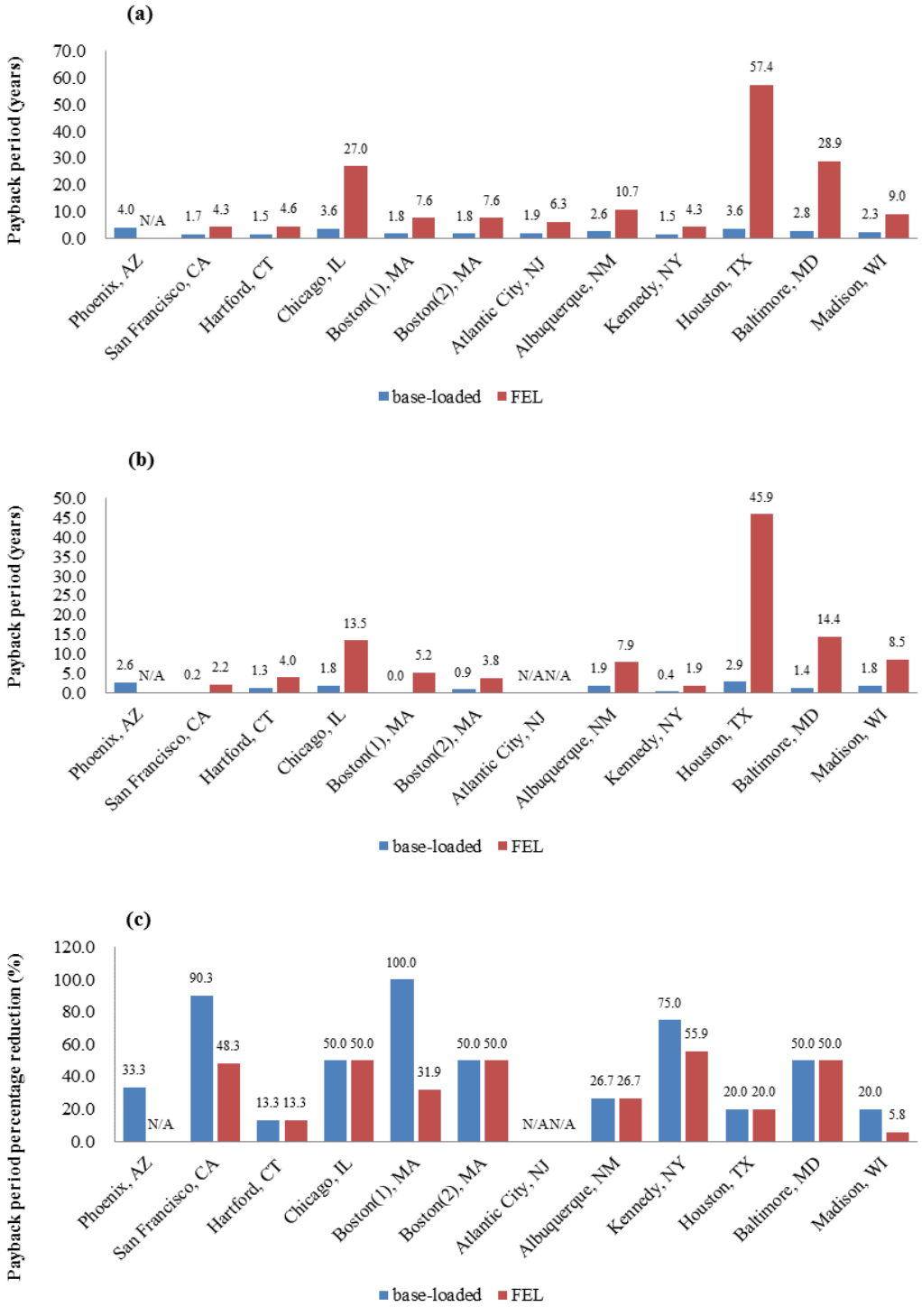

Figure 2.10 Results of payback period analysis for large hotel buildings: (a) Capital cost payback period of CHP systems without incentives; (b) Capital cost payback period of CHP systems with incentives; (c) Capital cost payback period percentage reduction

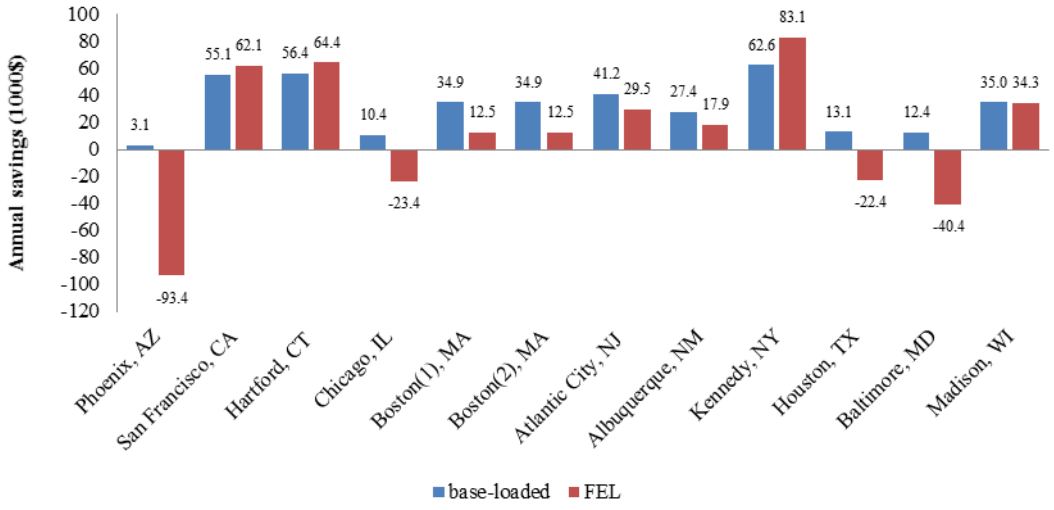

Figure 2.11 Annual savings in the energy consumption cost of different CHP operational strategies for secondary school buildings

Figure 2.12 (a) shows the capital cost payback period of CHP systems for secondary school buildings in different locations. As can be seen, the base-loaded CHP systems in the locations of San Francisco, CA, Hartford, CT, Boston, MA, Atlantic City, NJ, Albuquerque, NM, Kennedy, NY and Madison, WI have desirable payback periods, which are less than 5 years. For the FEL situation, the payback periods in these locations (if existing) are more than 10 years.

Figure 2.12 (b) and (c) show the capital cost payback period with incentives and the payback period percentage reduction due to incentives for secondary school buildings, respectively. Similar to the large hotel building, the payback period reduction for base-loaded CHP system in San Francisco, CA and Boston (1), MD can reach up to 100%. This is because, in these locations, the capital cost is less than the maximum amount offered by the incentive policies.

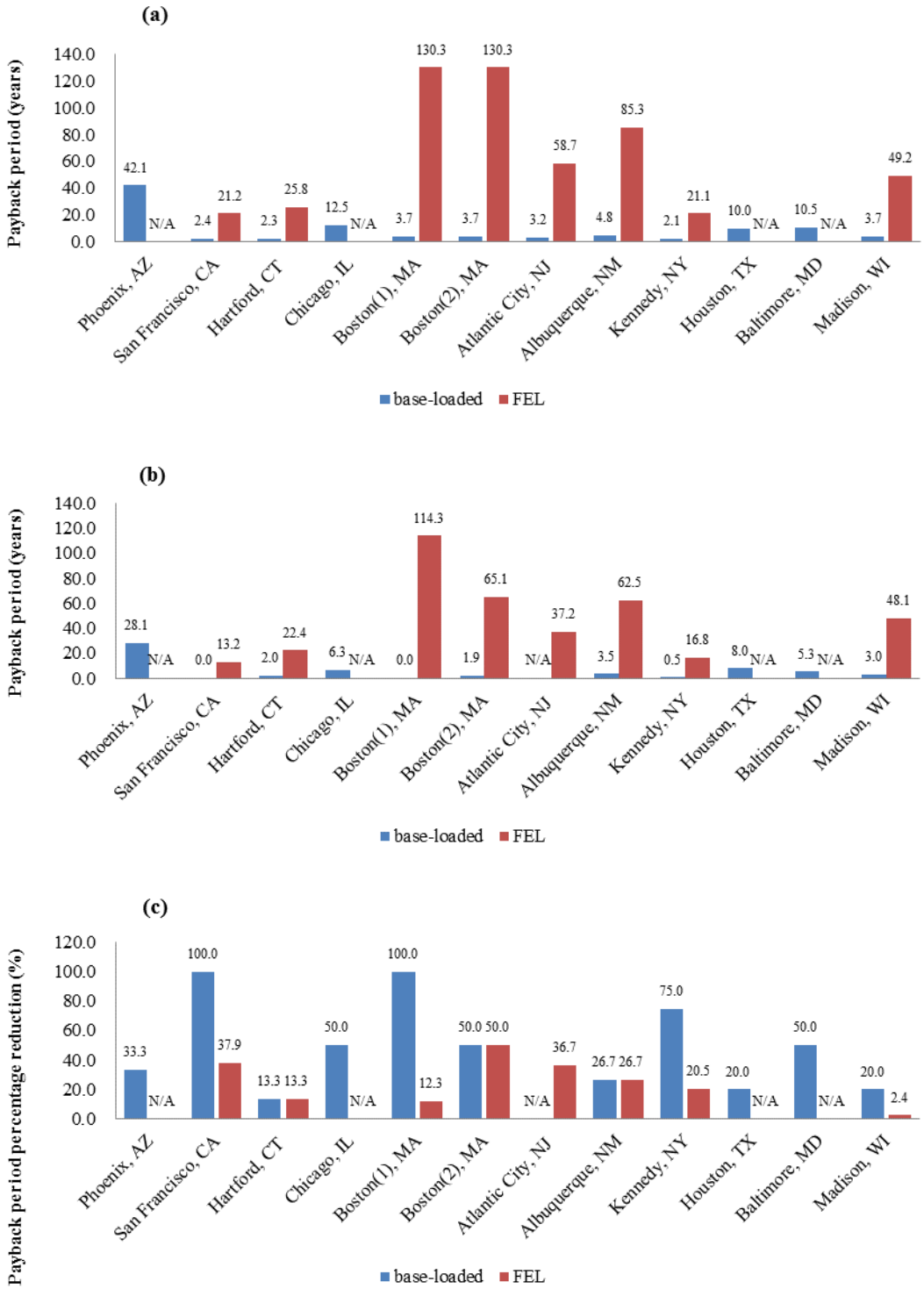

Figure 2.12 Results of payback period analysis for secondary school buildings: (a) Capital cost payback period of CHP systems without incentives; (b) Capital cost payback period of CHP systems with incentives; (c) Capital cost payback period percentage reduction

It is interesting to note that, when annual savings are not present in one or more locations for CHP operation with each building type, the locations that are not conducive all have cost ratios under 4. Examining Figure 2.5, Figure 2.7, Figure 2.9, and Figure 2.11, it is clear that Phoenix, AZ; Chicago, IL; Houston, TX; and Baltimore, MD are the locations, of those examined, least conducive to CHP operation, as all four buildings examined, aside from large hotel, do not provide annual savings under at least one CHP operational strategy in these locations. Each of these locations has a cost ratio below 3.8. Additionally, for a large office building, Boston, MA also yields negative annual savings for CHP-FEL operation. While Boston has a higher cost ratio than the afore-mentioned locations, it still has a ratio lower than 4, at 3.844, so it is not surprising that this location does not produce favorable results for all building types and CHP operational strategies. Finally, the large hotel building yields annual savings in all locations except Phoenix, AZ, which has the second lowest cost ratio of all locations examined.

This shows that, while cost ratio is certainly not the only factor impacting CHP locational performance, it certainly provides a substantial impact on CHP performance. Other factors that contribute to CHP location-based and building-type performance differences include the location-based ratio of annual electric load to annual thermal load and incentive structures currently in place in each location. All of these factors are contributing to overall CHP performance and impacting the results obtained, but it is worth reviewing load ratios, in particular, as results suggest that load ratios significantly contribute to explanations of why the large hotel shows the most favorable CHP results, even in low cost ratio locations; why Phoenix yields poor CHP operation regardless of building type; and why the large office building performs poorly in the most locations.

The large hotel has the most balanced (close to one) load ratio, overall, of the four buildings examined, ranging from about 0.7 in Madison, WI to about 1.9 in Phoenix, AZ. Thus, for the large hotel, the load ratio is least balanced (and highest) in the one location that yielded poor savings for CHP FEL operation. It is also worth noting that, for all building types, Phoenix, AZ has the highest electric to thermal load ratio of all locations examined. It should also be noted that, of all four buildings examined, the large office has the highest electric to thermal load ratio for each location. Thus, the electric to thermal load ratio contributes to the explanation of why the large hotel yields favorable CHP performance in the most locations compared to other building types and why the large office yields unfavorable CHP performance in the most locations compared to other building types, as well as why Phoenix is the only location that yields unfavorable performance for the large hotel building.

CHAPTER III

DESIGN AND TECHNO-ECONOMIC ANALYSIS FOR SOLAR PHOTOVOLTAIC (PV) SYSTEM

This chapter provides an analysis of the techno-economic performance of photovoltaic (PV) energy generation for selected locations. In this chapter, four types of buildings, including hospital, large office, large hotel, and secondary school, located in five different states which each have their own incentives, are selected and analyzed for the PV economic performance. Using the EnergyPlus simulation software, the energy consumption of each building is obtained. Then the simulation models of a PV system are established for each building type. From the simulation results, the payback period of the PV systems in different locations is calculated according to local incentive policies. This payback period is then compared to the one without regard for incentive policies. In this way, the techno-economic performance of PV system is evaluated, and existing incentive policies provided by utility companies in each state are analyzed and critiqued. Finally, a parametric analysis is conducted to investigate the influence of the parameters such as PV system capacity, capital cost of PV, sell back ratio, and the performance-based incentive rate on the performance of the PV system.

3.1 Solar Photovoltaic Analysis

The energy that can be obtained from a solar photovoltaic system is primarily a function of the performance characteristics of the solar PV modules comprised in the

array, with solar radiation and ambient temperature as environmental variables. PV performance characteristics should correspond to the specifications provided by the manufacturer based on experimental tests, and solar radiation data should be obtained from a reliable source that includes data measured over significant periods of time. In this analysis, Typical Meteorological Year 3 (TMY3) data is recommended and used. A defined time step is required for the analysis; one hour is used as the time step in this chapter. This section presents an analysis to determine the size of the photovoltaic array according to the methodologies used in Cho and Fumo [75] and Duffie and Beckman [76].

3.1.1 Solar Radiation

The equations proposed to estimate the total solar radiation G_T on the surface of the solar PV array are given in this section. The total solar radiation on the tilted surface of a module is the sum of the direct solar radiation $G_{b,s}$, diffuse solar radiation $G_{d,s}$, and ground reflected solar radiation $G_{r,s}$, which are defined in Eqs. (3.2), (3.3), and (3.4), respectively.

$$G_T = G_{b,s} + G_{d,s} + G_{r,s} \tag{3.1}$$

$$G_{b,s} = G_b \cos(\theta) \tag{3.2}$$

$$G_{d,s} = G_d \frac{1+\cos(\beta)}{2} \tag{3.3}$$

$$G_{r,s} = G_r \frac{1-\cos(\beta)}{2} \tag{3.4}$$

where θ is the solar angle of incidence and β is the surface tilt of the modules. The cosine of the angle of incidence is defined as

$$\cos(\theta) = \cos(\alpha_s)\cos(\gamma_s - \gamma)\sin(\beta) + \sin(\alpha_s)\cos(\beta) \tag{3.5}$$

where α_s is the solar altitude angle, γ_s is the solar azimuth angle, and γ is the surface (module's) azimuth angle. The solar altitude angle and the solar azimuth angle can be found using Eqs. (3.6) and (3.7), respectively.

$$\sin(\alpha_s) = \sin(\varphi)\sin(\delta_s) + \cos(\varphi)\cos(\delta_s)\cos(\omega_s) \tag{3.6}$$

$$\sin(\gamma_s) = \frac{\cos(\delta_s)\sin(\omega_s)}{\cos(\alpha_s)} \tag{3.7}$$

where φ is the latitude of the site, δ_s is the solar declination, and ω_s is the hour angle. The solar declination can be obtained using Eq. (3.8) with n as the day of the year (1 for January 1st and 365 for December 31st).

$$\delta_s = 23.45° \sin[360° \frac{n+284}{365}] \tag{3.8}$$

The ground reflected solar radiation can be calculated based on the direct and diffuse solar radiation and solar zenith angle [77] as shown in Eq. (3.9).

$$G_r = (G_b \cos(\Psi) + G_\mathrm{d})\rho \tag{3.9}$$

where Ψ is the solar zenith angle, which is the complementary angle of the solar altitude angle, α_s, and ρ is the ground reflectance. The ground reflectance is assumed to be 0.2, which is the commonly used value in the building energy simulations [77][78].

3.1.2 Solar Photovoltaic Module

The approach proposed in this study uses the model given in [79] as shown in Eq. (3.10). The total power levels of the PV array (P_{PV}) are assumed constant over the time step.

$$P_{PV} = A_{surf}\, f_{activ}\, G_T\, \eta_{cell}\, \eta_{invert} \tag{3.10}$$

where A_{surf} is the net surface area of PV modules, f_{activ} is the fraction of surface area with active solar cells, η_{cell} is the module conversion efficiency, and η_{invert}

is the DC to AC conversion efficiency. In general, the PV module conversion efficiency (η_{cell}) can be determined from the manufacturers' specifications.

3.1.3 Solar Availability

The solar maps show the monthly average daily total solar resource information on grid cells, i.e. the solar availability in each location. In solar maps, the values of insolation indicate the solar resource accessible to a photovoltaic panel oriented due south at an angle from horizontal equal to the location latitude, which is a typical orientation used in PV system installation [80].

Figure 3.1 illustrates the photovoltaic solar resource of the United States, specifically indicating the national solar PV resource potential for all states. In this chapter, five locations selected for investigation are Florida, Georgia, Hawaii, Nevada and Vermont. Table 3.1 shows the representative city as well as maximum and average solar availability for the selected states.

Table 3.1 Representative city and solar availability for five selected states

State	Representative city	Maximum solar availability (kWh/m^2/Day)	Average solar availability (kWh/m^2/Day)
Florida	Miami	6.0	5.5
Georgia	Atlanta	5.5	5.0
Hawaii	Honolulu	6.5	5.0
Nevada	Las. Vegas	6.5	5.75
Vermont	Montpelier	4.5	4.25

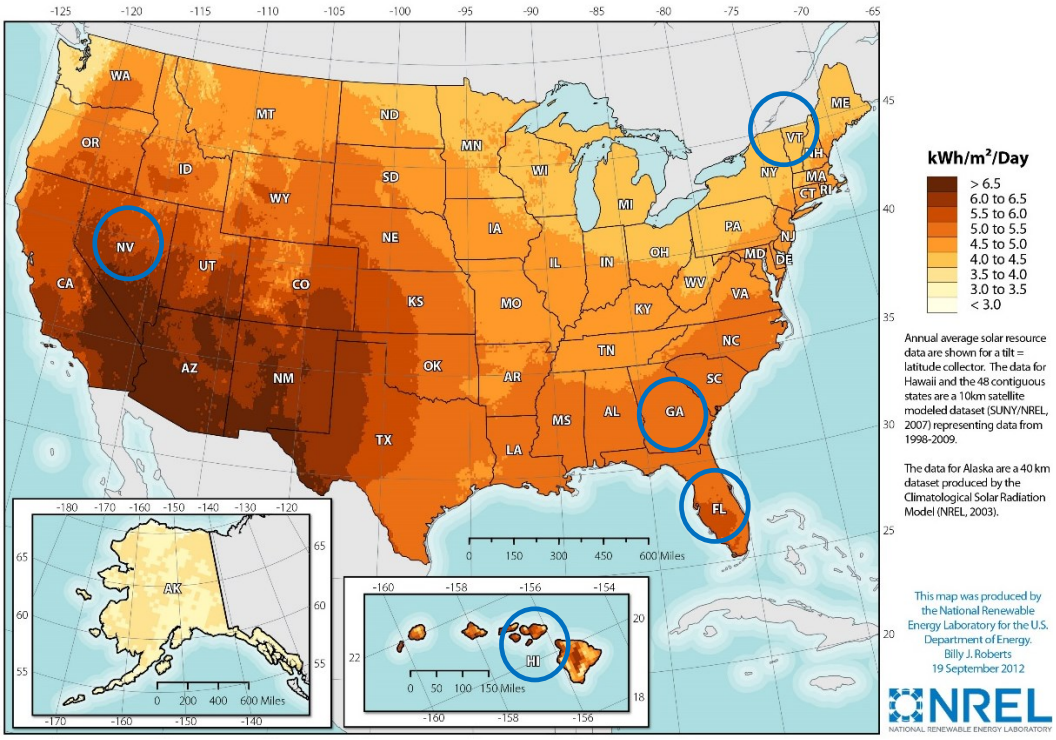

Figure 3.1 Photovoltaic Solar Resource of the United States [80]

3.2 Incentive Analysis

3.2.1 Payback Period Estimation

In order to determine the simple payback period of a PV system, the cost of installing a PV system and the annual savings earned from the PV system should be known. In this chapter, the focus is on the capital cost of a PV system, since it constitutes a large portion of the total cost of the PV system. For a commercial building, the cost for a medium-scale PV system (C_{PV}) in the U.S. averaged 2.25$/W [81], and this value is used to estimate the simple payback period. The capital cost of a PV system is calculated as:

$$Cost_{C,PV} = C_{PV} \cdot Cap_{PV} \tag{3.11}$$

where Cap_{PV} represents the capacity of the PV system.

The annual savings are calculated as:

$$\mathrm{AS} = E_{PV} \cdot Cost_e \tag{3.12}$$

where E_{PV} is the annual useable electricity energy generated by the PV system. $Cost_e$ is the cost of electricity (from the grid). Table 3.2 shows the electricity price used in the simulation for each location.

Table 3.2 Electricity prices used in the simulation for each location [82]

State	$Cost_e$($/kWh)
Florida	0.0965
Georgia	0.0975
Hawaii	0.2692
Nevada	0.0925
Vermont	0.1451

Then the payback period can be estimated as:

$$PBP = Cost_{C,PV}/AS \tag{3.13}$$

If the incentive is taken into the consideration, then the payback period is:

$$PBP_w = Cost_{C,PV}/(AS + In) \tag{3.14}$$

where PBP_w is the payback period with incentive policies. In is the amount of money which the PV system owner can obtain from the incentive policies.

3.2.2 Existing Incentive Structures

In many cases, local utility companies have incentive programs to encourage the use of renewable energy technologies, including PV. This section includes several examples from local utilities in the United States. Later, these examples will be compared and analyzed for effectiveness.

The solar Investment Tax Credit (ITC) is an important federal policy which aims at promoting the development of solar energy in the US. A tax credit allows a person or company to receive a dollar-for-dollar reduction in their income taxes. The ITC is calculated according to the amount of investment in solar systems. The ITC for both the residential and commercial applications are equal to 30 percent of the investment in solar systems [83].

Florida Power and Light (FPL) has a net metering program that allows customers to connect approved renewable energy systems (including PV arrays) to the grid. This system allows such customers to reduce their electricity bills as well as sell any excess electricity to FPL [84]. FPL also has a solar rebate program for residential and commercial customers who install PV arrays. Commercial customers can earn a rebate of up to $50,000 per location [85].

In 2012, Georgia Power, a local utility owned by Southern Company, initiated a plan called the Georgia Power Advanced Solar Initiative (GPASI) [86]. The goal of GPASI is to drive economic growth in the solar industry in Georgia, as well as to encourage development of renewable energy technologies as a whole, without negatively impacting prices or reliability for customers. Georgia Power has developed two programs to help meet that goal: 1) a net metering system to encourage customers to sell distributed

solar energy to the utility from small- and medium-scale projects; and 2) an auction scheme to allow solar developers to bring large-scale PV arrays to market.

In addition to GPASI, Georgia Power also provides residents a buyback program which pays a higher price than net metering for electricity generated by solar panels. This buyback program is available to both residential and commercial customers. Electricity generated by photovoltaic systems is purchased back by Georgia Power at a rate of $0.17/kWh, for any power capacity up to 5MW, as opposed to the buyback rate at a retail price (0.0975$/kWh in Georgia) for typical net metering[87].

Hawaiian Electric Company currently utilizes a feed-in tariff (FIT) program to promote renewable energy technologies. The Hawaii Public Utilities Commission has established three tiers for renewable energy technologies based on the type of technology, the capacity, and the island on which the project is located [88]. The tiers for PV on Oahu are presented in Table 3.3.

The energy payments are determined based on the tier, and therefore capacity, as shown in Table 3.4. According to the capacities investigated in this chapter, Tier 2 and 3 are selected for corresponding situations.

Table 3.3 Hawaii Public Utilities Commission Tiers

Tier	Project Size
1	0-20 kW
2	Greater than 20 kW and up to and including 500 kW
3	Greater than Tier 2 maximums and up to and including the lesser of 5 MW

Table 3.4 Hawaiian Electric PV Payment Rates

Tier	FIT Energy Payment Rate($/kWh)
1	0.218
2	0.189
3	0.197

Nevada Energy offers an incentive program called “RenewableGenerations.” Under this package, solar PV systems with capacities up to and including 25 kW receive an up-front incentive (UFI, dollars per watt), and systems with capacities higher than 25 kW receive a performance-based incentive (PBI, dollars per kilowatt hour). In the current investigation, only PBI is considered because the PV capacities under investigation in this chapter are all larger than 25 kW. The current structure of solar PV incentive rates [89] under the “RenewableGenerations” program is presented in Table 3.5.

Nevada Energy also provides a rebate program for small businesses and public buildings using solar applications. Eligible customers (up to 1MW) could get paid

$1.35/W for their solar energy systems with a maximum of $310,000 for public facilities; $67,500 for small business buildings; and $155,000 for schools [90].

Table 3.5 Nevada Energy PV Incentive Rates

Category	PBI($/kWh)
Public, low-income, non-profit	0.0317
Residential, commercial, industrial	0.0159

In Vermont, Green Mountain Power has an incentive program called "GMP Solar" for customers who generate electricity from solar arrays [91]. "GMP Solar" is a net metering program. In the event customers generate more energy than they use, customers are compensated for the excess energy according to Vermont state law. Systems with capacities of up to 500 kW are eligible for the net metering program. For those systems eligible for the net metering, an additional benefit of $0.043/kWh for the gross generation from solar sources is also available [92].

Table 3.6 presents a summary of the incentive benefits available in each examined region for commercial buildings. In the table, the column PBI includes not only the PBI incentive in Nevada, but also all the other incentives which pay the customers according to the amount of electricity (kilowatt hours) for their PV system, including the buyback program in Georgia, the FIT program in Hawaii, and the GMP solar program in Vermont.

Table 3.6 Incentive summary for each location

Company	PBI ($/kWh)	Net Metering	Others
Federal Incentive	NA	N	Tax credit (30% of investment)
Florida Power and Light	NA	Y	Rebate ($50,000)
Georgia Power	0.17 (up to 5 MW)	Y (if no PBI)	NA
Hawaiian Electric	0.189; 0.197 (based on capacity)	N	NA
Nevada Energy	0.0317; 0.0159 (based on building type)	N	Rebate ($1.35/W)
Green Mountain Power	0.043 (up to 500 kW)	Y(up to 500 kW)	NA

3.3 Building Model Description

As mentioned in last chapter, there are 16 commercial reference building models which are developed by the U.S. Department of Energy (DOE) and represent nearly 70% of the commercial buildings in the U.S [66][67]. With EnergyPlus simulation software, these reference buildings could provide complete descriptions for whole building energy analysis. In this chapter, four types of buildings are selected: hospital, large office, large hotel, and secondary school. Figure 3.2 shows the drawings of the four types of buildings [93], respectively. The characteristics of each building type are the same with the ones in Table 2.1.

These four building types were chosen because the electrical energy consumptions in those buildings are relatively large compared to other DOE's commercial reference building models, so that the existing PV incentives can be

effectively evaluated with the consideration of its capacity limit in some states' incentive policies. In addition, the feasibility of PV systems in different types of buildings can be effectively demonstrated using those four building types because each building has unique electric load profiles.

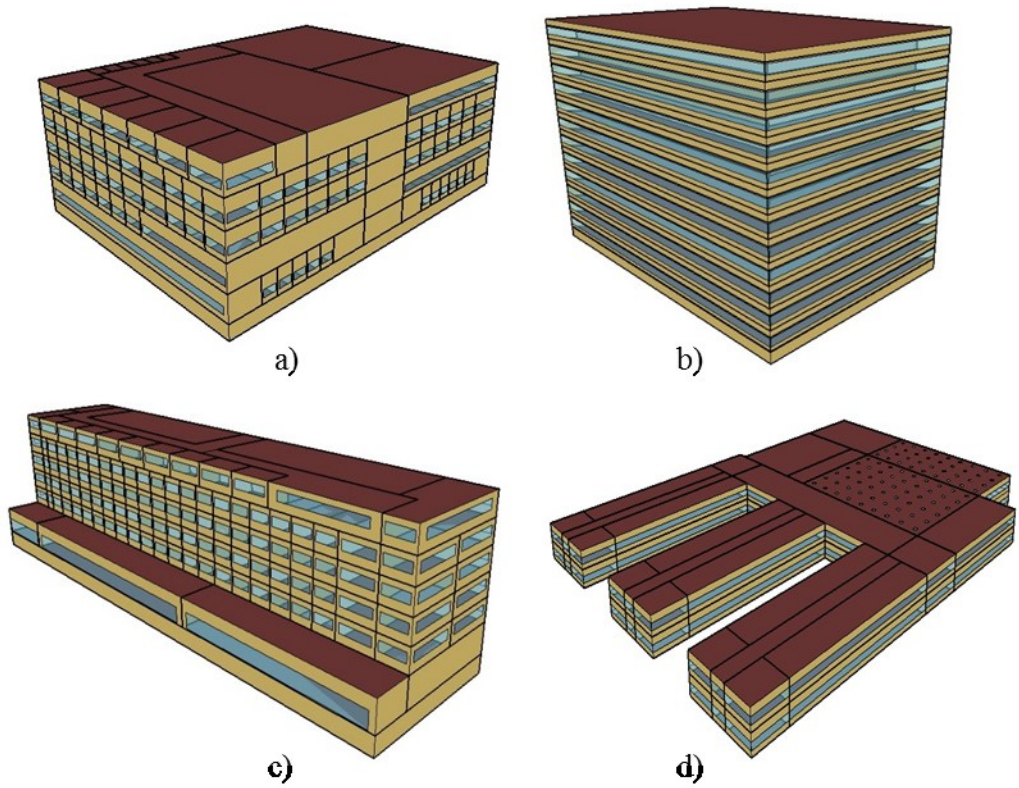

Figure 3.2 Drawings of the four types of buildings; a) hospital; b) large office; c) large hotel; d) secondary school

In this chapter, the hourly electric energy consumptions, e_{con}, for each building in different locations are obtained by simulating those reference building models in EnergyPlus software. Then the PV models are run in the Mathcad software to simulate

the hourly electricity generation, e_{gen}, of the PV system. The hourly difference between onsite electric energy consumption and generation can be estimated as:

$$\Delta e = e_{gen} - e_{con} \tag{3-15}$$

When $\Delta e > 0$, part of the electricity generated by the PV is not used by the building, thus is wasted if not considering any incentives (e.g., net metering or feed-in-tariff). A larger Δe value implies that more electricity would be wasted. When $\Delta e < 0$, excess electricity needs be imported from the grid to meet the electricity demand of the building. A larger magnitude negative Δe value means that more electricity would be imported. Figure 3.3 shows the hourly electricity consumption, generation and difference in an arbitrary day for a building. Furthermore, the annual positive difference (PD) and negative difference (ND) can be determined by summing positive Δe and negative Δe for the entire simulation period, respectively, as shown Eqs. (3-16) and (3-17).

$$PD = \sum_{i=1}^{8760} \Delta e_i \qquad \text{if } \Delta e_i > 0 \tag{3-16}$$

$$ND = \sum_{i=1}^{8760} \Delta e_i \qquad \text{if } \Delta e_i < 0 \tag{3-17}$$

Then the PD and ND can be normalized by its PV capacity using Eqs. (3-18) and (3-19) and the normalized PD and ND values are shown in Table 3.7.

$$\overline{PD} = \frac{PD}{Cap_{PV}} \tag{3-18}$$

$$\overline{ND} = \frac{ND}{Cap_{PV}} \tag{3-19}$$

$\overline{PD}$ indicates the excess electricity generated onsite per kilowatt capacity and $\overline{ND}$ shows the electricity imported from the grid per kilowatt capacity. By normalizing the PD and ND, the influence of PV capacity on the annual difference can be estimated. This

information will be useful when the payback periods with/without any incentives for various buildings are compared in subsequent discussions for Figure 3.5.

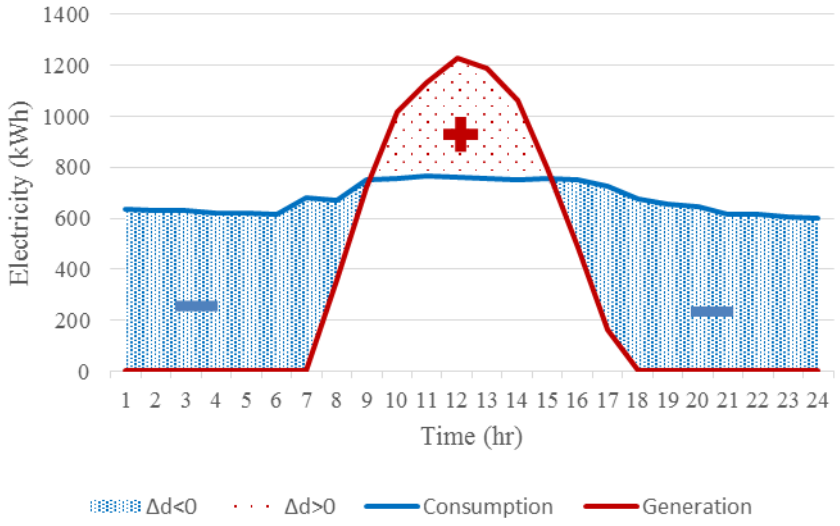

Figure 3.3 Hourly electricity consumption, generation and the difference in an arbitrary day

Table 3.7 Annual total difference between hourly electricity generation and consumption normalized by its PV capacity (MWh/kW)

	Hospital		Large office		Large hotel		Secondary school	
	$\overline{PD}$	$\overline{ND}$	$\overline{PD}$	$\overline{ND}$	$\overline{PD}$	$\overline{ND}$	$\overline{PD}$	$\overline{ND}$
FL	0.053	-4.047	0.181	-2.591	0.268	-3.400	0.437	-1.474
GA	0.086	-3.407	0.244	-2.157	0.395	-2.933	0.605	-1.019
HI	0.080	-3.397	0.218	-2.281	0.352	-3.148	0.512	-1.262
NV	0.244	-2.803	0.486	-1.751	0.634	-2.702	0.902	-0.935
VT	0.095	-3.234	0.255	-2.018	0.327	-2.752	0.566	-0.927

Table 3.8 indicates the peak electricity load for four kinds of buildings in all locations. This information will be used to decide the capacity of PV array for each kind of building in subsequent discussions for Figure 3.5.

Table 3.8 Peak electricity load for each kind of building in all locations [Unit: kW]

	Hospital	Large office	Large hotel	Secondary school
Florida	1341	1689	434	1228
Georgia	1262	1553	426	1101
Hawaii	1218	1565	417	1108
Nevada	1188	1478	476	1202
Vermont	1182	1497	404	938

Figure 3.4 shows the monthly electric load for the four kinds of reference buildings in all five locations. It can be seen from Figure 3.4 that the electric load for the hospital and large office buildings are much higher than that for the large hotel and secondary school buildings. For each building type, the electric load in Florida and Hawaii are higher than that in other states during most times of the year due to larger air conditioning requirement, and the electric load in Vermont is the least among five locations.

3.4 Results and Discussion

In this section, the results of payback periods for each building type in all locations are compared with each other. Then the parameter study is conducted in order to reveal the influence of each parameter on the payback period of a PV system. Note that

all incentives listed in Table 3.6 are used for the calculation of the payback period with incentive in each figure unless specifically mentioned otherwise.

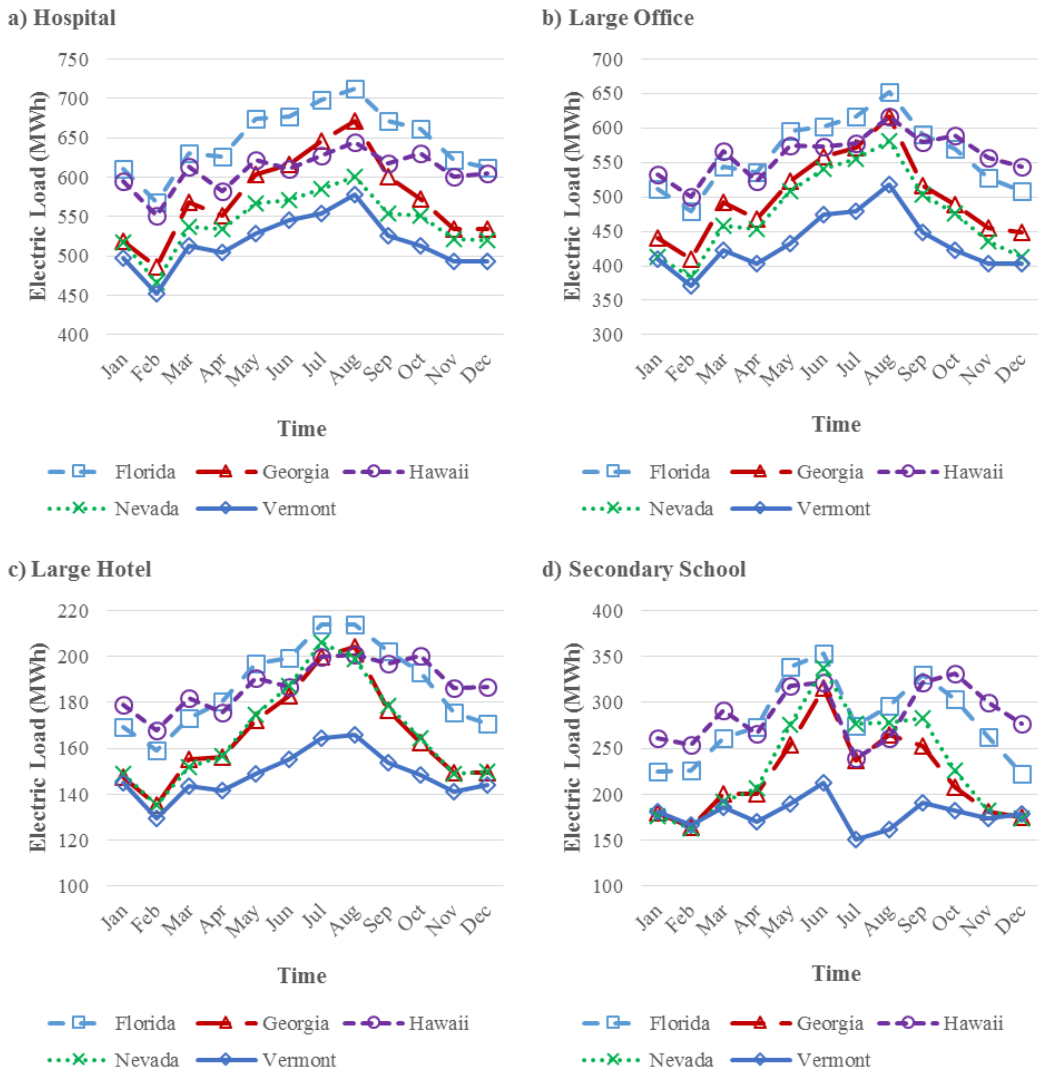

Figure 3.4 Monthly electric load for the reference buildings in all locations; a) hospital; b) large office; c) large hotel; d) secondary school

Figure 3.5 shows the results of payback period analysis with and without the existing incentive policies in each location for four different buildings including hospital,

large office, large hotel, and secondary school. In this part, the capacity of the PV array is selected based on the maximum electricity load of each building type. The selected capacities are 1400 kW, 1700 kW, 480 kW, and 1300 kW for the hospital, large office, large hotel, and secondary school, respectively. For each building type, the payback period of a PV system is calculated based on the local incentive policies (as described in Section 3.2) and then compared to the case without considering incentives. The findings from the simulation results shown in Figure 3.5 are discussed in detail below:

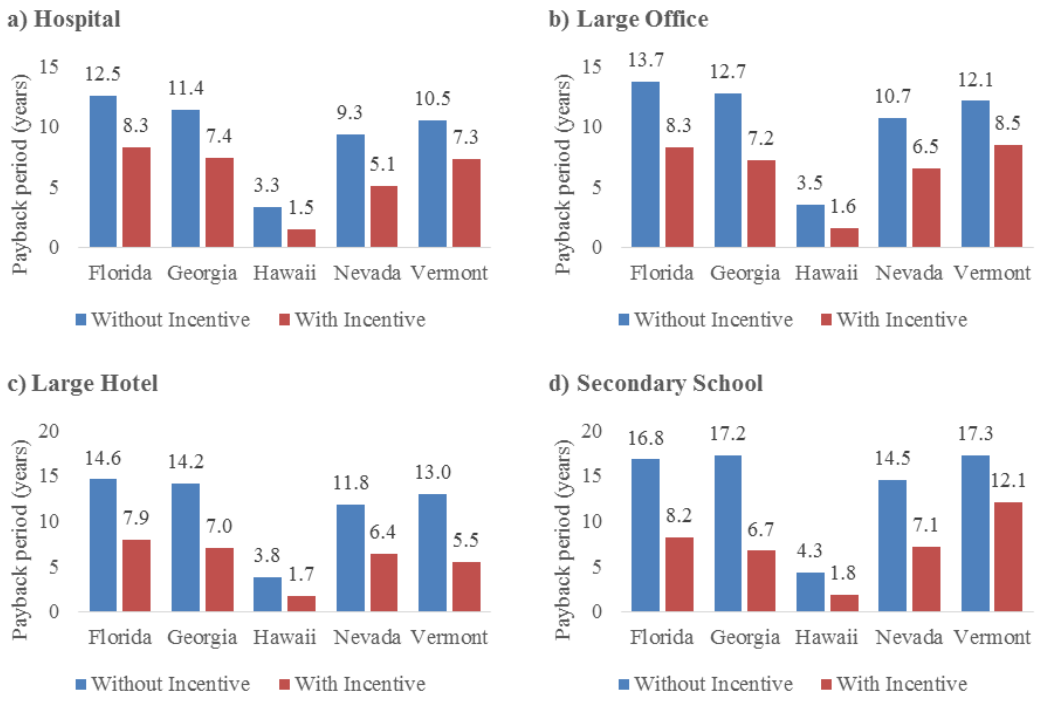

Figure 3.5 Results of payback period analysis for four kinds of buildings; a) hospital; b) large office; c) large hotel; d) secondary school

In all locations, the PV system for hospital building possesses the shortest payback period before incentive policies are taken into consideration, while the PV

system for secondary school has the longest payback period. As can be seen from Table 3.7, the hospital building in each location processes the lowest normalized positive difference ($\overline{PD}$), which means the waste of the generated electricity is the lowest among all building types when the incentive policies are not taken into consideration. This explains well why the hospital has the shortest payback period without incentives. Table 3.7 also shows that $\overline{PD}$ becomes larger in the order of hospital, large office, large hotel and secondary school although the order magnitude of their PV capacities do not follow this order. With this observation, one can explain why the payback period becomes bigger in the order of hospital, large office, large hotel and secondary school in Figure 3.5.

When the incentive policies are adopted, the payback period can be significantly reduced in most locations and building types. The payback periods for all building types in most locations become less than 10 years after the incentives are applied. Considering the expected lifespan of the PV modules in the market is between 20 and 30 years [38], reducing the payback period below 10 years with the incentives in each selected state can effectively promote the PV installations in their states. However, the level of reduction can vary depending on the location and building type (i.e., the reduction in the payback period varies approximately from 2 to 11 years). Interestingly, one can also observe from Figure 3.5 that the level of payback period reduction decreases in the order of secondary school, large hotel, large office and hospital when the incentives are considered in the calculation. This is the exact opposite trend compared to that without the incentives mentioned above. It means that the larger $\overline{PD}$ would result the larger reduction of

payback period because those buildings have more excess electricity would benefit more from the PBI and net metering policies.

It is important to mention here that the incentive policy from Green Mountain Power in Vermont (i.e., a PBI of 0.043 $/kWh and net metering) is only for the system under 500 kW. Thus, among the four building types, only the PV system for a large hotel is eligible for the incentive policy from Green Mountain Power. That is why the payback period with incentive for large hotel in Vermont is much shorter than that for other building types in Vermont.

Notably, for all building types, the payback periods in Hawaii are quite attractive (all below 5 years) even without including the incentive policy. This is due to the influence of the solar availability and electricity cost. From Table 3.1 and Table 3.2, it can be seen that Hawaii possesses high solar availability and high electricity cost. Higher solar availability means that the PV system can generate more electricity under the same conditions, and higher electricity cost means that more money can be saved when using the electricity generated from PV instead of grid electricity. As a comparison, Nevada also has the same or even higher solar availability, but much lower electricity cost compared to Hawaii; thus, the payback period in Nevada is much higher than that in Hawaii. Similarly, even though the solar availability in Vermont is lower than that in Florida and Georgia, the payback period without incentive of PV system in Vermont is still better than that in Florida and Georgia (except for the case of secondary school) due to much higher electricity cost in Vermont compared to that in Florida and Georgia. The exception for the secondary school can be explained in such a way that the negative normalized difference for secondary school is smaller than that for other building types,

which reduces the influence of electricity cost on the payback period because a smaller normalized negative difference means less electricity is imported from the grid. The above mentioned analysis shows that, while electricity cost is certainly not the only factor impacting PV locational performance, it definitely provides a substantial impact on PV cost performance.

Besides the two factors solar availability and electricity cost (which have been discussed before), there are several other factors that can influence the payback period of a PV system: capacity of the PV system, capital cost of PV, sell back electricity rate, and PBI rate. It can be seen from Figure 3.5 that the trends of the variation of the payback period with the locations among different building types are similar. For this reason, the hospital building is taken as a representative building type to perform a parametric analysis to illustrate the impact on the payback period by each factor (capacity of PV system, capital cost of PV, sell back electricity rate and PBI rate) in the following paragraphs. In this parametric analysis, it is assumed that the baseline scenarios include the existing incentive policies for each location (e.g., a PBI rate is reflected in the payback results for Hawaii in the baseline scenario to evaluate the impact of the aforementioned factors).

The influence of each parameter on the payback period is analyzed and presented in the following paragraphs, and Figure 3.6 to Figure 3.9 show the results of the parameter study. Figure 3.6 illustrates the influence of the capacity of PV system on the payback period for hospital buildings for the locations of Florida, Georgia, Hawaii, Nevada, and Vermont. As the capacity of PV system varies from 400 kW to 2000 kW, the payback periods with/without incentives are compared to each other. As shown in the

figure, the payback period without incentive increases with the increase of the PV capacity for all locations. For the payback periods without incentives in all locations, 1200 kW is an inflection point. When the capacity is smaller than 1200 kW, the payback period increases slowly with the change of PV capacity. However, when the capacity exceeds 1200 kW, the payback period increases quickly with the change of PV capacity. This is because the maximum electricity load in all locations is around 1200 kW (see Table 3.8). When the PV capacity is larger than the maximum electricity load, the PV system generates more electricity than the building consumes, so without any incentives (i.e., buy-back policies), the excess electricity is wasted. However, when net metering or PBI incentives are included, the excess electricity serves to diminish the payback period. Among the five locations, the payback periods are more sensitive to the variation of the PV capacity in Nevada and Vermont than in other locations, while the influence of the PV capacity is not significant in Hawaii, nor is it significant in Florida and Georgia when incentive polices are taken into consideration. This is due to the high PBI (i.e., feed-in tariff rate) in Hawaii and Georgia, as well as the net metering policy in Florida. For those locations that do not provide either a high PBI or a net metering policy, the users need to be aware that choosing an appropriate size is critical to achieve a desired payback period, while the policy makers may consider this as an opportunity to promote the PV systems in their states by implementing either a PBI or a net metering policy. As shown in Figure 3.6 (d)-(e), the payback period can vary from 2 to 6 years in Nevada and from 5 to 8 years in Vermont as the PV capacity increase from 400 kW to 1200 kW.

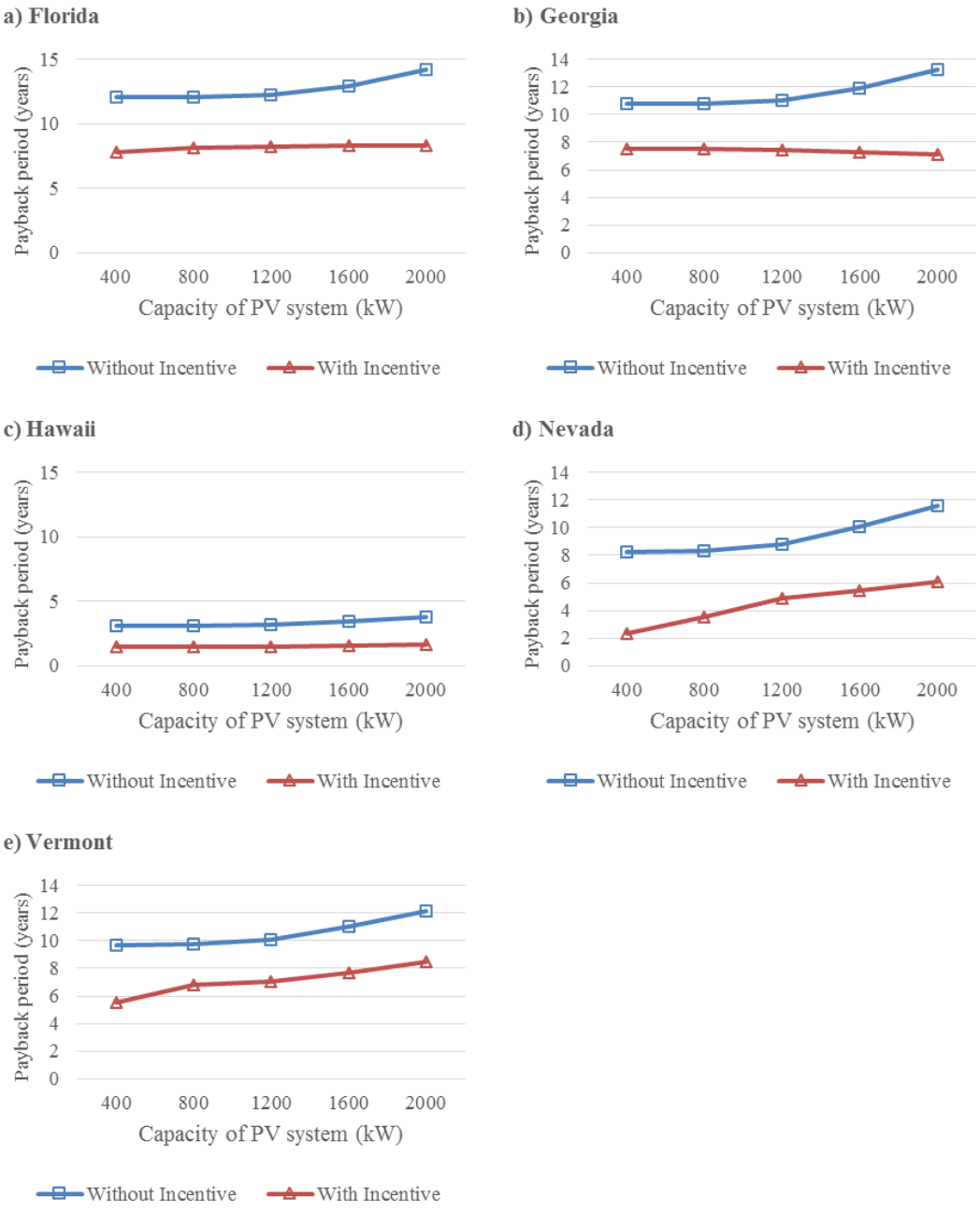

Figure 3.6 Influence of the PV capacity on the payback period for hospital buildings; a) Florida; b) Georgia; c) Hawaii; d) Nevada; e) Vermont

Figure 3.7 shows the variation trend of PV system payback period for hospital buildings when the capital cost of PV system changes from 0.5 $/W to 5 $/W. In this

case, the capacity of the PV system is set to a value of 1400 kW, which is based on the maximum electrical load of the hospital buildings among the five locations. As can be seen in the figure, the payback period increases linearly with the increase of capital cost of PV in all five locations, no matter whether the incentive is taken into consideration or not.

The slope of the line in the figure indicates how deeply the payback period is influenced by the capital cost of PV. For example, when the cost of PV changes from 0.5 to 5 $/W, the payback period without incentive varies from 2 years to almost 30 years in Florida, while it only varies from 2 years to nearly 10 years in Hawaii. Furthermore, from the figure, the conclusion can be drawn that if the capital cost goes down in the future (now the average price is about 2.25 $/W), the payback period of a PV system will be more attractive. The results shown in this figure are useful for both PV users and policy makers. On one hand, the potential PV users can estimate the payback periods of PV systems with the capital cost of PV in their locations and then determine whether it is worthwhile to install a PV system. On the other hand, the policy makers can consider providing an UFI and determine incentive rate based on the capital cost of PV in their locations. Taking Florida as an example, if a UFI of 1 $/W is given, the equal effect is the capital cost of PV system reduces from 2.25 $/W to 1.25 $/W, and then the payback period reduces from 12 to 7 years (without the existing incentives) and from 8 to 5 years (with the existing incentives).

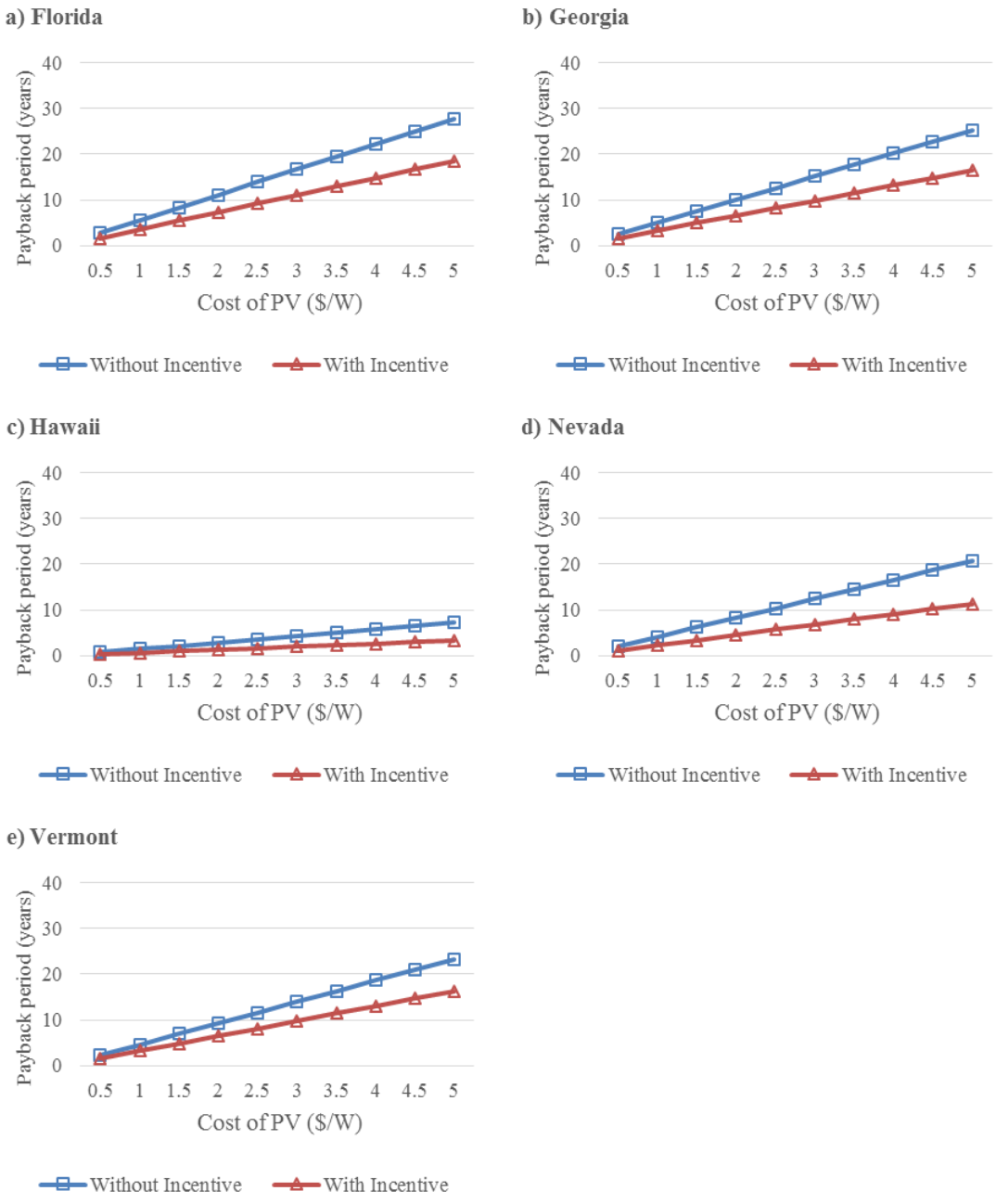

Figure 3.7 Influence of the capital cost of PV on the payback period for hospital buildings; a) Florida; b) Georgia; c) Hawaii; d) Nevada; e) Vermont

The influence of the sell back ratio on the payback period for hospital buildings is illustrated in Figure 3.8. In this part, when calculating the payback period with incentive,

the net metering incentive will not be applied directly, but instead assumes that the PV users in all the five locations can sell excess electricity back to a utility company. The sell back price is given out by defining a new parameter, sell back ratio. Namely, the sell back ratio indicates the ratio of the sell back rate of electricity to the local purchase rate charged by the utility company. In this case, the variation range of the sell back ratio is from 0.1 to 1, with an interval of 0.1. When the sell back ratio equals to 1, it means that net metering is available for the PV system. The capacities of PV systems are set to 1400 kW and 2000 kW. The reason why a 2000 kW capacity is added here is to supply enough excess electricity generation to adequately analyze the influence of the net metering on the payback period. Apparently, the payback period without incentive remains a constant value for a specific location and capacity. Also, in the same location, the payback period of the PV system with a capacity of 2000 kW is larger than that of the PV system with a capacity of 1400 kW. When the incentive policies are applied, the payback period decreases with the increase of the sell back ratio, which is especially significant for the cases with 2000 kW capacity. This is because at the capacity of 2000 kW, the PV system generates much more excess electricity to sell back than the case at the capacity of 1400 kW; thus, the influence of the sell back ratio on the payback period is more significant. Notably, when the sell back ratio equals to 1, i.e., net metering is adopted, the 2000 kW capacity PV system has almost the same payback period as the 1400 kW PV system. This indicates that the users need to be aware that they need to carefully size their PV systems based on their maximum electricity demand in their buildings when there are no policies to sell excess electricity back to a utility company in their locations.

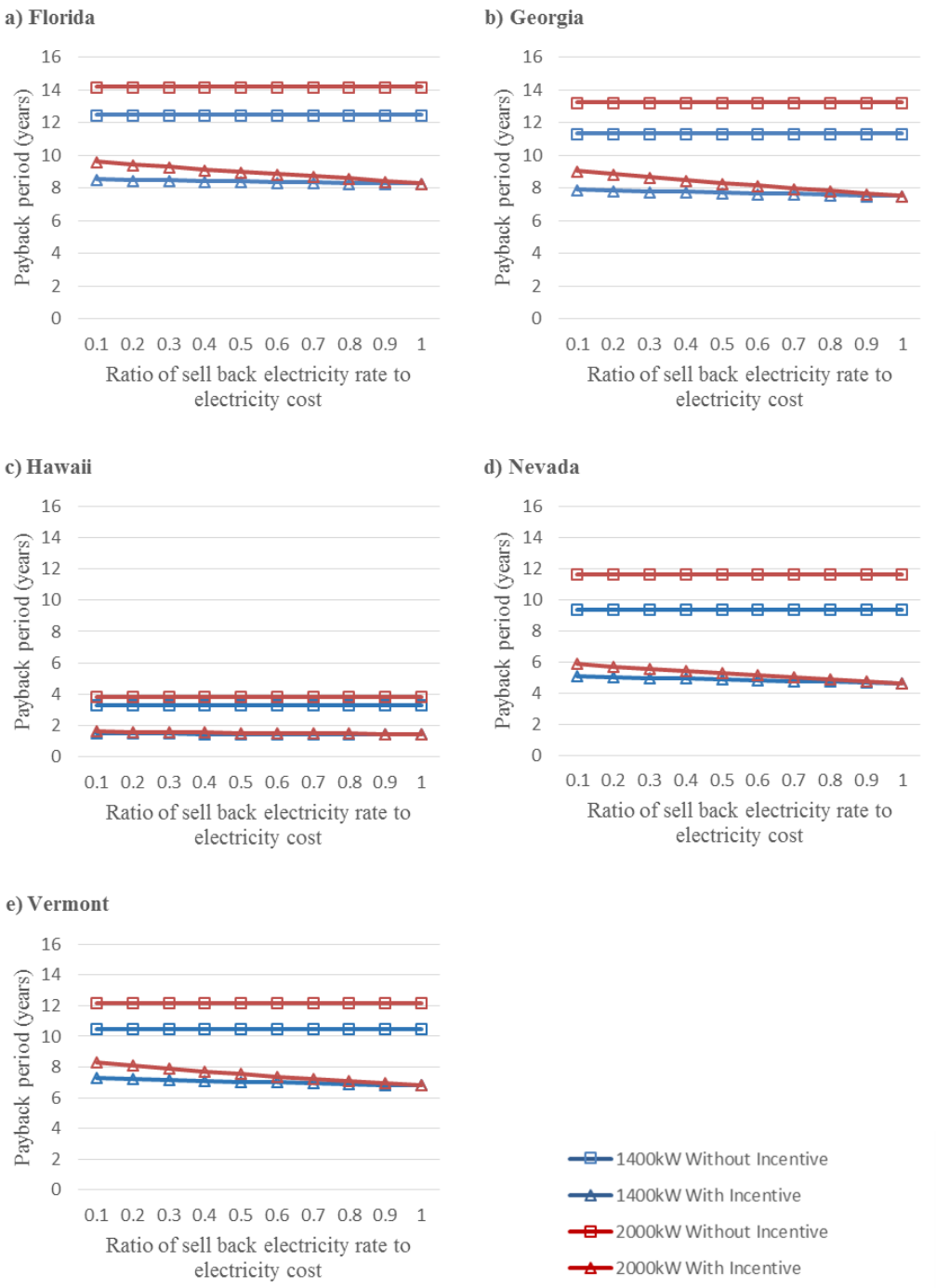

Figure 3.8 Influence of the sell back ratio on the payback period for hospital buildings; a) Florida; b) Georgia; c) Hawaii; d) Nevada; e) Vermont

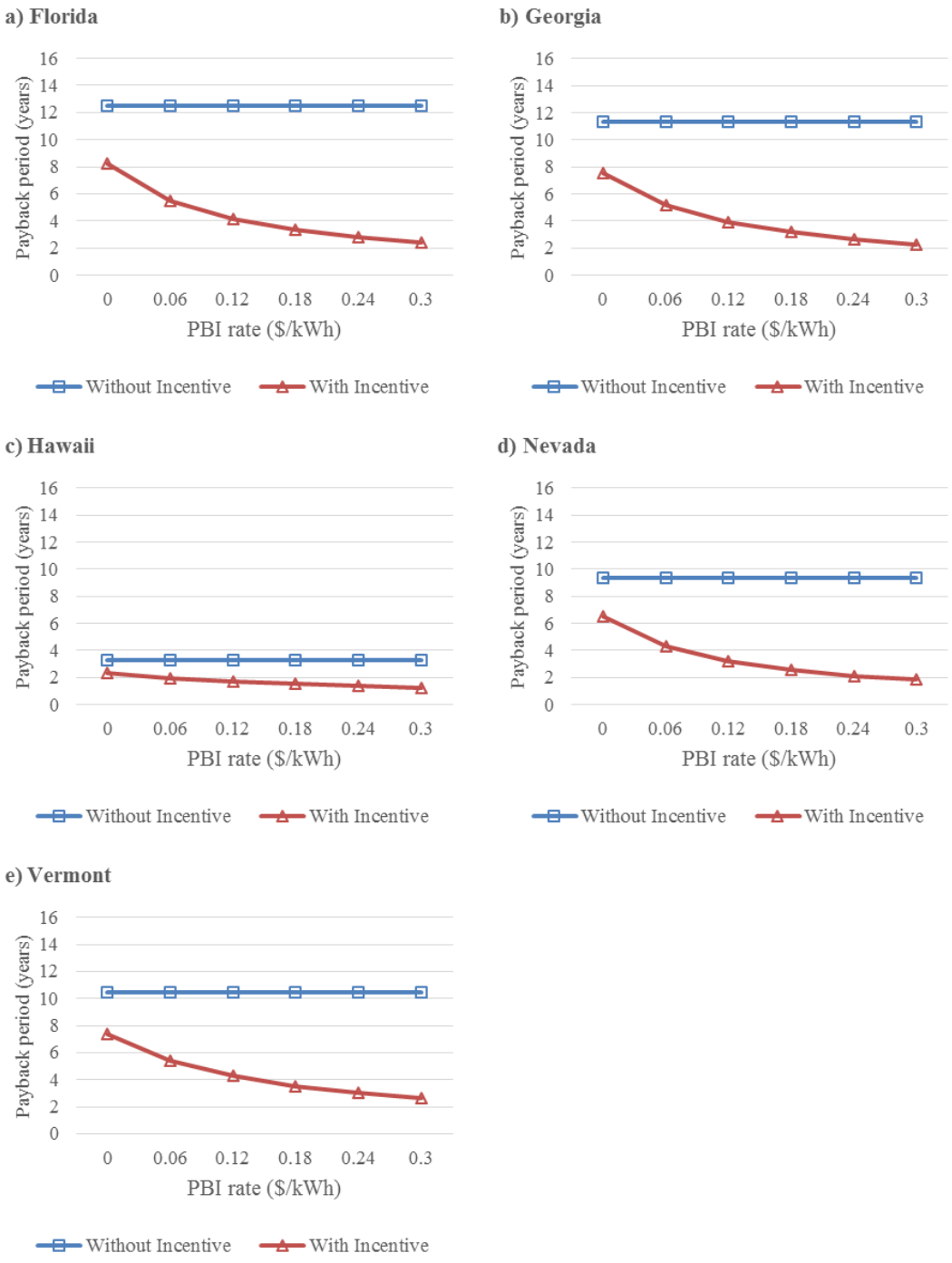

Figure 3.9 Influence of the PBI rate on the payback period for hospital buildings; a) Florida; b) Georgia; c) Hawaii; d) Nevada; e) Vermont

Figure 3.9 shows the influence of the PBI rate on the payback period for hospital buildings. In this case, the capacity of PV system is set to 1400 kW for all locations. When calculating the payback period with incentive, instead of using existing PBI rate for each location, it is assumed that in all the locations, the PV customers are eligible for a PBI of which the rate ranges from 0-0.3 $/kWh. Additionally, the other incentives summarized in Section 3.2.2.7 are still available with the exception of the existing PBI. Note that, in this part, customers are assumed to be paid for the amount of the electricity generated by their PV systems, no matter whether they use the electricity only in their properties or export it to the grid. Just like the variation trend shown in Figure 3.8, the payback period without incentive here remains a constant value for a specific location. However, the payback period decreases as a decay curve with the increasing PBI rate when the incentive is taken into consideration. In all locations, increasing the PBI is an effective way to improve the payback period of PV system. It is important to mention here that the payback period in Hawaii does not reduce drastically because it already has a low payback period even without regarding to incentive. With these results, the policy makers can effectively determine a PBI rate in a particular location to promote the PV systems.

CHAPTER IV

DESIGN AND TECHNO-ECONOMIC ANALYSIS FOR INTEGRATED PHOTOVOLTAIC AND BATTERY ENERGY STORAGE (PV-BES) SYSTEMS

This chapter presents an analysis of integrated photovoltaic and battery energy storage (PV-BES) systems. A mathematical model of the PV-BES system to evaluate annual energy performance is developed in this chapter. Four types of buildings (i.e., hospital, large office, large hotel, and secondary school) located in four different states, which each has their own PV and/or BES incentives, are selected and analyzed. Based on the energy performance data for each building type, the simple payback period (PBP) for the PV-BES system in different locations is calculated according to the local incentive policies. The PBP is chosen as an indicator to evaluate the effectiveness of incentive policies for different locations and building types by comparing it to the PBP for the same PV-BES systems without incentive policies. The reduction of carbon dioxide emission (RCDE) due to the PV generation is also investigated since it indicates the potential to reduce the PBP for a further step when a high carbon credit is available. Furthermore, a parametric analysis is conducted to determine the sensitivity and contribution of parameters such as the capacity of the PV-BES system, the capital cost of PV module and the battery storage on the performance of the PV-BES system.

4.1 Solar Photovoltaic Analysis

This section presents the proposed model and inputs used to evaluate the technical performance of the photovoltaic array. The proposed PV model is established according to the methodologies used in Ref. [76]. The solar radiation data used in this paper is obtained from the Typical Meteorological Year 3 (TMY3) data [94].

4.1.1 Solar Radiation

The equations proposed to estimate the total solar radiation, G_T, on the surface of the solar PV array are given in this section. The total solar radiation on the tilted surface of a PV panel is the sum of the direct solar radiation, $G_{b,s}$, diffuse solar radiation, $G_{d,s}$, and ground reflected solar radiation, $G_{r,s}$, which are defined in Eqs. (4-2), (4-3), and (4-4), respectively,

$$G_T = G_{b,s} + G_{d,s} + G_{r,s} \tag{4-1}$$

$$G_{b,s} = G_b \cos(\theta) \tag{4-2}$$

$$G_{d,s} = G_d \frac{1+\cos(\beta)}{2} \tag{4-3}$$

$$G_{r,s} = G_r \frac{1-\cos(\beta)}{2} \tag{4-4}$$

where θ is the solar angle of incidence and β is the surface tilt of the modules. In this paper, the surface tilt angle is set equal to the local latitude (Φ). The cosine of the angle of incidence is defined as,

$$\cos(\theta) = \cos(\alpha_s)\cos(\gamma_s - \gamma)\sin(\beta) + \sin(\alpha_s)\cos(\beta) \tag{4-5}$$

where α_s is the solar altitude angle, γ_s is the solar azimuth angle, and γ is the surface (module's) azimuth angle. The surface azimuth angle is set to 0 in the calculation. The

solar altitude angle and the solar azimuth angle can be found using Eqs. (4-6) and (4-7), respectively,

$$\sin(\alpha_s) = \sin(\varphi)\sin(\delta_s) + \cos(\varphi)\cos(\delta_s)\cos(\omega_s) \quad (4\text{-}6)$$

$$\sin(\gamma_s) = \frac{\cos(\delta_s)\sin(\omega_s)}{\cos(\alpha_s)} \quad (4\text{-}7)$$

where φ is the latitude of the site, δ_s is the solar declination, and ω_s is the hour angle. The solar declination can be obtained using Eq. (4-8) with n as the day of the year (1 for January 1st and 365 for December 31st).

$$\delta_s = 23.45° \sin[360° \frac{n+284}{365}] \quad (4\text{-}8)$$

The ground reflected solar radiation can be calculated based on the direct and diffuse solar radiation and solar zenith angle [77] as shown in Eq. (4-9),

$$G_r = (G_b \cos(\Psi) + G_\mathrm{d})\rho \quad (4\text{-}9)$$

where Ψ is the solar zenith angle, which is the complementary angle of the solar altitude angle, α_s, and ρ is the ground reflectance. The ground reflectance is assumed to be 0.2, which is the commonly used value in the building energy simulations [77].

4.1.2 Solar Photovoltaic Module

The approach proposed in this study uses the model given in Ref. [79] as shown in Eq. (4-10). The total power levels of the PV array (P_{PV}) are assumed constant over the time step,

$$P_{PV} = A_{surf} \cdot f_{activ} \cdot G_T \cdot \eta_{cell} \cdot \eta_{invert} \cdot N \cdot [1 - (t-1) \cdot d_{PV}] \quad (4\text{-}10)$$

where A_{surf} is the net surface area of PV modules, f_{activ} is the fraction of surface area with active solar cells, η_{cell} is the module conversion efficiency, η_{invert} is the DC to AC conversion efficiency, N is the quantity of the PV modules, t is the time expressed in

years ($t \geq 1$), and d_{PV} is the degradation rate of the PV system. In general, the PV module conversion efficiency (η_{cell}) can be determined from the manufacturers' specifications. The values of PV module parameters adopted in this paper are listed in Table 4.1. The d_{PV} is set to 0.5%/year in this paper according to Refs. [95][96]. It is important to mention here that the temperature and dust and snow losses are not considered in this study because those loss values are not available for all locations selected in this study and considering general, uniform losses in different locations to the simplified equation, presented in Eq. (4-10), may not improve the accuracy of PV performance results.

Table 4.1 Parameters used in the simulation of the PV module [76][97]

PV module parameter	Value
A_{surf} (m^2)	1.66
f_{activ}	0.85
η_{cell}	0.18
η_{invert}	0.95
d_{PV}	0.5%

4.1.3 Solar Availability

Figure 4.1 illustrates the average daily solar radiation flux of the United States, specifically indicating the national solar PV resource potential for all states [80]. In this paper, the four locations selected for investigation are California, Hawaii, New Jersey, and New York. Table 4.2 shows the representative city, in each selected state, as well as solar availability range for the selected locations. These locations were selected since, to

the best of authors' knowledge, they were the only ones providing detailed incentive values for battery energy storage at the time this study was conducted.

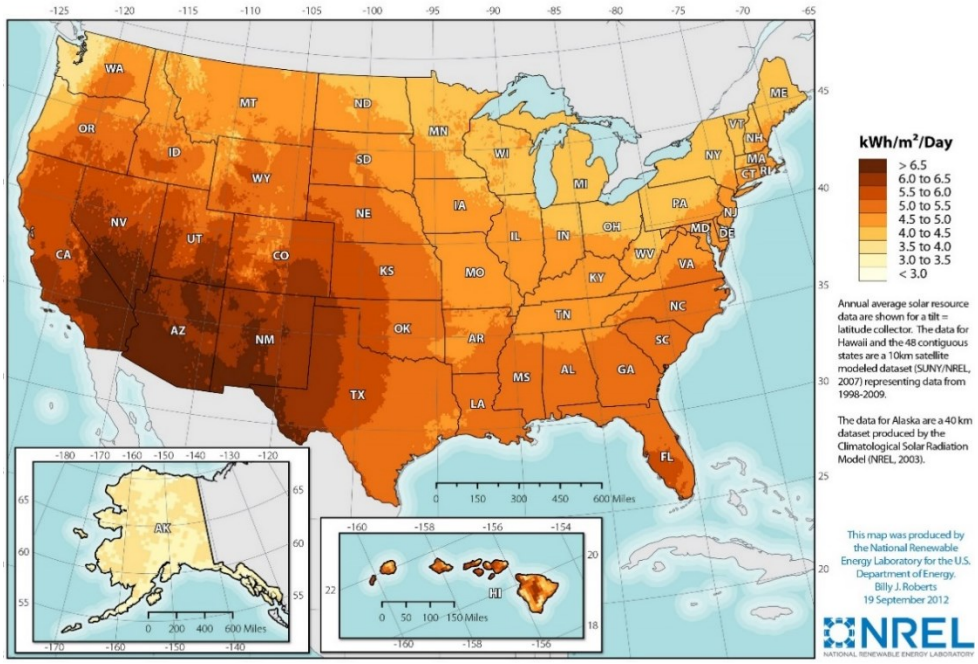

Figure 4.1 Average daily solar radiation flux of the United States [80]

Table 4.2 Representative city and solar availability for four selected states

State	Representative city	Solar availability range (kWh/m^2/Day)
California	Los Angeles	6.0-6.5
Hawaii	Honolulu	6.0-6.5
New Jersey	Atlantic City	4.5-5.0
New York	Kennedy	4.0-4.5

4.2 Building model description

There are 16 commercial reference building models developed by the U.S. Department of Energy (DOE) which can represent almost 70% of the commercial buildings in the U.S. region [66][67]. This work focuses on the commercial building sector because many incentives evaluated in this study are designed for large-scale commercial buildings (e.g., PV incentive in Hawaii, PV and BES incentives in New York). These reference building models are used in the EnergyPlus simulation software to generate simulation data of building energy usage profile. In this paper, four building types were selected: hospital, large office, large hotel, and secondary school. The reason for choosing these four building types is that those buildings possess relatively large electrical energy consumptions compared to residential building and other DOE's commercial reference building models, so that the existing incentives can be effectively evaluated considering the capacity limit in some states' incentive policies (like Hawaii and New York).

The drawings of the selected building types are shown in Figure 4.2 and the characteristics of each building type are listed in Table 4.3.

Table 4.3 Types and characteristics of the selected reference buildings

Building type	Floor area (m^2)	Number of floors
Hospital	22,422	5
Large office	46,320	12
Large hotel	11,345	6
Secondary school	19,592	2

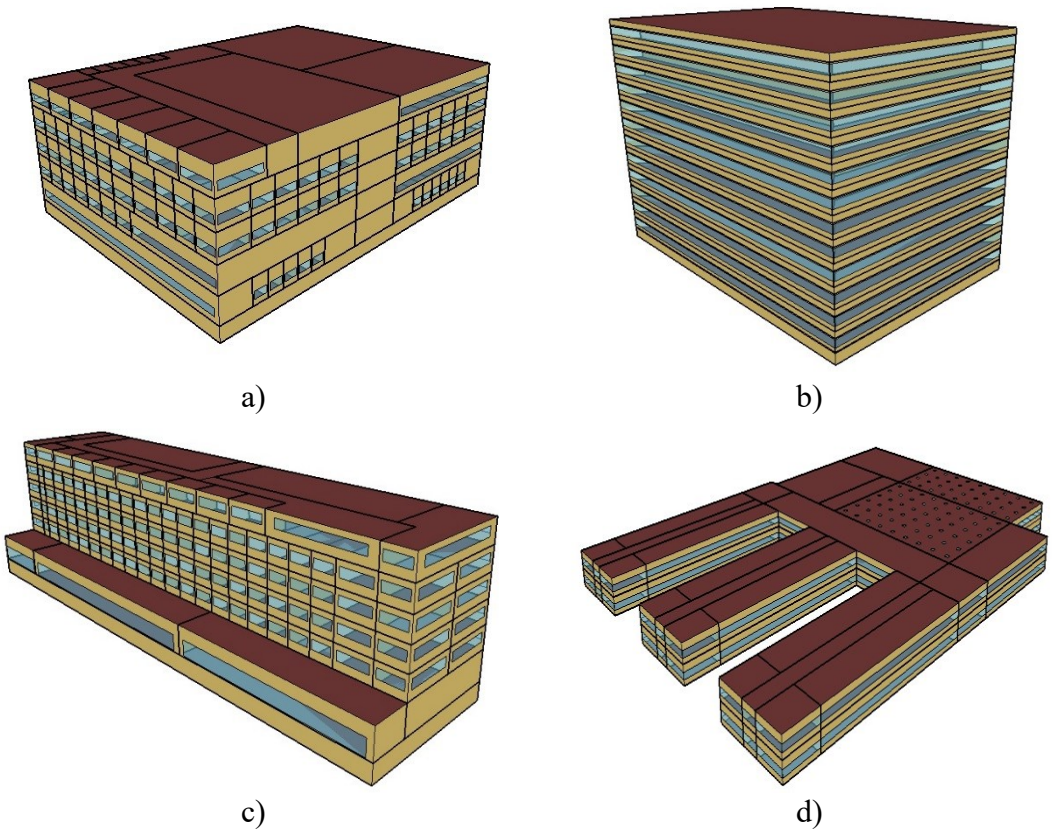

Figure 4.2 Drawings of the selected building types; a) hospital; b) large office; c) large hotel; d) secondary school [66]

Table 4.4 indicates the electrical energy consumption of the selected reference buildings in the different locations. In this table, E_{max} is the maximum hourly building electric load and E_{ave} is the average hourly building electric load. The maximum hourly electricity load is used to size the PV system, that is, decide the nominal capacity of PV system for each building type in each location. With the nominal capacity of PV system, as well as the climate data, the hourly PV generation can be calculated.

Table 4.4 Hourly electrical energy consumption of selected reference buildings in different locations

	Hospital		Large Office		Large Hotel		Secondary School	
Location	E_{max} (kWh)	E_{ave} (kWh)	E_{max} (kWh)	E_{ave} (kWh)	E_{max} (kWh)	E_{ave} (kWh)	E_{max} (kWh)	E_{ave} (kWh)
CA	1156	759	1460	639	367	214	819	255
HI	1218	833	1565	769	417	257	1108	393
NJ	1260	748	1611	628	421	214	1154	267
NY	1266	747	1597	628	428	215	1170	270

4.3 Battery energy storage system design

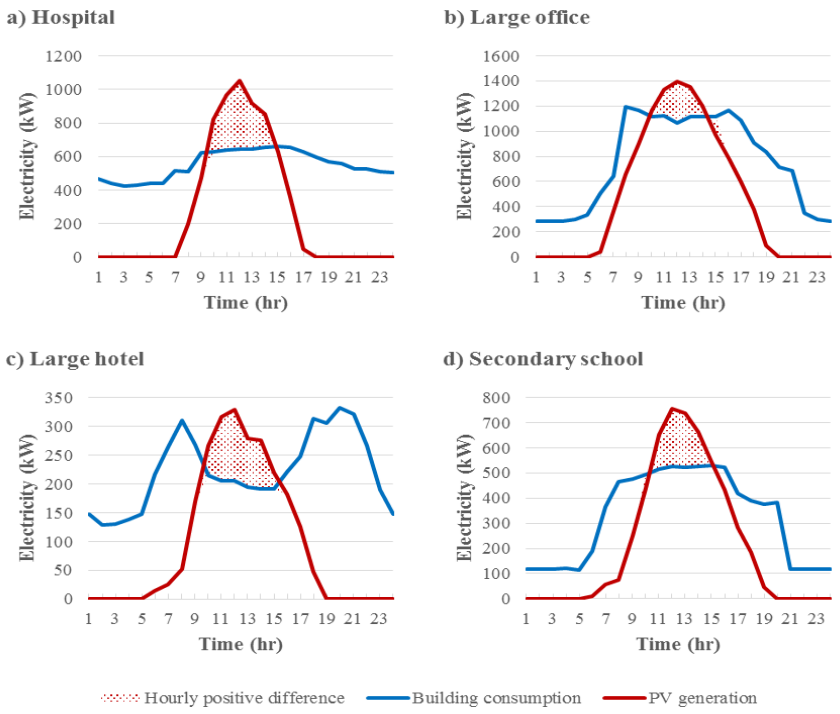

Figure 4.3 Hourly building electricity consumption, PV generation and positive difference on an arbitrary day in California; a) Hospital; b) Large office; c) Large hotel; d) Secondary school

The battery energy storage system is designed to store the excess energy generated by the PV system. Thus, the battery is sized based on the hourly positive difference (PD) between PV generation and the building electric load. The hourly building electric load $E_{load}(h)$ is obtained from the simulation results of EnergyPlus. The PV generation at time h is calculated by:

$$E_{PV}(h) = P_{PV}(h) \cdot \Delta t \tag{4-11}$$

where h represents time in hours, which varies from 1 to 8760 during one year, and Δt is an hourly time step. Note that $E_{PV}(h)$ is used to calculate the hourly PV generation for each year within the life span. However, since the yearly degradation of PV system is considered for $P_{PV}(h)$ in Eq. (4-10), thus, $E_{PV}(h)$ also degrades year by year. The hourly positive difference can be obtained by the equations below:

$$PD(h) = \begin{cases} E_{PV}(h) - E_{load}(h), & E_{PV}(h) > E_{load}(h) \\ 0, & \text{others} \end{cases} \tag{4-12}$$

then, the daily positive difference is:

$$D(n) = \sum_{i=24n-23}^{24n} PD(i) \tag{4-13}$$

where n is the day of the year (1 for January 1st and 365 for December 31st). Figure 4.3 shows the hourly electricity consumption, PV generation and positive difference in an arbitrary day for 4 building types in California.

The battery capacity is designed to meet the maximum daily positive difference and could be expressed as:

$$Ebat = Max(D(n)) \tag{4-14}$$

In addition to the hourly positive difference, the hourly absolute difference (AD) between PV generation and the building electric load is defined as:

$$AD(h) = |E_{PV}(h) - E_{load}(h)| \quad (4\text{-}15)$$

The rated power of BES system is designed based on the maximum hourly absolute difference:

$$Pbat = \frac{Max(AD(h))}{1hr} \quad (4\text{-}16)$$

According to the maximum hourly building electric load as well as the method mentioned above, the PV capacity (Cap_{PV}), battery capacity, and rated power of BES are set as shown in Table 4.5.

Table 4.5 PV capacity, battery capacity, and rated power of BES

	Hospital			Large Office			Large Hotel			Secondary School		
	Cap_{PV} (kW)	$Ebat$ (kWh)	$Pbat$ (kW)	Cap_{PV} (kW)	$Ebat$ (kWh)	$Pbat$ (kW)	Cap_{PV} (kW)	$Ebat$ (kWh)	$Pbat$ (kW)	Cap_{PV} (kW)	$Ebat$ (kWh)	$Pbat$ (kW)
CA	1200	2200	1100	1500	7400	1300	370	900	370	820	4600	720
HI	1200	1400	1200	1600	6900	1400	420	730	420	1100	5600	900
NJ	1300	2800	1100	1600	8100	1400	420	1200	420	1200	7200	1100
NY	1300	2700	1100	1600	8100	1400	430	1400	430	1200	7300	1000

With the hourly building electric load known and battery capacity selected, two dimensionless parameters, electricity ratio (r_e) and battery ratio (r_b), can be defined as

$$r_e = E_{ave}/E_{max} \quad (4\text{-}17)$$

$$r_b = E_{bat}/E_{ave} \quad (4\text{-}18)$$

The electricity ratio, r_e, reflects the characteristics of the building electricity consumption. A larger r_e value indicates a more even hourly electricity consumption, which means the building can utilize the PV generation better since the PV is sized based

on E_{max}. The battery ratio, r_b, shows the characteristics of the energy storage. The larger the r_b is, the longer the battery can supply the building once fully charged. The r_e and r_b values for each building type and location are shown in Table 4.6. This information will be useful for payback analysis in Section 6.

Table 4.6 Electric ratio and battery ratio for each building type and location

	Hospital		Large Office		Large Hotel		Secondary School	
Location	r_e	r_b	r_e	r_b	r_e	r_b	r_e	r_b
CA	0.66	2.90	0.44	11.58	0.58	4.21	0.31	18.04
HI	0.68	1.68	0.49	8.97	0.62	2.84	0.35	14.25
NJ	0.59	3.74	0.39	12.90	0.51	5.61	0.23	26.97
NY	0.59	3.61	0.39	12.90	0.50	6.51	0.23	27.04

The PV-BES system operation strategy is summarized in Figure 4.4. When the battery is charging, the charging power $P_C(h)$ is expressed as:

$$P_C(h) = \begin{cases} P_{PV}(h) - P_{load}(h), & 0 \le P_{PV}(h) - P_{load}(h) < Pbat \\ Pbat, & P_{PV}(h) - P_{load}(h) \ge Pbat \end{cases} \quad (4\text{-}19)$$

where $P_{load}(h)$ is the building electric power at time h, which is obtained from the simulation results of EnergyPlus.

The effect of $P_C(h)$ on the state of charge (SOC) of the battery is given by:

$$SOC(h) = SOC(h-1) + [P_C(h)/Ebat] \cdot \Delta t \cdot \eta_C \quad (4\text{-}20)$$

where η_C is the battery charging efficiency and equals to 90% in our case [98][51].

When the battery is discharging, the discharging power $P_{DC}(h)$ can be estimated as:

$$P_{DC}(h) = \begin{cases} P_{load}(h) - P_{PV}(h), & 0 \le P_{load}(h) - P_{PV}(h) < Pbat \\ Pbat, & P_{load}(h) - P_{PV}(h) \ge Pbat \end{cases} \quad (4\text{-}21)$$

The effect of $P_{DC}(h)$ on the SOC of the battery is given by:

$$SOC(h) = SOC(h-1) + [P_{DC}(h)/Ebat] \cdot \Delta t \cdot (1/\eta_{DC}) \quad (4\text{-}22)$$

where η_{DC} is the battery discharging efficiency and equals to 90% in this paper [98][51].

The initial value of SOC is $SOC(0)$ and occurs when h=1. In this paper, SOC_{max} and SOC_{min} are set to 100% and 0%, respectively [99][100].

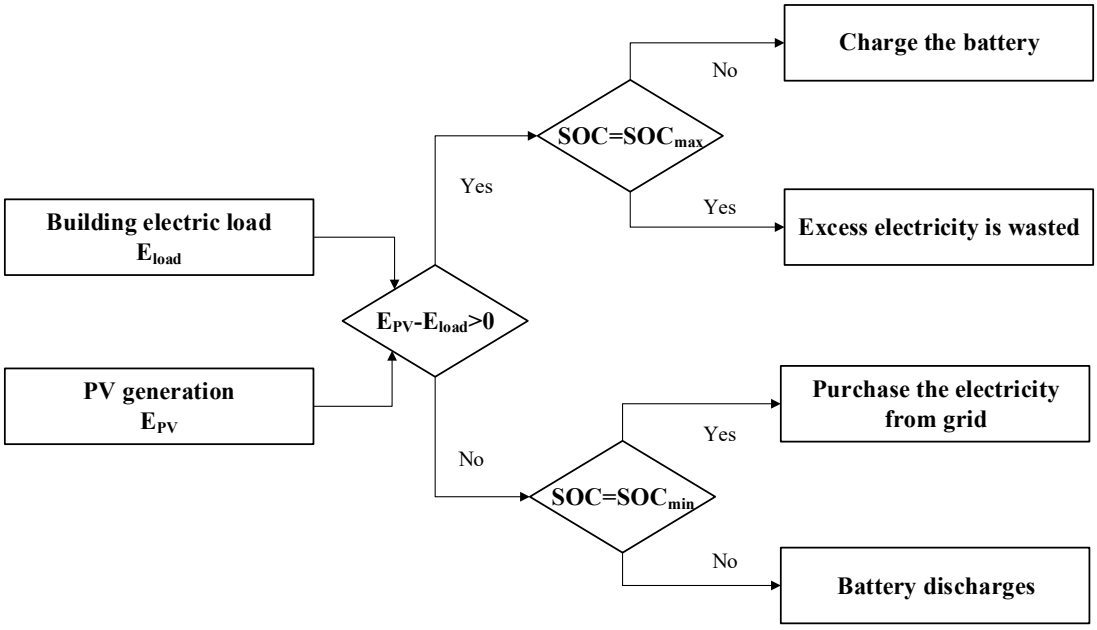

Figure 4.4 Operation strategy of PV-BES system

4.4 Incentive Analysis

In this paper, the PBP is chosen as an important indicator to evaluate the effectiveness of the incentive policies for PV and energy storage system. In order to

determine the PBP, the cost of installing a battery storage system integrated with a PV system is estimated as follows:

$$Cost_{C,PV} = C_{PV} \cdot Cap_{PV} \tag{4-23}$$

The capital cost of the inverter can be estimated by:

$$Cost_{C,inv} = C_{inv} \cdot Cap_{PV} \tag{4-24}$$

It is important to mention that the detailed costs of PV, from Ref. [96], are adopted in this paper but they are classified into two parts, the inverter cost (C_{inv}) and the PV major cost (C_{PV}). The PV major cost includes all the costs except inverter cost like module cost, install labor & equipment cost, and sales tax, etc.

The capital cost of the BES system is [101][102]:

$$Cost_{C,BES} = C_P \cdot Pbat + C_E \cdot Ebat \tag{4-25}$$

The operating and maintenance cost of the PV system (PV modules and inverter) can be decided by:

$$Cost_{OM,PV} = C_m \cdot Cap_{PV} \tag{4-26}$$

The operating and maintenance cost of the BES system per year is:

$$Cost_{OM,BES} = C_f \cdot Pbat + C_v \cdot E \tag{4-27}$$

where E is the annual discharge energy of the BES system. Since the variable operating and maintenance cost is negligible compared to the fixed one, the C_v is set to 0 [101].

The total capital cost of the PV-BES system is the sum of above items in the equations from Eq. (4-23) to (4-25):

$$Cost_{C,total} = Cost_{C,PV} + Cost_{C,inv} + Cost_{C,BES} \tag{4-28}$$

The parameters used in the above-mentioned equations are presented in Table 4.7

Table 4.7 Parameters for PBP estimation

Parameter	Meaning	Value [96][101][103][104]
C_P	Specific power cost of BES	\$400/kW
C_E	Specific capacity cost of BES	\$330/kWh
C_f	Fixed O&M cost of BES	\$20/kW.yr
C_v	Variable operating and maintenance cost of BES	0
C_{pv}	PV major cost	\$1930/kW
C_{inv}	Inverter cost	\$130/kW
C_m	Operating and maintenance cost of PV	\$34 kW.yr

With the PV-BES system operating, part of the building electric load is supplied by the system instead of purchasing from the grid. The annual saving, i.e. reduction of electric cost can be determined as:

$$AS = (E_{grid} - E_{grid,PV-BES}) \cdot Cost_e \quad (4\text{-}29)$$

where $Cost_e$ is the electricity cost. E_{grid} is the electricity purchased from the grid during one year before the PV-BES system is applied to the reference building, which equals to the annual building electric load. While $E_{grid,PV-BES}$ is the electricity purchased from the grid with the PV-BES system applied to the reference building.

At the same time, the reduction of carbon dioxide emission (RCDE) due to the clean generation (PV system) can be estimated as:

$$RCDE = (E_{grid} - E_{grid,PV-BES}) \cdot EF_e \quad (4\text{-}30)$$

where EF_e is grid emission factor. The electricity cost and the grid emission factor for selected locations are summarized in Table 4.8.

Table 4.8 Electricity cost [82] and grid emission factor [105] for each location

State	$Cost_e$ (\$/kWh)	EF_e (kg/kWh)
CA	0.1573	0.258
HI	0.2693	0.671
NJ	0.1279	0.376
NY	0.1531	0.166

With the total cost and annual saving known, the PBP of PV-BES system can be decided:

$$PBP = Cost_{C,total}/(AS - Cost_{OM,PV} - Cost_{OM,BESS}) \quad (4\text{-}31)$$

If the incentive policies are applied, the PBP becomes:

$$PBP_w = (Cost_{C,total} - In_1)/\left(AS + In_2 - Cost_{OM,PV} - Cost_{OM,BESS}\right) \quad (4\text{-}32)$$

where PBP_w is the payback period with considering the incentive policies. In_1 and In_2 are the incentives on the installation costs (e.g., rebates, grant and tax incentives) and the utility rates (e.g., feed-in tariff), respectively. The incentives on the installation costs (In_1) help diminish the total capital cost while the incentives on the utility rates (In_2) increase the annual savings from the operation.

The PBP is an easy and straightforward way to reflect how long the cost of an investment could be recovered. However, since the cash earned in later time is worth less than cash in the current period, the discounted cash flow analysis is added in addition to

PBP analysis to take the time value of money into consideration. The cash flows can be estimated:

$$CF(0) = -Cost_{C,total} \tag{4-33}$$

$$CF(t) = \frac{AS - Cost_{OM,PV} - Cost_{OM,BESS}}{[(1+i)/(1+j)]^t} \tag{4-34}$$

where CF indicates the cash flow at number t year ($CF(0)$ is the initial cash flow at 2016), i is the discount rate, and j is the inflation rate. In this paper, the values of i and j are set to 7% and 2.5%, respectively [96].

Table 4.9 Incentive policies for PV systems

Location	Incentive policy
Federal	Tax credit (equal to 30% of investment) [83]
Los Angeles, CA	*Rebate:* $0.40/W for PV system. Up to 50% of project costs for commercial systems. The maximum system size is 1MW [106][107]
Honolulu, HI	*Feed-in tariff* program: 0.189$/kWh; 0.197$/kWh (based on capacity*)[88]
Atlantic City, NJ	NA
Kennedy, NY	*Grant* program for first 3 years: $0.0114/kWh** [108]

* For the PV systems greater than 20 kW and up to and including 500 kW, the payment rate is 0.189 $/kWh. While for those greater than 500 kW and up to and including 5 MW, the payment changes to 0.197 $/kWh.
** The minimum capacity is 200 kW.

The incentive policies for PV system and BES system are summarized in Table 4.9 and Table 4.10, respectively. As mentioned before, only 4 locations were selected in this study because, to the best of authors' knowledge, those locations were the only ones providing incentive values for battery energy storage at the time this study was

conducted. Some states (e.g., Florida, New Mexico, and Washington) also provide incentive policies but incentive values are not publically available, so that those states are not included in this study.

Table 4.10 Incentive policies for BES systems [109]

Location	Incentive policy
Federal	NA
Los Angeles, CA	$1.31/W for energy storage system which capped at 3MW
Honolulu, HI	20% investment tax credit or a utilization credit equal to $0.08/kWh of capacity for the first 10 years of the project
Atlantic City, NJ	Payments no greater than $500,000 per project or 30% of the project's total installed cost whichever is less
Kennedy, NY	Provides customers with $2,100/kW for battery storage and $2,600/kW for thermal storage. Capped at 50% of the project cost

4.5 Result and Analysis

The simulation results obtained from the model described in Sections 2 to 5 are presented in this section. The incentive analysis results for each building type in all locations are presented in Section 6.1, followed by a parametric analysis to reveal the influence of each parameter on the PBP on a PV-BES system in Section 6.2. In this section, both the PBP and the discounted payback period (DPBP) are discussed. For the calculation of PBP, a constant cost is applied, while for the DPBP, the current cost is used, which means all the costs are discounted to the initial year of investment.

4.5.1 Incentive Analysis

The results of incentive analysis for the selected building type and locations are presented in this section. In this part, the PV-BES system is sized according to Table 4.5. The average annual savings in electricity consumption cost for each building type and location are presented in Figure 4.5. For all locations, the average annual savings increase in the order of large hotel, secondary school, hospital and large office, which is in agreement with the order of magnitude of their PV capacity listed in Table 4.5. For all building types except for the secondary school, the average annual savings become larger in the order of New Jersey, New York, California and Hawaii, which is in agreement with their electricity cost shown in Table 4.8. This demonstrates that the average annual savings for a specific building type is mainly affected by the local electricity price.

Figure 4.6 provides the result of CDE reduction for selected building types and locations. As shown in the figure, the CDE reduction increases in the same order with annual savings do for a specific location. For a specific building type, the CDE reduction becomes larger in the order of New York, California, New Jersey and Hawaii, which is in agreement with their grid emission factor, CF_{CDE}, shown in Table 4.8. The CDE reduction could be used to reduce the operation cost if carbon credits are available. For example, the Regional Greenhouse Gas Initiative which involves nine states in the US (Connecticut, Delaware, Massachusetts, New Hampshire, New York, Rhode Island, and Vermont) has provided carbon credits since 2008 between about $2/ton and $5.5/ton and the cap-and-trade program in California has allowed carbon trades since 2012 between about $10-14 per ton [110]. However, these carbon credits are still too low to have a dramatic impact on reducing the PBP since the benefits due to carbon credits are

negligible compared to the annual savings. Take the hospital in California as an example, the carbon credit in 2015 was $12.1 per ton [110], then the benefit due to carbon credit is $6969.6 ($12.1 per ton times 576 tons) which is negligible compared to the annual saving of $351K. Even though the influence is not significant at present, the CDE reduction can be used to improve the PBP for a further step if a much higher carbon credit is available in future.

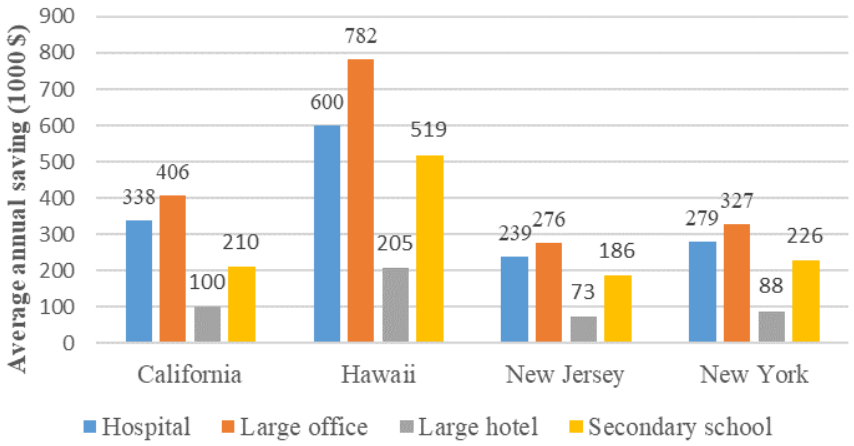

Figure 4.5 Average annual savings in the electricity consumption cost for selected building types and locations

Figure 4.7 presents the results of PBP analysis considering different incentive levels (e.g., no incentive, PV incentive only, BES incentive only, both PV and BES incentives) in each location for four different building types including hospital, large office, large hotel, and secondary school. The findings from the analysis results demonstrated in Figure 4.7 are discussed in detail below:

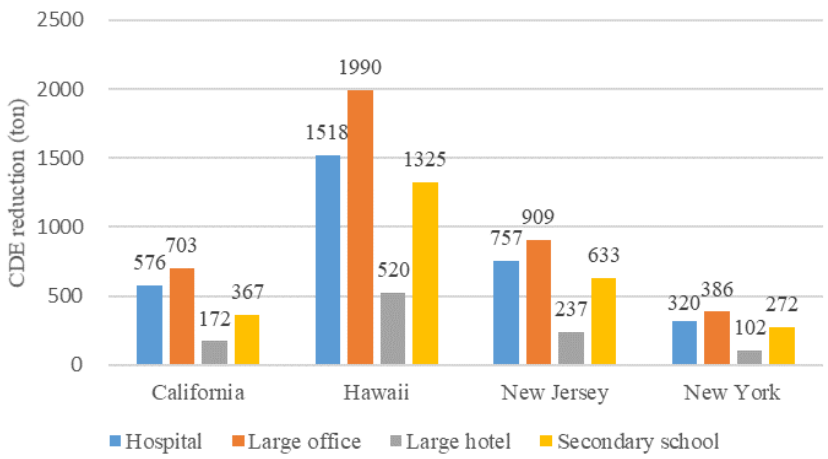

Figure 4.6 CDE reduction for selected building types and locations

In all locations, the PBP of PV-BES system for hospital building is the shortest before any incentive policies are taken into consideration, while the PBP for secondary school is the longest. As can be seen from Table 4.6, the hospital building in each location has the highest electricity ratio, which means the hourly electricity consumption is the most even among all building types. From Figure 4.7, one can see the PBP without incentives becomes larger in the order of hospital, large hotel, large office and secondary school, which is in agreement with their r_b value and on the contrary with their r_e value. This observation demonstrates that the PV-BES system is not cost effective (i.e., longer payback periods) when the PV and BES are sized bigger and used more. With this observation, one can explain why the PBP increases in the order of hospital, large hotel, large office and secondary school in Figure 4.7 even though the order of magnitude of their annual savings do not follow this order.

When the incentive policies are applied, the PBP can be reduced at different levels. The level of reduction varies depending on the location and building type.

Generally, the reduction in the PBP varies approximately from 1 to 8 years when PV incentive is applied, 0 to 9 years when BES incentive is applied and in total 2 to 16 years when both incentives are applied. The PBPs for all building types in California and Hawaii become less than 10 years after both the PV and BES incentives are adopted. Considering the maximum lifetime of the PV modules in the market can reach up to 30 years [38] and 12 years for lead-acid battery [111], decreasing the PBP to less than 10 years with the incentives can promote the installations of PV-BES system in these states. However, the PBP for most building types in New Jersey and New York are not acceptable. Especially in New Jersey, the PBPs for all building type are larger than 15 years even after both the PV and BES incentives are applied.

It is important to mention here that the PV incentive policy in Hawaii is classified based on the PV capacity. For the PV systems greater than 20 kW and up to and including 500 kW (large hotel in our case), the payment rate is 0.189 $/kWh. While for those greater than 500 kW and up to and including 5 MW, the payment changes to 0.197 $/kWh. The BES incentive policy in Hawaii is no longer available, but it is still considered in this study to estimate the benefits if it would have been still available. In this paper, a 20% investment tax credit is adopted as BES incentive in Hawaii.

Notably, for all building types, the PBPs in Hawaii seem more attractive (all below 10 years even without considering any incentives) than other locations. This is because of the influence of the solar availability and electricity cost. As can be seen from Table 4.2 and Table 4.8, Hawaii has high solar availability and high electricity cost. Higher solar availability implies more electricity is generated by the PV system under the same conditions, and higher electricity cost means more money is saved when using the

PV generated electricity instead of grid electricity. As a comparison, California also has the same solar availability, but much lower electricity cost; thus, the PBP without incentive in California is much longer than that in Hawaii. Similarly, even though the solar availability in New York is lower than that in New Jersey, the PBP without incentives in New York is still better than that in New Jersey due to a higher electricity cost in New York compared to that in New Jersey.

Figure 4.8 shows the cash flow analysis for large office buildings in selected locations when both the incentive policies and the impact of discount rate as well as inflation rate are taken into consideration. The cash flow analysis is conducted for 25 years, which is of twice the lead acid battery lifetime but still within the PV modules lifetime. Thus, a replacement of battery system is needed at the 12^{th} year. It is assumed that the incentives for battery energy storage in each location are still available for the replacement. As can be seen in the figure, the discounted payback period (DPBP) for PV-BES system in California and Hawaii are around 19 and 8 years, respectively. Furthermore, within the twice battery lifetime period, the users in California can benefit by about half million dollars from the PV-BES system, while in Hawaii have a substantial benefit of around 3 million. However, the users in New Jersey and New York cannot get a payback within the twice battery lifetime period under the existing incentive policies. For these two locations, the PV-BES system cannot be promoted until more powerful incentive policies are provided or the lifetime of battery is improved.

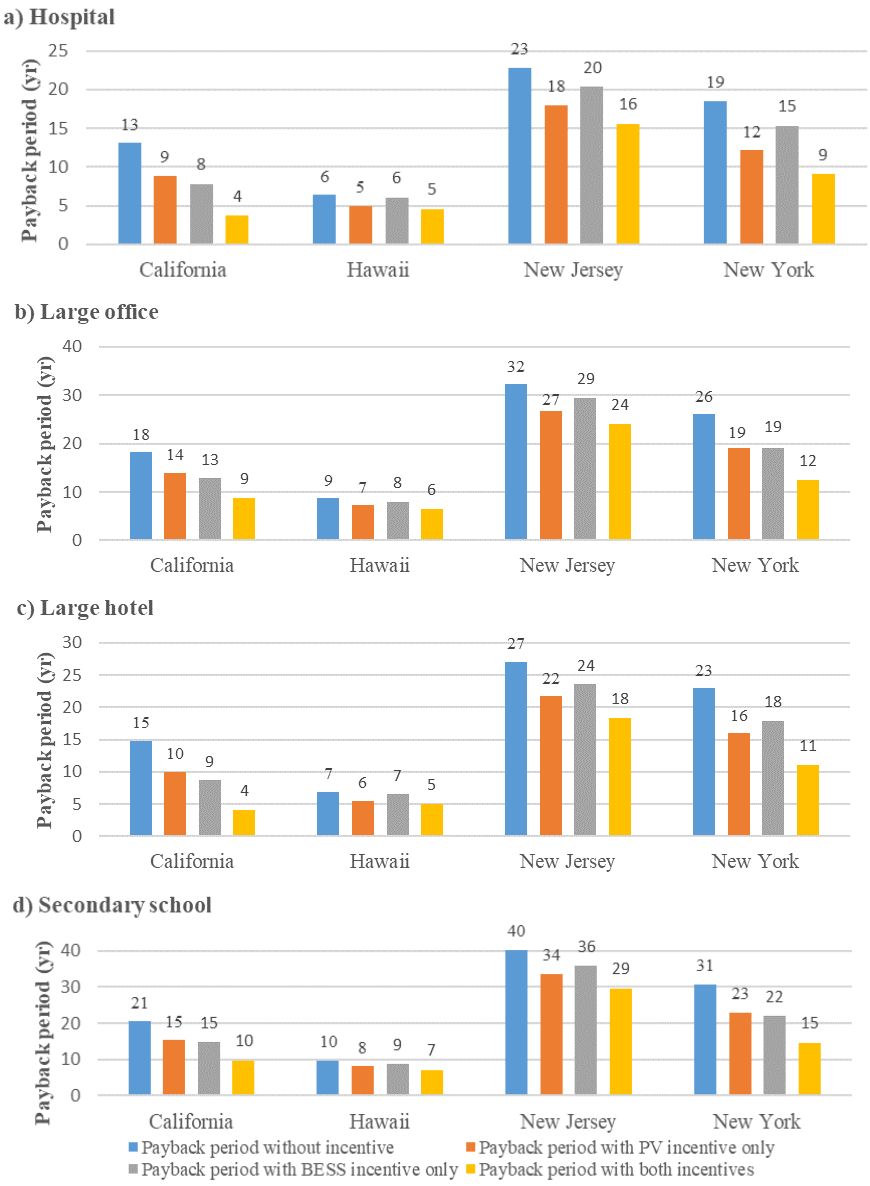

Figure 4.7 Results of PBP analysis for selected building types and locations; a) hospital; b) large office; c) large hotel; d) secondary school

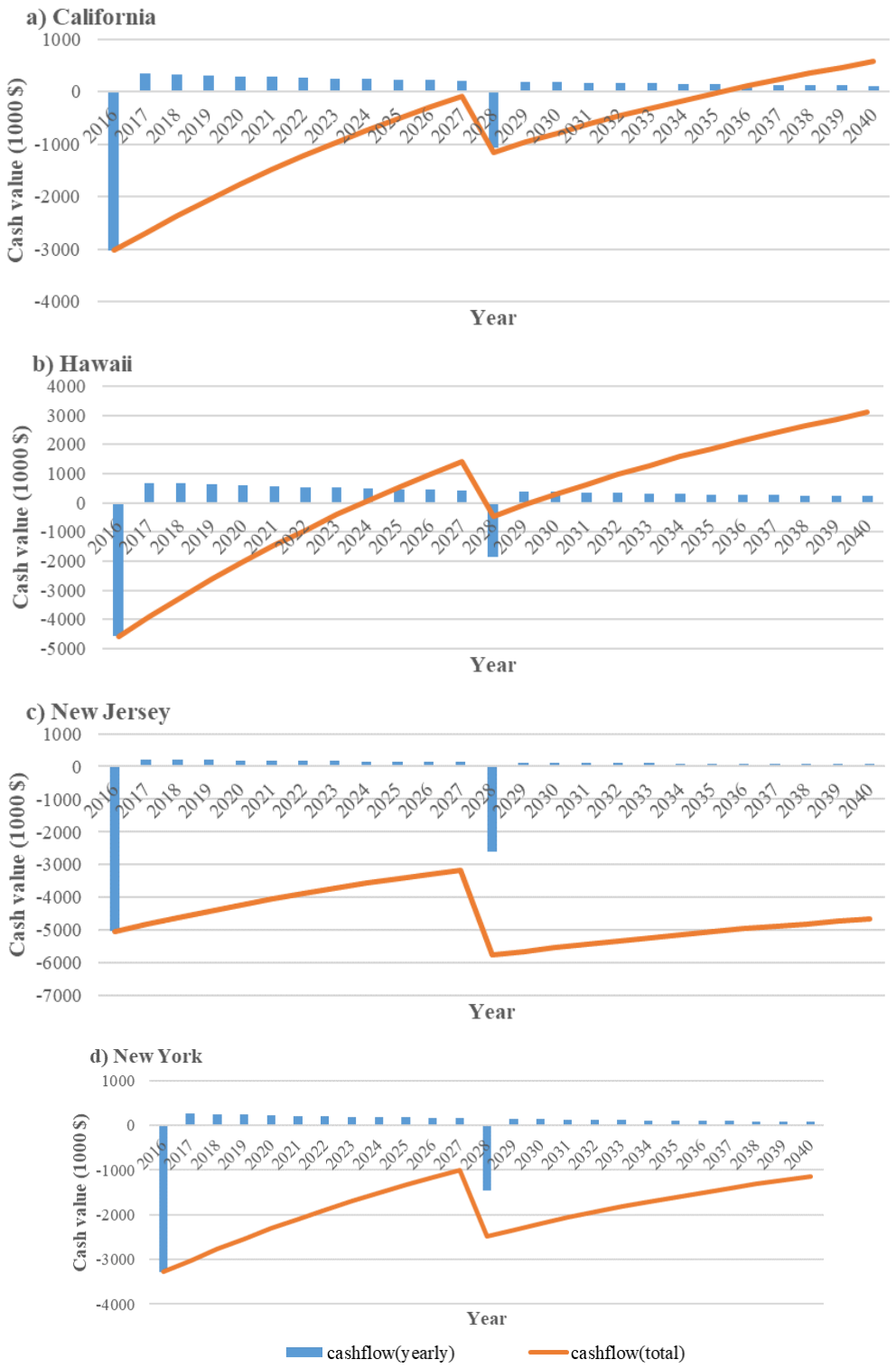

Figure 4.8 Cash flow analysis for large office buildings in selected locations; a) California; b) Hawaii; c) New Jersey; d) New York

4.5.2 Parametric analysis

In addition to the two factors, solar availability and electricity cost discussed before, there are several other factors that have an influence on the PBP of a PV-BES system, e.g., capacity of the PV-BES system and capital cost of the PV module and battery storage. As can be seen in Figure 4.7, the trends of the variation of the PBP among different locations building types are similar. For this reason, the large office in California is taken as a representative building type and location to perform the parametric analysis. Besides, the DPBP generally exists when the simple PBP is within the lifetime of the system [112]. Therefore, the PBP is still used as an indicator of the parametric analysis to illustrate the impact of factors including capacity and capital cost in the following paragraphs.

Figure 4.9 shows the effect of the PV capacity and battery capacity on the PBP for the large office buildings in California. Notably, the PV capacity and battery capacity mentioned in this section indicate the normalized capacity, which are normalized by Cap_{PV} and $Ebat$, respectively. In this figure, the PV capacity changes from 1.0 to 1.6 and the battery capacity changes from 0.1 to 1. The reason an oversized PV capacity was chosen is to generate more electricity for storing. As can be seen from Figure 4.9, when the battery capacity is small (i.e. the battery capacity equals to 0.1), the PBP without incentive increases with the increasing PV capacity. When the battery capacity becomes larger than 0.1, the PBP without incentive decreases firstly before increasing again when the PV capacity increases. Similarly, with most PV capacities (from 1.2 to 1.6), the PBP without incentive decreases first and then increases again with the increase of battery capacity. Interestingly, for the condition regardless any incentives, a middle size of

battery storage (e.g. 0.4 and 0.5) can diminish the PBP difference between different PV capacities. When the incentives are applied, the PBPs become much lower. At a certain PV capacity condition, the PBP increases directly with the increasing battery capacity, which shows a different trend with that in the situation without incentive. Overall, the shortest PBP occurs at the lowest PV capacity condition (1.0) and the lowest battery capacity (0.1) no matter whether the incentive is applied or not. This observation demonstrates that the PV-BES system is still not cost effective at present capital and operational cost levels.

Figure 4.10 presents the variation trend of PV-BES system PBPs for large office building with the change of specific energy cost and power cost of PV-BES. Note that the energy cost is based on the capacity (kWh) while the power cost is based on the rated power (kW). In this part, the PV capacity, battery capacity, and rated power of PV-BES system are selected according to Table 4.5. The red arrow indicates the location where the lowest PBP is obtained. As can be seen in the figure, the PBP increases linearly with both the energy and power cost no matter whether the incentive is taken into account or not. Furthermore, the PBP is more deeply influenced by the energy cost than by the power cost since the PBP increases dramatically with increasing energy cost while increases mildly with increasing power cost. In addition, from the figure, the conclusion can be drawn that if the energy and power cost go down in the future (now is about 330 $/kWh and 400 $/kW, respectively), the PBP of a PV-BES system will be more attractive. The results shown here are useful for both system users and policy makers. On one hand, the potential PV-BES system users can estimate the PBPs with the energy cost and power cost in their locations and then determine whether it is worthwhile to install a

PV-BES system. On the other hand, the policy makers can consider providing incentives based on the energy cost in their locations since the PBP is deeply affected by the energy cost. For example, at the power cost of 100 $/kW, the PBP without incentive changes from 30.94 yr to 11.65 yr when the energy cost decreases from 900 $/kWh to 100 $/kWh, showing a slope of 0.024 yr/($/kWh), which means that if the policy makers provide an incentive of 100 $/kWh based on the energy capacity, the equivalent effect would be a decreasing of 100 $/kWh in the energy cost and the PBP could be reduced about 2.4 years.

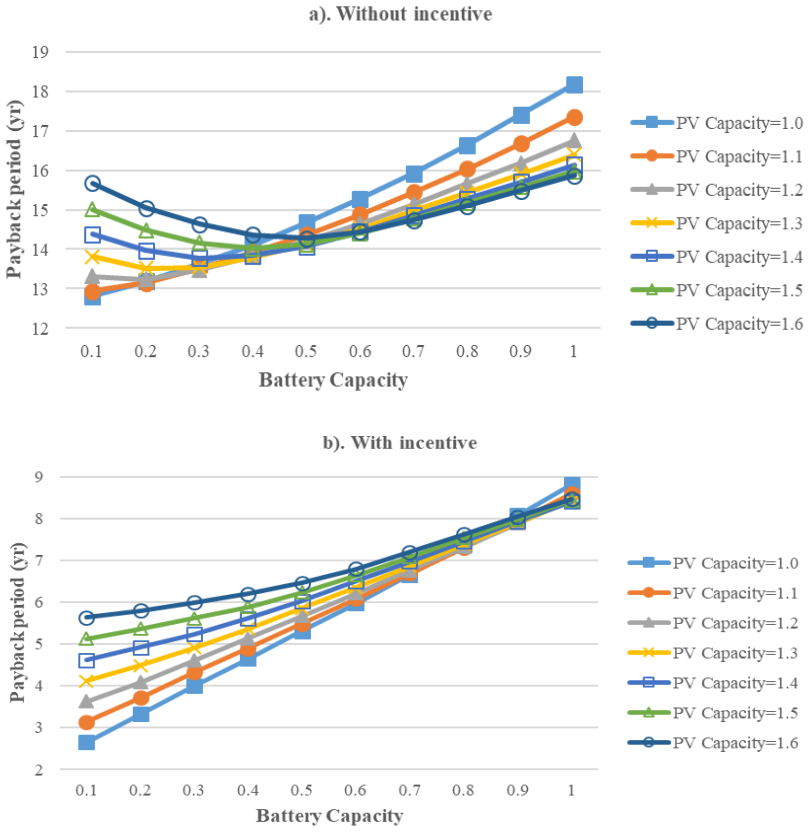

Figure 4.9 Influence of battery capacity on the PBP under different PV capacity situations for large office building in California

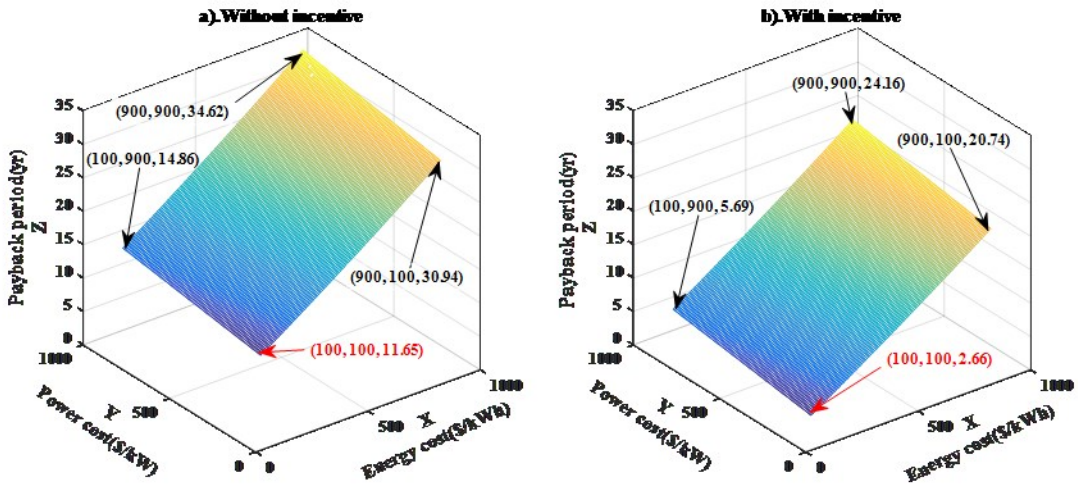

Figure 4.10 Influence of battery capital cost on the PBP for large office building in California

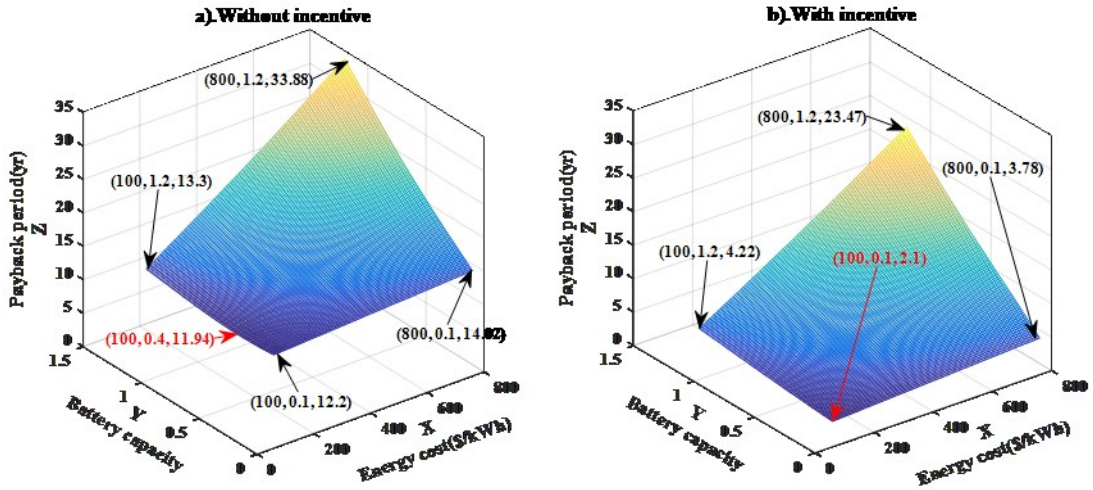

Figure 4.11 Influence of energy cost and capacity of battery on the PBP for large office building in California

Figure 4.11 shows the influence of energy cost and battery capacity on the PBP for the large office buildings in the locations of California. In this part of analysis, the PV capacity and the rated power of BES are decided according to Table 4.5. The variation range of energy cost is from \$100/kWh to \$800/kWh, and the variation range of battery capacity is from 0.1 to 1.2. The point marked out in the figure shows the shortest PBP as

well as the corresponding energy cost and battery capacity. Based on the analysis in Figure 4.10, the PBP without incentive increases with the energy cost increasing. Furthermore, Figure 4.11 shows that the influence of the energy cost on the PBP becomes more and more significant with increasing battery capacity. Similarly, the battery capacity has a stronger influence on the PBP with increasing energy cost. It is interesting to notice that, when the energy cost is too high (e.g., $800/kWh), the PBP increases dramatically with the battery capacity. In this case, the users need to be aware that they need to carefully size their BES or even just installing a PV system without BES in order to get a better PBP. However, if the energy cost becomes cheap, the PBP will decrease slightly before mildly increasing with the battery capacity. In this case, the users can consider installing a PV integrated with BES, that is, a PV-BES system. Besides, the effect of both the energy cost and the battery capacity on the PBP can be diminished when the incentives are taken into consideration.

Figure 4.12 presents the influence of capital cost and capacity of PV on the PBP for large office buildings. The variation range of PV cost is from 1500 $/kW to 2500 $/kW, and the variation range of PV capacity is from 1 to 2. The point marked out in the figure shows the shortest PBP as well as the corresponding PV cost and PV capacity. In this case, the battery capacity and the rated power of BES are selected based on Table 4.5. The energy cost and power cost are equal to the values shown in Table 4.7. As shown in Figure 4.12, the PBPs increase linearly with the PV cost no matter whether the incentives are taken into consideration. Also, oversize the PV capacity to a certain extent can reduce the PBP within the whole range of the PV cost (e.g., 1.8 when PV cost equals to 1500 $/kW). This result demonstrates that with the existing battery capacity and the

rated power of BES, the users can benefit more by oversizing the PV even for PV costs as high as 2500 $/kW.

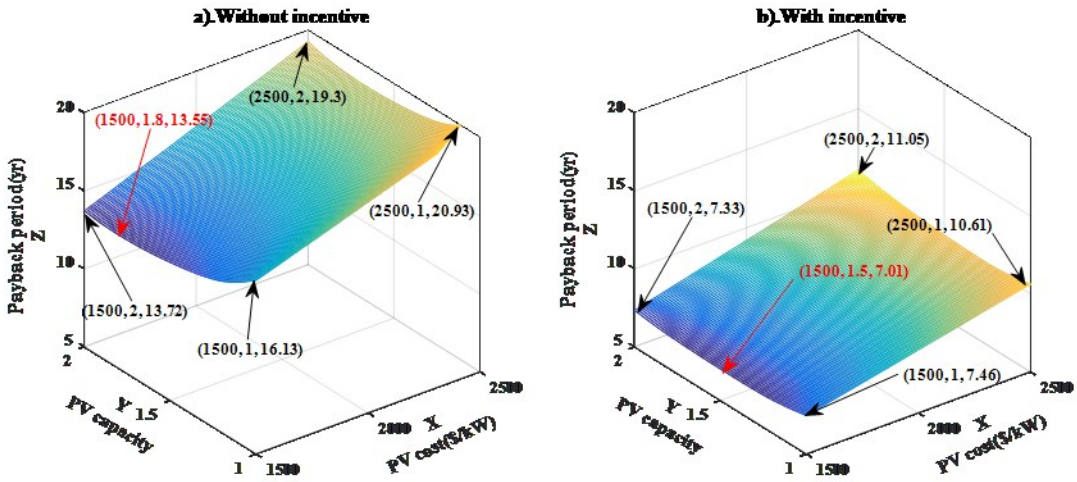

Figure 4.12 Influence of capital cost and capacity of PV on the PBP for large office building in California

CHAPTER V

MULTI-OBJECTIVE DESIGN OPTIMIZATION FOR DISTRIBUTED ENERGY SYSTEMS WITH ENERGY STORAGE

In this chapter, an integrated distributed energy system including photovoltaics (PV), combined heat and power (CHP) and electric and thermal energy storage for commercial buildings (i.e., a hospital and a large hotel) is designed. The subsystems mentioned in previous chapters are integrated based on a proposed control strategy to meet the electric and thermal energy demand of a building. A multi-objective particle swarm optimization (PSO) is performed for an optimal design. The objective is to minimize the payback period and maximize the reduction of carbon dioxide emissions by selecting the optimal size of each subsystem.

5.1 Model Description

Figure 5.1 shows a schematic of the proposed distributed energy system with energy storage. As can be seen in the figure, PV panels are considered in the system design to provide electricity to a building during the daytime. Battery energy storage (BES) is adopted to moderate the generation volatility of PV by storing the excess electricity when the PV generation is sufficient and provide the electricity to the building when the PV generation cannot satisfy the building electric load. Also, a combined heat and power (CHP) system is designed to supply the space heating and hot water demand partially or entirely, and at the same time acting as a compliment to power generation. A

boiler is considered to fulfill the remaining required heat in case the heat recovered from the power generation unit (PGU) in the CHP system is not sufficient to meet the thermal energy requirement of the building. If the recovered heat is more than the demand, a thermal energy storage (TES) is used to store the excess thermal energy. The operation strategy of the distributed energy system is presented in Figure 5.2. Since mathematical models for other subsystems have been developed in chapters from Chapter II to Chapter IV, thus, in this section, only the mathematical model for TES is established.

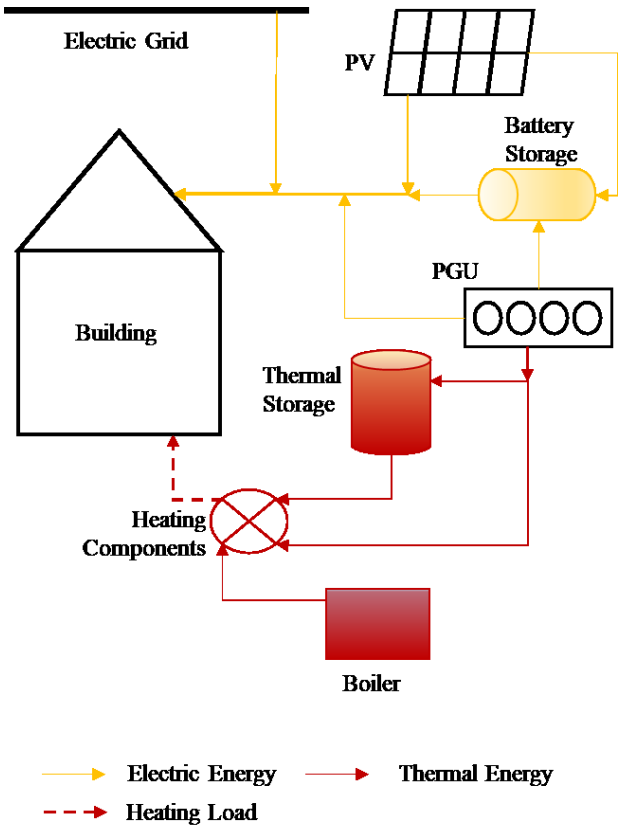

Figure 5.1 Schematic of the distributed energy system with energy storage

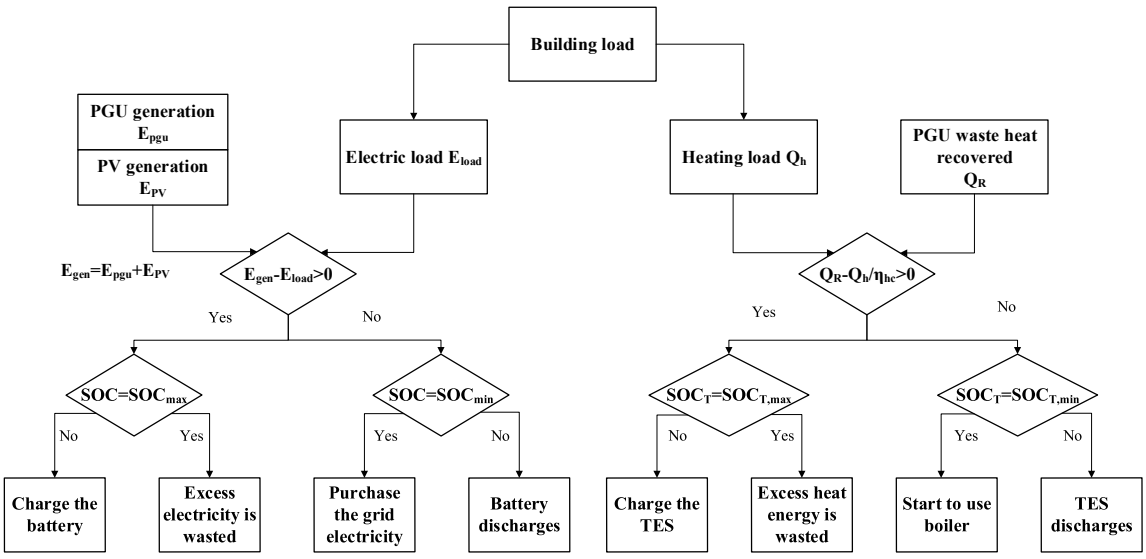

Figure 5.2 Flow chart of the operation strategy of the distributed energy system

In this dissertation, a hot water tank is used as the TES system. The storage tank is assumed to be well insulated, so the heat loss of the TES system is not considered in this analysis. The energy balance of the TES system is shown as following.

When the heat recovered from the PGU exceeds the thermal load of the building, the excess heat serves to charge the TES system. The state of charge of TES system (SOC_T) is estimated as:

$$SOC_T(h) = SOC_T(h-1) + [(Q_R - Q_{hc})/Etes] \cdot \eta_{tC} \quad (5\text{-}1)$$

where Q_R is the heat recovered from the PGU, Q_{hc} is the thermal load of the building, $Etes$ is the energy capacity of TES in kWh, and η_{tC} is the TES charging efficiency.

When the heat recovered from the PGU is not sufficient, the TES system is discharging. The state of charge of TES is then expressed as:

$$SOC_T(h) = SOC_T(h-1) + [(Q_{hc} - Q_R)/Etes] \cdot (1/\eta_{tDC}) \quad (5\text{-}2)$$

where η_{tDC} is the TES discharging efficiency.

5.2 Building Model Description

In this chapter, two building types, a hospital and a large hotel, are selected and analyzed in two locations, i.e., California and Texas. The reason for choosing these two locations is because both locations have sufficient solar radiation, which is desired since PV system is included in our distributed energy system. Figure 5.3 shows the drawings of the two types of buildings [93], respectively. The peak electricity load of the selected building types in both locations are listed in

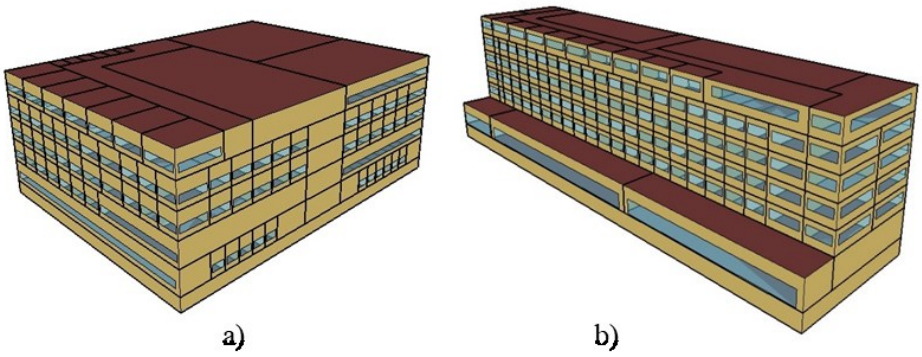

Figure 5.3 Drawings of the buildings; (a) hospital; (b) large hotel

Table 5.1 Peak electricity load for each kind of building in all locations [Unit: kW]

	Hospital	Large hotel
CA	1147	361
TX	1326	434

5.3 Multi-objective optimization

5.3.1 Objective function and decision variables

In this chapter, the payback period (PBP) of the proposed distributed system and the reduction of carbon dioxide emission (RCDE) are selected as two conflict objectives. The optimization program is designed to decide the minimum PBP and the maximum RCDE. The following decision variables are used for optimizing algorithm.

Cap_{PV} : Capacity of PV (kW)

$Ebat$: Capacity of battery storage (kWh)

$Pbat$: Rated power of battery storage (kW)

P_{pgu} : Rated power of PGU (kW)

$Etes$: Capacity of thermal storage (kWh)

With these decision variables, the multi-objective design optimization model for the distributed energy system can be expressed as:

$$\min(PBP) = f_1(Cap_{PV}, Ebat, Pbat, P_{pgu}, Etes) \quad (5\text{-}3)$$

$$\max(\text{RCDE}) = f_2(Cap_{PV}, Ebat, Pbat, P_{pgu}, Etes) \quad (5\text{-}4)$$

The logical bounds of the decision variables aforementioned are summarized in Table 5.2. Figure 5.4 shows the flow chart of the multi-objective particle swarm optimization.

Table 5.2 Logical bounds of the decision variables

Situations	PV Capacity (kW)	BES Capacity (kWh)	BES Rated Power (kW)	PGU Power (kW)	TES Capacity (kWh)
Hospital	[0, 2000]	[0, 2200]	[0, 1100]	[0, 1200]	[0, 2000]
Large hotel	[0, 750]	[0, 1200]	[0, 400]	[0, 400]	[0, 700]

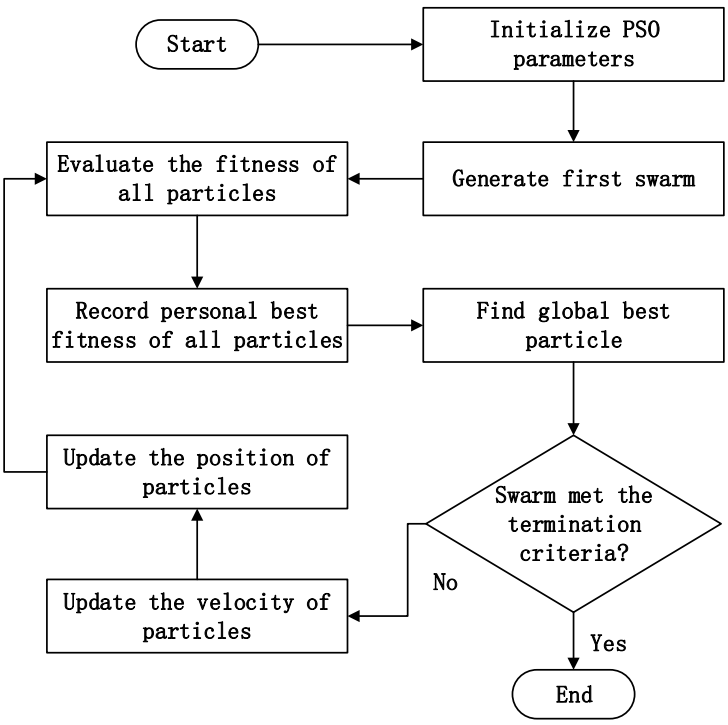

Figure 5.4 Flow chart of the multi-objective particle swarm optimization (PSO)

In order to estimate the PBP, the cost of installing the distributed energy system as well as the financial benefits obtained from the system are given as follows:

The capital cost of the PV modules is calculated as:

$$Cost_{C,PV} = C_{PV} \cdot Cap_{PV} \tag{5-5}$$

The capital cost of the inverter is given by:

$$Cost_{C,inv} = C_{inv} \cdot Cap_{PV} \tag{5-6}$$

Note that the detailed costs of PV, from Ref. [96], are classified into two parts, that is, the inverter cost (C_{inv}) and the PV major cost (C_{PV}) in this paper. The PV major cost, C_{PV}, consists of all the expenditures except for inverter like module cost, install labor & equipment cost, and sales tax, etc.

The capital cost of the BES system could be calculated as [101][102]:

$$Cost_{C,BES} = C_P \cdot Pbat + C_E \cdot Ebat \tag{5-7}$$

The capital cost of the PGU system is:

$$Cost_{C,pgu} = C_{pgu} \cdot P_{pgu} \tag{5-8}$$

The capital cost of the TES (hot water tank) is estimated as:

$$Cost_{C,tes} = C_{tes} \cdot Etes \tag{5-9}$$

The O&M cost of the PV system (PV modules and inverter) is given by:

$$Cost_{OM,PV} = C_m \cdot Cap_{PV} \tag{5-10}$$

While the O&M cost of the BES system per year is:

$$Cost_{OM,BES} = C_f \cdot Pbat + C_v \cdot E \tag{5-11}$$

where E is the amount of annual discharge energy of the BES system. However, the value of C_v is set to 0 because the variable operating and maintenance cost is negligible compared to the fixed one [101].

The total capital cost of the distributed energy system is the sum of above mentioned costs in the equations from Eq. (5-5) to (5-9):

$$Cost_{C,total} = Cost_{C,PV} + Cost_{C,inv} + Cost_{C,BES} + Cost_{C,pgu} + Cost_{C,tes} \tag{5-12}$$

The parameters used in the equations above are summarized in Table 5.3.

When the distributed energy system is operating, the building electric load is partly provided by the system instead of importing from the grid. In addition, the thermal load is also supplied entirely or partially by the distributed energy system. The annual saving, i.e. reduction in electric and gas bill can be determined as:

$$AS = \left(E_{grid} - E_{grid,DES}\right) \cdot Cost_e + (F_l - F_{l,DES}) \cdot Cost_f \quad (5\text{-}13)$$

where $Cost_e$ is the electricity cost. E_{grid} is the electricity imported from the grid before the distributed energy system is applied to the reference building, while $E_{grid,DES}$ is the electricity purchased from the grid with the distributed energy system operating. Similarly, $Cost_f$ is the fuel cost (nature gas in this case). F_l is the original fuel purchased without operating the proposed distributed energy system, and $F_{l,DES}$ is the one with distributed system operating.

Table 5.3 Parameters for PBP estimation

Parameter	Meaning	Value [96][101][103][104]
C_P	Specific power cost of BES	$400/kW
C_E	Specific capacity cost of BES	$330/kWh
C_f	Fixed O&M cost of BES	$20/kW.yr
C_v	Variable operating and maintenance cost of BES	0
C_{pv}	PV major cost	$1930/kW
C_{inv}	Inverter cost	$130/kW
C_m	Operating and maintenance cost of PV	$34 kW.yr
C_{pgu}	Specific capacity cost of PGU	$1400/kW
C_{tes}	Specific capacity cost of TES	$31/kWh

Once the total cost and annual saving is known, the PBP of distributed energy system can be decided:

$$PBP = (Cost_{C,total} - In)/\left(AS - Cost_{OM,PV} - Cost_{OM,BESS}\right) \quad (5\text{-}14)$$

where In is the incentives provided by the governments and/or the utility companies which help to diminish the installation costs. Incentives for the selected locations and specified systems are summarized in Table 5.5 to Table 5.7.

Simultaneously, the reduction of carbon dioxide emission (RCDE) due to the contribution of the distributed energy system can be estimated as:

$$RCDE = \left(E_{grid} - E_{grid,DES}\right) \cdot EF_e + \left(F_l - F_{l,DES}\right) \cdot EF_f \quad (5\text{-}15)$$

where EF_e and EF_f are grid emission factor and natural gas emission factor, respectively. The electricity and nature gas cost as well as both emission factors for selected locations are summarized in Table 5.4.

Table 5.4 Electricity and fuel cost [82] and carbon dioxide emission factor [105] for each location

State	$Cost_e$ (\$/kWh)	$Cost_f$ (\$/kWh)	EF_e (kg/kWh)	EF_f (kg/kWh)
CA	0.1515	0.028	0.259	0.18
TX	0.0831	0.023	0.521	0.18

Table 5.5 CCHP incentive polies for selected locations

City	Incentive policy
CA	*Grant* for Internal Combustion Engine (CHP): \$0.42/W. *
TX	*Grant:* Offset 20% of the upfront implementation costs. **

*. N.C. Clean Energy Technology Center. Self-Generation Incentive Program. http://programs.dsireusa.org/system/program/detail/552 (accessed November 30, 2017).
**. United States Environmental Protection Agency. dCCHP (CHP Policies and Incentives Database). https://www.epa.gov/chp/dchpp-chp-policies-and-incentives-database#CityofHoustonEnergyEfficiencyIncentiveProgram (accessed May 23, 2018).

Table 5.6 PV incentive polies for selected locations

Location	Incentive policy
Federal	Tax credit (equal to 30% of investment) *
CA	*Rebate:* $0.40/W for PV system. Up to 50% of project costs for commercial systems. The maximum system size is 1MW **
TX	*Rebate:* $0.25/W for PV system and up to 100 kW***

*. Solar Energy Industries Association (SEIA). Solar Investment Tax Credit (ITC). https://www.seia.org/policy/finance-tax/solar-investment-tax-credit (accessed on 01 Aug. 2017).
**. U.S. Department of Energy (DOE). LADWP – Solar Incentive Program. https://energy.gov/savings/ladwp-solar-incentive-program (accessed on 01 Aug. 2017).
***. AEP Texas. Welcome to the SMART Source Solar PV Program. https:// http://www.txreincentives.com/apv/index.php (accessed May 23, 2018).

Table 5.7 BES incentive polies for selected locations*

Location	Incentive policy
CA	$1.31/W for energy storage system which capped at 3MW.
TX	N/A

*. National Renewable Energy Laboratory (NREL). Issue Brief: A Survey of State Policies to Support Utility-Scale and Distributed-Energy Storage. http://www.nrel.gov/docs/fy14osti/62726.pdf (accessed on 01 Aug. 2017).

5.3.2 Decision making process

Since two conflicting objectives are involved in the optimization, it is not possible to obtain a single solution that can optimize both objectives at the same time. A common way to solve this problem is to find the Pareto optimal solutions (i.e. Pareto frontier) first and then obtain a final solution by employing an appropriate multi-criteria decision analysis method. In this study, the TOPSIS (Technique for Order Preference by Similarity to an Ideal Solution) is used. The essence of the TOPSIS method is to select an alternative which has the longest geometric distance from the non-ideal point, and also

has the shortest geometric distance from the ideal point. Figure 5.5 shows an example of Pareto frontier and selected result of the distributed energy system for large hotel building in California. A detailed description of TOPSIS method is illustrated in Ref. [113].

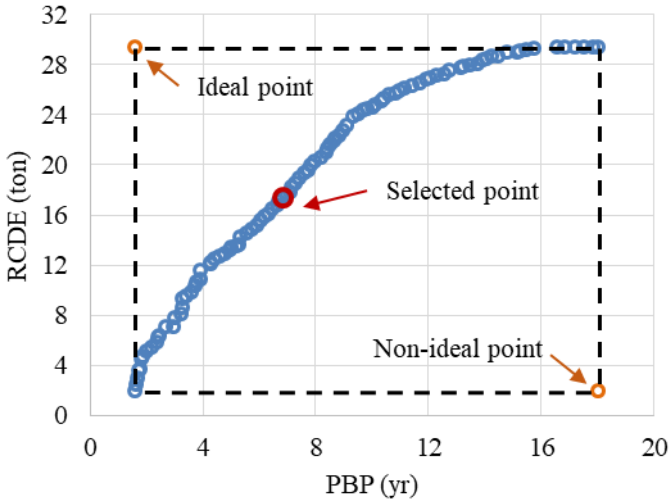

Figure 5.5 Pareto frontier of payback period and reduction of carbon dioxide emission

5.4 Results and Discussion

In this research, the distributed energy systems are designed and optimized based on the models and methods described in previous sections for a hospital and a large hotel in California and Texas. In order to simplify the optimization, the simulation period is set to 6 weeks, i.e., 1008 hours instead of one year (8760 hours). The 6 weeks selected for simulation are Jan 1st to Jan 7th, Jan 21st to Jan 27th, Apr 1st to Apr 7th, Jul 1st to Jul 7th, Jul 21st to Jul 27th, and Oct 21st to Oct 27th, among which two weeks are in winter, two weeks are in summer, and the remaining two weeks are in the transition season (spring and fall).

The selection of decision variables (subsystem capacities in our case) based on the TOPSIS method are presented in Table 5.8. Notably, the optimal capacity and rated power of BES for both the hospital and the large hotel in Texas are 0, which means for that case, a distributed energy system without BES is more beneficial. This is mainly because the BES is not cost effective in Texas considering the electricity price there is quite low.

Table 5.8 Selection of decision variables based on TOPSIS method

Situations	PV Capacity (kW)	BES Capacity (kWh)	BES Rated Power (kW)	PGU Power (kW)	TES Capacity (kWh)
Hospital in CA	1386	386	107	94	52
Large hotel in CA	271	573	123	100	614
Hospital in TX	1297	0	0	153	43
Large hotel in TX	198	0	0	107	576

Based on the optimal sizing listed in Table 5.8, the capital cost of each subsystem for selected building types and locations are presented in Figure 5.6. As can be seen in the figure, for all building types and locations, the capital cost of PV system takes up the largest portion of the total capital cost and the TES takes up the least portion. The cost of TES is even negligible compared to the total cost. Besides, the second costliest subsystem for both building types in CA is the BES while in TX is the PGU since BES is not adopted. The savings during the simulation period (6 weeks) based on the optimal sizing results shown in Table 5.8 for selected building types and locations are presented in Figure 5.7. Note that the savings here include the savings on both the electricity and natural gas bills. Generally, the larger the system size is, the more savings could be

achieved. This demonstrate why the savings for the hospital in each location are more than that those for the large hotel. Besides, the savings for same building type in CA are more than twice as the savings in TX, even though the total capital cost in CA is slightly more. The reason is that the electricity price in CA is higher than that in TX, which means one can obtain more savings when using the electricity generated by the distributed energy systems instead of purchasing the grid electricity.

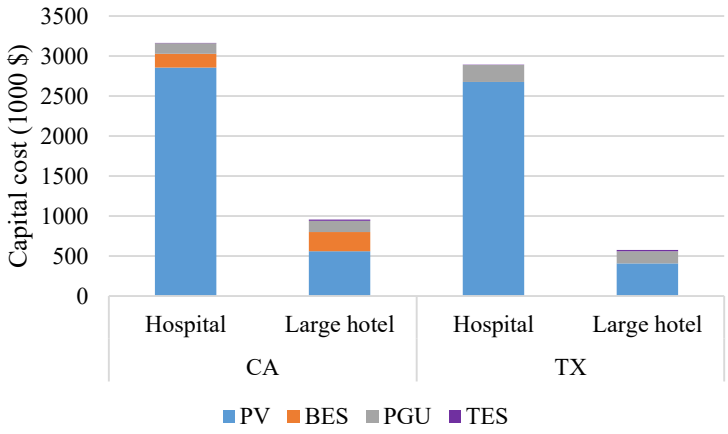

Figure 5.6 Capital cost of each subsystem for selected buildings and locations

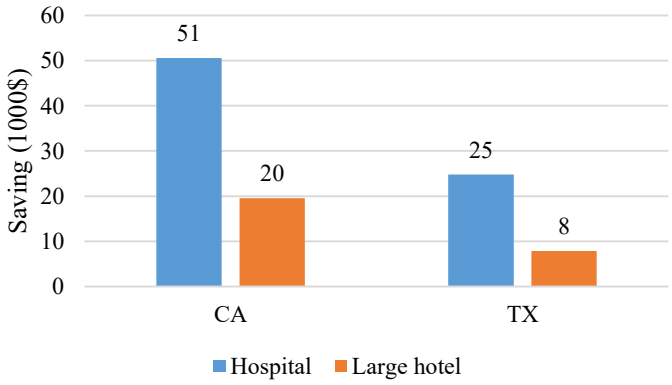

Figure 5.7 Savings for selected building types and locations

The optimal PBP and RCDE are illustrated in Figure 5.8 and Figure 5.9, respectively. As discussed before, it is impossible to obtain the minimum PBP and the maximum RCDE simultaneously. Thus, the optimization result shown here is a tradeoff between the PBP and RCDE. Figure 5.8 presents the PBP for selected building types including the hospital and the large hotel in each location. As can be seen in Figure 5.8, the PBP for the selected building types and locations except for hospital in TX are less than 10 years (even below 5 years for both building types in CA). Considering the lifespan of each subsystems of distributed energy system, reaching a PBP less than 10 years in the selected states can effectively promote the installations of distributed energy system in their states. For both building types, the PBP in Texas is worse than that in California, especially for the hospital building, which reaches up to 13 years. Moreover, for each location, the PBP for large hotel is better than that for hospital.

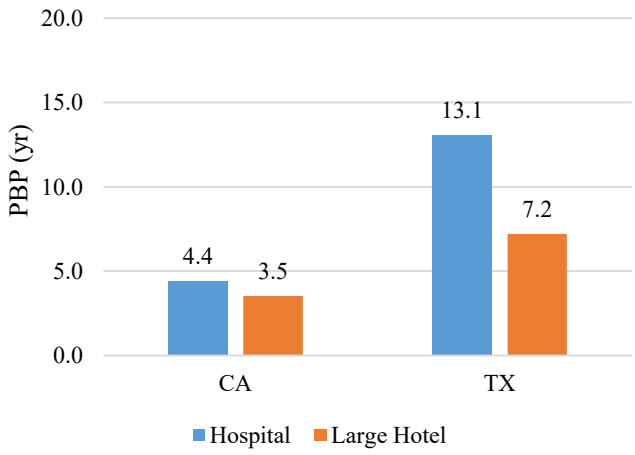

Figure 5.8 Optimization results of PBP for selected building types and locations

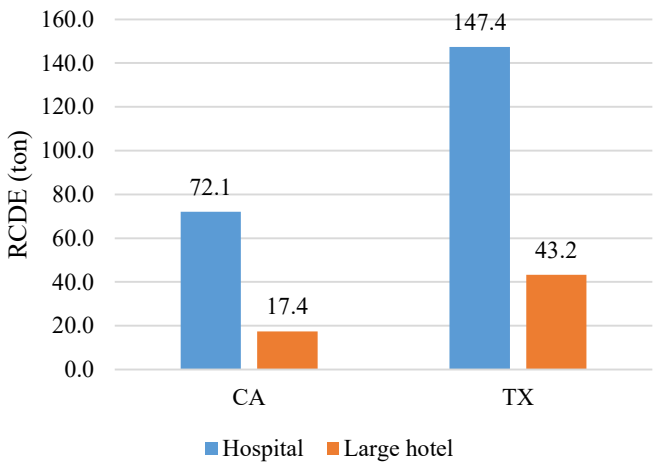

Figure 5.9 Optimization results of RCDE for selected building types and locations

Figure 5.9 provides the results of RCDE for the selected building types and locations. It is important to mention here, the values shown in Figure 5.9 represent the results for only 6 weeks rather than the whole year. As can be seen from Table 5.4, the grid emission factor in California is smaller than the grid emission factor in Texas, which means the electricity in California is "cleaner." When the distributed system is designed to provide electric and thermal energy to the building, the "savings" in carbon dioxide emission due to the trade-off effect between cost and environmental aspects is relatively low. Therefore, from Figure 5.9, one can see that the RCDE in Texas is much higher than that in California for both building types. In addition, if the use of carbon credit is accessible for those locations, the operation cost of the distributed energy system could be further reduced. By now, there are several states in the U.S. providing carbon credits in the range from \$2 /ton to \$14 /ton [110]. However, current carbon credits are still too low to make a significant influence on diminishing the PBP because the benefits from carbon credits seem to be tiny compared to the annual savings. For example, the carbon

credit for California in 2015 was $12.1 /ton [110], thus, the benefit from the carbon credit for the hospital building in California is around $872.4 ($\$12.1/ton \times 72.1\ ton$), which is too small to have an impact on the PBP. If a much higher carbon credit could be achieved in future, the influence of the carbon credit of the PBP will have a more significant impact.

Figure 5.10 presents the electric energy demand and supply including the building electricity load, PV and PGU generation, battery storage usage, electricity imported form the grid, and the amount of electricity that wasted during the simulation period. As can be seen from Figure 5.10, for the hospital building in both locations, the amount of electric energy supply becomes larger in the order of PGU generation, PV generation, and grid import. Due to the contribution of the distributed energy system, the amount of electricity from the grid is reduced compared to the original electricity load. Take the hospital building in California as an example, the electricity load is 764 MWh, which need to be imported from the grid without applying the distributed energy system. However, because of the operation of the distributed energy system, only 411 MWh of electricity is imported form the grid. It is important to mention here, the item "battery usage" in the figure contains the amount of both charging and discharging of the battery during the simulation period. Thus, the amount of electricity supplied by the battery is approximately half of the value shown in the figure. No matter whether the battery storage system exits or not, electricity waste still exits. Note that the item "electricity wasted" in the figure refers to the excess electricity generation which have to be abandoned because of the absence of BES (in TX) or the limitation of BES capacity/rated power (in CA) but not includes the electric energy losses due to the battery charging and

discharging efficiency. Furthermore, if some policies like “net metering” or “feed-in tariff” are available, the electricity which is wasted could be exported or sold back to the electric grid to obtain more savings and even the battery storage system in California can be displaced.

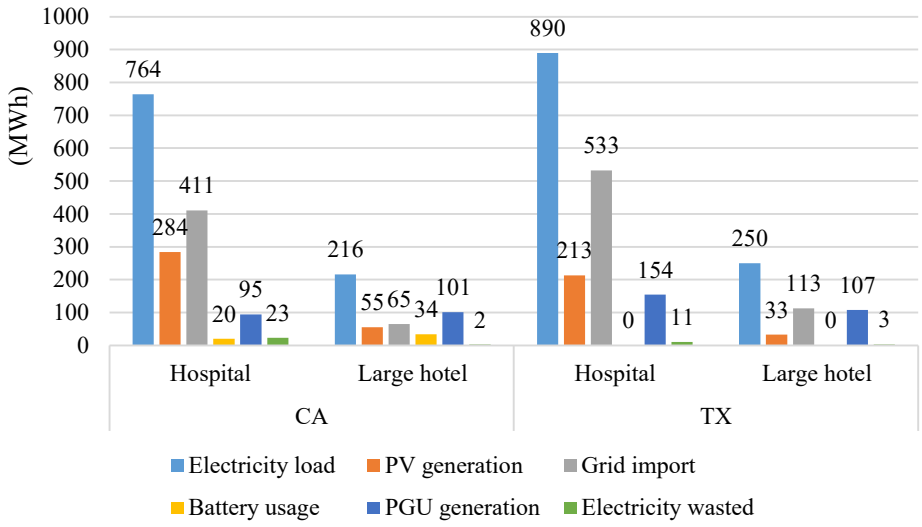

Figure 5.10 Electric energy demand and supply during the simulation period for selected building types and locations

The fuel and thermal energy demand and supply during the simulation period for selected building types and locations are illustrated in Figure 5.11. In this figure, fuel load refers to the original fuel requirement for the reference building, that is, fuel consumption without operating the distributed energy system. The “heat recovered” derives from the waste heat of the PGU which is normally discarded in many applications. Similar to the “battery usage” in Figure 5.10, the “TES usage” contains the amount of both charging and discharging of the TES during the simulation period as well.

Also, the "heat wasted" is the excess heat energy that can neither be used nor stored in the TES due to the capacity limitation. As can be seen from Figure 5.11, the fuel requirement to operate the distributed energy system, i.e., sum of the boiler fuel and PGU fuel in the figure, is much larger than the original fuel load of the reference building. This is because of the facts that a portion of the electricity load as well as the heating load of the building is provided by the PGU. Therefore, the fuel consumption increases significantly with the operation of the distributed energy system.

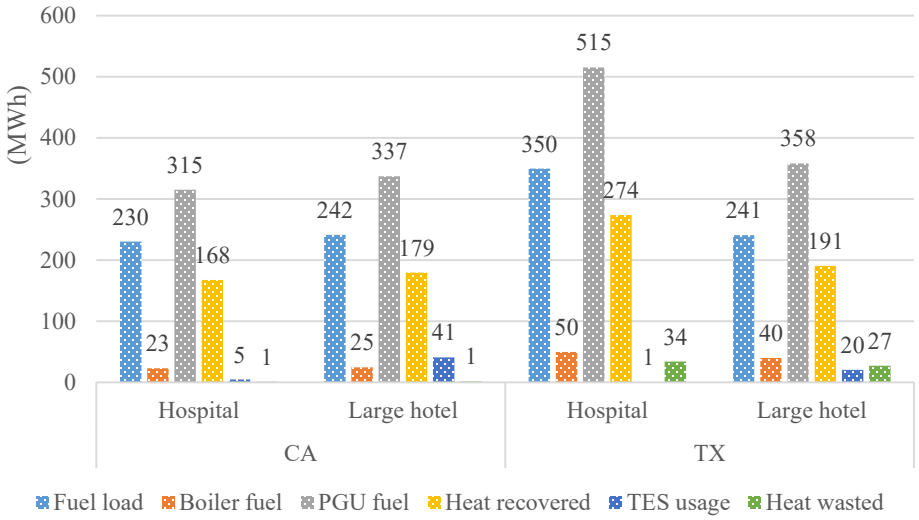

Figure 5.11 Fuel and thermal energy demand and supply during the simulation period for selected building types and locations

Figure 5.12 and Figure 5.13 show the energy demand and supply characteristics for the hospital building in California for an arbitrary day in winter, summer, and transition season. Figure 5.12 shows the building electric load, which is the original load of the hospital building before applying the distributed energy system. It also shows the

PGU and PV generation, the electricity imported and wasted, as well as the battery storage remaining. For the winter day (Figure 5.12 (a)), the PV generation is relatively low and little electricity generation is stored in the battery storage system. Thus, no electricity is wasted within the 24 hours as shown in Figure 5.12 (a). By comparing the grid electricity, i.e. the electricity imported form the grid after operating the distributed energy system, to the building electricity load, one can see that an approximating 100kW peak shaving is achieved. For the summer day, as can be seen in Figure 5.12 (b), the building electricity load is slightly larger than that in winter and transition season. This is because of the cooling requirement, which is originally fulfilled by electricity, that increases in the summer time. In addition, the PV system generates more electricity so that the battery storage is fully charged around 14:00. Due to the contribution of the distributed energy system, less electricity needs to be imported form the grid and an approximately 350 kW peak shaving is achieved. As for the transition season, the tendency of the electricity use and provision is similar to that for the summer day, while the peak shaving is almost 400 kW.

Similarly, Figure 5.13 shows the original building fuel requirement to operate the boiler before applying the distributed energy system for the hospital building in California on an arbitrary day. It also shows the heat energy recovered and wasted, the boiler fuel purchased (after operating distributed energy system), and the TES remaining. It is important to mention here, the boiler along with the heat energy recovered from the exhaust of PGU are used to supply the hot water and the space heating for the building when the distributed energy system is operating. This demonstrates why the boiler fuel purchased during the summer day is less than that for the winter day since the space

heating requirement in summer is lower. It can be seen from Figure 5.13 (a), the excess heat energy is stored in the thermal storage system. Furthermore, the peak load of boiler fuel after applying the distributed energy system is 80 kW, which is much lower than the original boiler fuel peak requirement (i.e., 306 kW). Similarly, as shown in Figure 5.13 (b) and (c), a peak shaving of 200 kW in boiler fuel load could be achieved during the selected day in summer and transition season, respectively.

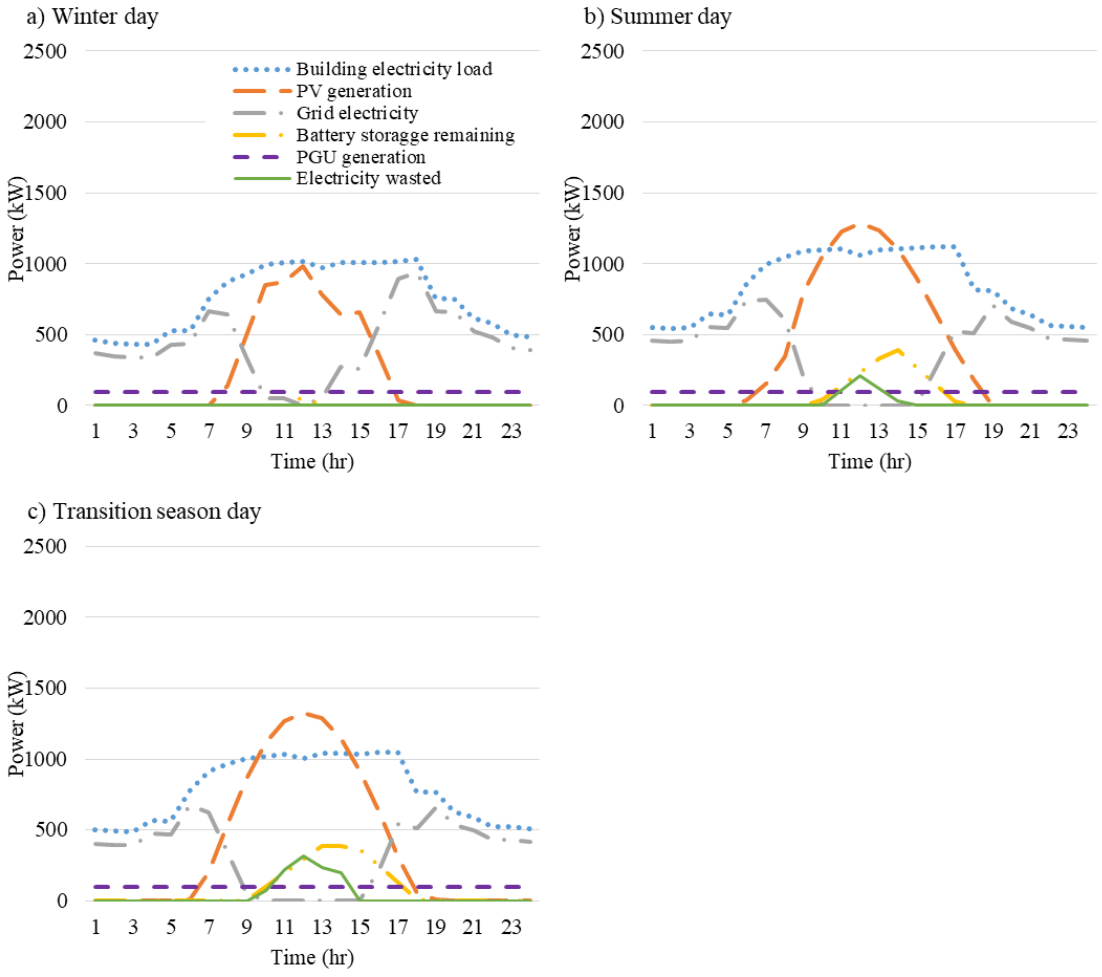

Figure 5.12 Electricity use and provision for hospital in California; a) Winter day; b) Summer day; c) Transition season

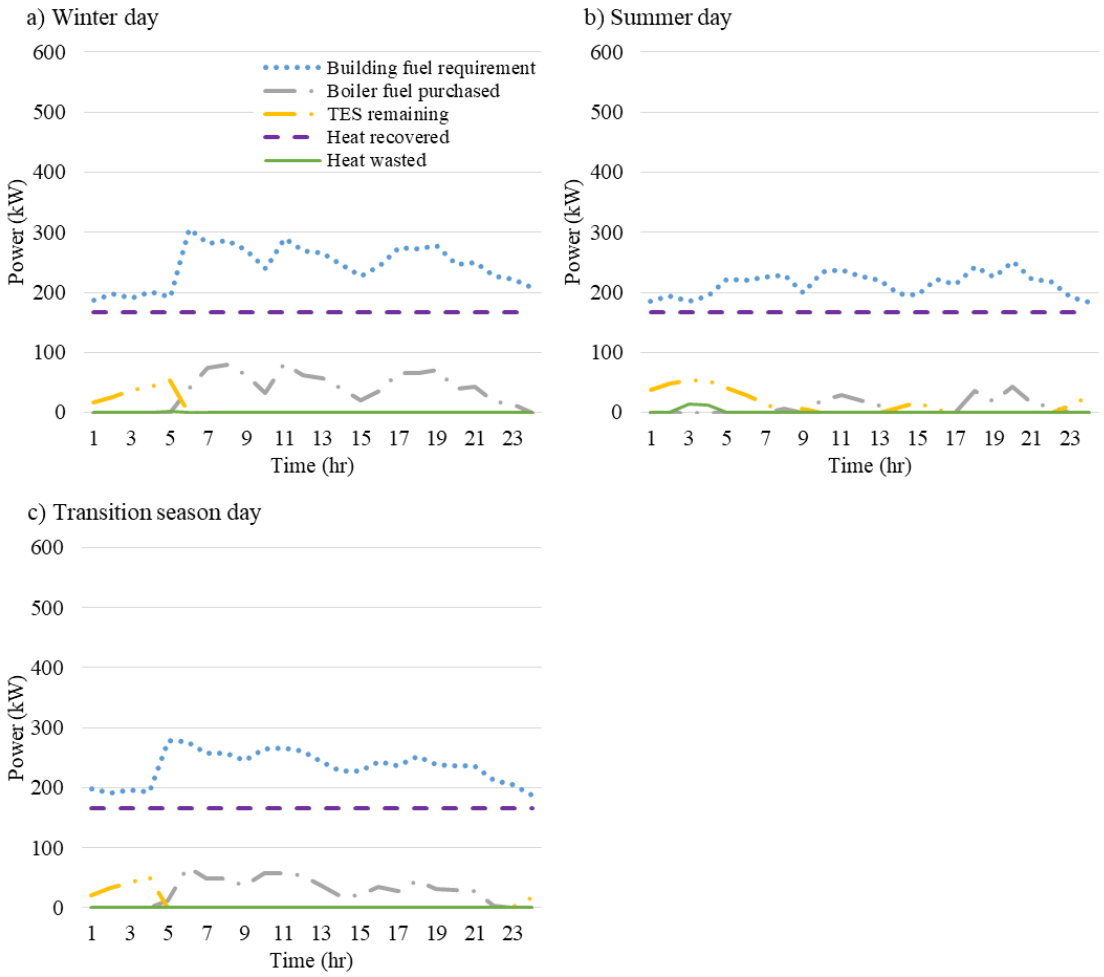

Figure 5.13 Fuel and thermal energy use and provision for hospital in California; a) Winter day; b) Summer day; c) Transition season

CHAPTER VI

CONCLUSIONS

In this dissertation, distributed energy systems were analyzed for their techno-economic performance and potential to reduce emissions. Subsystems including CHP, PV, BES, and TES were first modeled and analyzed individually and then integrated together based on a proposed control strategy. A multi-objective particle swarm optimization algorithm was applied to optimize the integrated distributed energy system with the objective of minimizing the payback period and maximizing the reduction of carbon dioxide emission.

CHAPTER I presented the background of distributed energy systems and reviewed previous and current researches about different aspects of distributed energy systems.

CHAPTER II modeled the CHP system, analyzed the techno-economic performance of the CHP system, and evaluated the CHP incentive policies. The CHP system was operated in two different modes, the base-loaded mode and the FEL mode. The results demonstrated that for most situations (locations and building types), the base-loaded CHP systems had better PBP than the FEL CHP systems. Meanwhile, with the same incentive policy, the PBP of base-loaded CHP systems were reduced more significantly than that for the FEL CHP systems. For each location, the large hotel buildings were extremely suitable to adopt the base-loaded CHP systems since the capital

cost payback periods were all within 5 years. As for other building types, the conclusions vary with the locations. For those situations in which the PBP is too long (decades) or non-existent, instead of only offering financial support, the policy maker should encourage the users to choose an appropriate capacity and operational strategy in order to get a faster PBP. The ratio of electricity cost to fuel (natural gas) cost ($Cost_e/Cost_f$) is a key factor affecting the PBP significantly. The larger the value of ($Cost_e/Cost_f$) is, the more money that can be saved when using a CHP system to generate electricity instead of purchasing electricity from the grid. According to the results of the payback period percentage reduction, incentives for San Francisco, CA, Boston, MA, and Kennedy, NY seem to be most supportive. Based on the feature of incentives for these areas, an incentive with a capital grant larger than $400/kW, or with a production incentive larger than $0.1/kWh, should provide substantial benefits for CHP system implementation.

CHAPTER III focused on the techno-economic and parametric analysis of PV systems. It is shown that the solar availability and electricity cost are key factors which affect the PBP significantly. For larger solar availability, more electricity can be generated by the PV system under the same condition, while larger electricity cost values lead to more cost savings when using a PV system to generate electricity, instead of purchasing electricity from the grid. When the PV capacity is larger than the maximum electricity load, the PBP without incentive increases in most locations as the PV capacity increases. Thus, for those locations that do not provide either a high performance based incentive or a net metering policy, the users need to be aware that choosing an appropriate size of the PV system is critical to achieve a desired PBP. In addition, the PBP increases linearly with the increase of capital cost of PV in all of the selected

locations, no matter whether the incentive is taken into consideration or not. The slope of variation line shows how deeply the PBP is influenced by the capital cost of PV for each location (e.g. when the cost of PV changes from 0.5 to 5 $/W, the PBP without incentive varies from 2 years to almost 30 years in Florida, while it only varies from 2 years to nearly 10 years in Hawaii). As for the sell back ratio, when the sell back ratio equals to 1, i.e., net metering is available, it can reduce the impact of the PV capacity on the PBP. This means that the PV users could install a larger capacity PV system without sacrificing the PBP.

CHAPTER IV investigated the performance of an integrated PV and battery storage system and determined the effects of parameters including capacity of the PV-BES system, capital cost of PV module and battery storage on the performance of the PV-BES system. The analysis results lead to the conclusions below:

1. For all the building types in California and Hawaii, the existing incentive policy could reduce the PBP effectively below 10 years. However, the PBP for most building types in New Jersey and New York were too long even when both the PV and BES incentive policies were taken into account.
2. With a specific battery capacity, the PBP without an incentive decreased firstly before increasing again when the PV capacity increases. However, with most PV capacities, the payback period without incentive increased dramatically with the increase of battery capacity. (i.e. the shortest payback periods occurred at the middle PV capacity condition (1.4 or 1.5) but the lowest battery capacity (0.5) for all locations).

3. The PBP increased linearly with both the energy and power cost in most locations (except New York), no matter whether the incentive was taken into account or not. Furthermore, for all locations, the PBP was influenced more deeply by the energy cost than by the power cost.
4. The battery capacity had a greater influence on the PBP when the energy cost increased. When the energy cost was too high (e.g., $800/kWh), the PBP increased dramatically with the battery capacity. In this case, the users need to be aware that they need to be carefully size their BES or even just installing a PV system without BES in order to get a better payback period. However, for reduced energy costs, the payback period would decrease slightly before mildly increasing with the battery capacity. In this case, the users can consider installing a PV integrated with a BES.

CHAPTER V presented a case study of design optimization for integrated distributed energy systems including PV, CHP, and electric and thermal energy storage for commercial buildings (i.e., a hospital and a large hotel). The subsystems were integrated together based on a proposed control strategy to meet the electric and thermal energy demand of the building. A multi-objective particle swarm optimization (PSO) was performed to determine the optimal size of each subsystem with objectives to minimize the payback period and maximize the reduction of carbon dioxide emission. The results show that the proposed method could be effectively utilized to obtain an optimized design of distributed energy systems that can get a tradeoff between the environmental and economic impacts for different buildings. For all building types and locations, the capital cost of PV system was the largest expenditure among the total capital cost and the

TES was the least one. The cost of TES was even negligible compared to the total cost. With the optimal sized distributed energy system, an approximating 300kW electricity peak shaving and 610 kW boiler fuel reduction could be achieved for the hospital building in California for the winter day. For the summer and transition season, only electricity peak shaving is achieved and the amounts are 800 kW and 600 kW, respectively.

REFERENCES

[1] U.S. Environmental Protection Agency Combined Heat and Power Partnership. Catalog of CHP Technologies. 2017.

[2] Busch R, Hodkinson G. Distributed energy systems 2015:1–119. https://www.siemens.com/content/dam/internet/siemens-com/fairs-events/fairs/2016/intersolar-2016/DES_Summary for decision makers.pdf.

[3] Giarola S, Forte O, Lanzini A, Gandiglio M, Santarelli M, Hawkes A. Techno-economic assessment of biogas-fed solid oxide fuel cell combined heat and power system at industrial scale. Appl Energy 2018;211:689–704. doi:10.1016/J.APENERGY.2017.11.029.

[4] Zhang J, Cho H, Knizley A. Evaluation of financial incentives for combined heat and power (CHP) systems in U.S. regions. Renew Sustain Energy Rev 2016;59:738–62. doi:10.1016/j.rser.2016.01.012.

[5] Zhang N, Wang Z, Lior N, Han W. Advancement of distributed energy methods by a novel high efficiency solar-assisted combined cooling, heating and power system. Appl Energy 2018;219:179–86. doi:10.1016/J.APENERGY.2018.03.050.

[6] Bianchini A, Gambuti M, Pellegrini M, Saccani C. Performance analysis and economic assessment of different photovoltaic technologies based on experimental measurements. Renew Energy 2016;85:1–11. doi:10.1016/j.renene.2015.06.017.

[7] Zhang J, Knizley A, Cho H. Investigation of existing financial incentive policies for solar photovoltaic systems in U.S. regions. AIMS Energy 2017;5:974–96. doi:10.3934/energy.2017.6.974.

[8] Sardi J, Mithulananthan N, Gallagher M, Hung DQ. Multiple community energy storage planning in distribution networks using a cost-benefit analysis. Appl Energy 2017;190:453–63. doi:10.1016/J.APENERGY.2016.12.144.

[9] Parra D, Norman SA, Walker GS, Gillott M. Optimum community energy storage for renewable energy and demand load management. Appl Energy 2017;200:358–69. doi:10.1016/J.APENERGY.2017.05.048.

[10] Soares JB, Szklo AS, Tolmasquim MT. Alternative depreciation policies for promoting combined heat and power (CHP) development in Brazil. Energy 2006;31:1151–66. doi:10.1016/j.energy.2005.05.004.

[11] Yuan C, Liu S, Yang Y, Chen D, Fang Z, Shui L. An analysis on investment policy effect of China's photovoltaic industry based on feedback model. Appl Energy 2014;135:423–8. doi:10.1016/j.apenergy.2014.08.103.

[12] Sani Hassan A, Cipcigan L, Jenkins N. Optimal battery storage operation for PV systems with tariff incentives. Appl Energy 2017;203:422–41. doi:10.1016/j.apenergy.2017.06.043.

[13] Li G, Zhang R, Jiang T, Chen H, Bai L, Cui H, et al. Optimal dispatch strategy for integrated energy systems with CCHP and wind power. Appl Energy 2017;192:408–19. doi:10.1016/j.apenergy.2016.08.139.

[14] Mohammadi A, Mehrpooya M. Energy and exergy analyses of a combined desalination and CCHP system driven by geothermal energy. Appl Therm Eng 2017;116:685–94. doi:10.1016/j.applthermaleng.2017.01.114.

[15] Arsalis A, Alexandrou AN, Georghiou GE. Thermoeconomic modeling of a small-scale gas turbine-photovoltaic-electrolyzer combined-cooling-heating-and-power system for distributed energy applications. J Clean Prod 2018;188:443–55. doi:10.1016/J.JCLEPRO.2018.04.001.

[16] Zhang J, Cho H, Luck R, Mago PJ. Integrated photovoltaic and battery energy storage (PV-BES) systems: An analysis of existing financial incentive policies in the US. Appl Energy 2018;212:895–908. doi:10.1016/j.apenergy.2017.12.091.

[17] Hung DQ, Mithulananthan N, Bansal RC. Integration of PV and BES units in commercial distribution systems considering energy loss and voltage stability. Appl Energy 2014;113:1162–70. doi:10.1016/J.APENERGY.2013.08.069.

[18] Huang Y, Wang YD, Chen H, Zhang X, Mondol J, Shah N, et al. Performance analysis of biofuel fired trigeneration systems with energy storage for remote households. Appl Energy 2017;186:530–8. doi:10.1016/J.APENERGY.2016.03.028.

[19] Mago PJ, Luck R. Evaluation of a base-loaded combined heating and power system with thermal storage for different small building applications. Int J Energy Res 2013;37:179–88. doi:10.1002/er.1892.

[20] Çakir U, Çomakli K, Yüksel F. The role of cogeneration systems in sustainability of energy. Energy Convers Manag 2012;63:196–202. doi:10.1016/j.enconman.2012.01.041.

[21] Akorede MF, Hizam H, Pouresmaeil E. Distributed energy resources and benefits to the environment. Renew Sustain Energy Rev 2010;14:724–34. doi:10.1016/j.rser.2009.10.025.

[22] Liu M, Shi Y, Fang F. Combined cooling, heating and power systems: A survey. Renew Sustain Energy Rev 2014;35:1–22. doi:10.1016/j.rser.2014.03.054.

[23] Fu L, Zhao XL, Zhang SG, Jiang Y, Li H, Yang WW. Laboratory research on combined cooling, heating and power (CCHP) systems. Energy Convers Manag 2009;50:977–82. doi:10.1016/j.enconman.2008.12.013.

[24] Al-Sulaiman F a., Hamdullahpur F, Dincer I. Performance assessment of a novel system using parabolic trough solar collectors for combined cooling, heating, and power production. Renew Energy 2012;48:161–72. doi:10.1016/j.renene.2012.04.034.

[25] Larsson S, Fantazzini D, Davidsson S, Kullander S, Höök M. Reviewing electricity production cost assessments. Renew Sustain Energy Rev 2014;30:170–83. doi:10.1016/j.rser.2013.09.028.

[26] Abusoglu A, Kanoglu M. Exergoeconomic analysis and optimization of combined heat and power production: A review. Renew Sustain Energy Rev 2009;13:2295–308. doi:10.1016/j.rser.2009.05.004.

[27] Wang H-C, Jiao W-L, Lahdelma R, Zou P-H. Techno-economic analysis of a coal-fired CHP based combined heating system with gas-fired boilers for peak load compensation. Energy Policy 2011;39:7950–62. doi:10.1016/j.enpol.2011.09.050.

[28] International Energy Agency (IEA). Combined Heat and Power: Evaluating the Benefits of Greater Global Investement 2008. https://www.iea.org/publications/freepublications/publication/chp_report.pdf (accessed June 3, 2018).

[29] U.S. Environmental Protection Agency (EPA). Combined heat and power: A clean energy solution 2012. https://www.energy.gov/sites/prod/files/2013/11/f4/chp_clean_energy_solution.pdf (accessed June 3, 2018).

[30] International Energy Agency (IEA). Tracking Industrial Energy Efficiency and CO 2 Emissions. Paris (France): 2007.

[31] Bernotat K, Sandberg T. Biomass fired small-scale CHP in Sweden and the Baltic States: A case study on the potential of clustered dwellings. Biomass and Bioenergy 2004;27:521–30. doi:10.1016/j.biombioe.2003.10.010.

[32] Konstantakos V, Pilavachi P a., Polyzakis A, Theofylaktos C. A decision support model for combined heat and power economic evaluation. Appl Therm Eng 2012;42:129–35. doi:10.1016/j.applthermaleng.2012.03.018.

[33] Knizley A, Mago PJ. Evaluation of combined heat and power (CHP) systems performance with dual power generation units for different building configurations. Int J Energy Res 2013;37:1529–38. doi:10.1002/er.2965.

[34] Knizley AA, Mago PJ, Smith AD. Evaluation of the performance of combined cooling, heating, and power systems with dual power generation units. Energy Policy 2014;66:654–65. doi:10.1016/j.enpol.2013.11.017.

[35] Cho H, Mago PJ, Luck R, Chamra LM. Evaluation of CCHP systems performance based on operational cost, primary energy consumption, and carbon dioxide emission by utilizing an optimal operation scheme. Appl Energy 2009;86:2540–9. doi:10.1016/j.apenergy.2009.04.012.

[36] Hu M, Cho H. A probability constrained multi-objective optimization model for CCHP system operation decision support. Appl Energy 2014;116:230–42. doi:10.1016/j.apenergy.2013.11.065.

[37] Yun KT, Cho H, Luck R, Mago PJ. Modeling of reciprocating internal combustion engines for power generation and heat recovery. Appl Energy 2013;102:327–35. doi:10.1016/J.APENERGY.2012.07.020.

[38] International Energy Agency. Technology Roadmap Solar Photovoltaic Energy 2014. http://www.iea.org/publications/freepublications/publication/TechnologyRoadmapSolarPhotovoltaicEnergy_2014edition.pdf (accessed May 18, 2017).

[39] International Energy Agency. Tracking Clean Energy Progress 2016. http://www.iea.org/publications/freepublications/publication/TrackingCleanEnergyProgress2016.pdf (accessed June 3, 2018).

[40] Zhang J, Cho H, Knizley A. Evaluation of financial incentives for combined heat and power (CHP) systems in U.S. regions. Renew Sustain Energy Rev 2016;59:738–62. doi:10.1016/j.rser.2016.01.012.

[41] Ershad AM, Brecha RJ, Hallinan K. Analysis of solar photovoltaic and wind power potential in Afghanistan. Renew Energy 2016;85:445–53. doi:10.1016/j.renene.2015.06.067.

[42] Mamia I, Appelbaum J. Shadow analysis of wind turbines for dual use of land for combined wind and solar photovoltaic power generation. Renew Sustain Energy Rev 2016;55:713–8. doi:10.1016/j.rser.2015.11.009.

[43] Pandey AK, Tyagi VV, Selvaraj JA, Rahim NA, Tyagi SK. Recent advances in solar photovoltaic systems for emerging trends and advanced applications. Renew Sustain Energy Rev 2016;53:859–84. doi:10.1016/j.rser.2015.09.043.

[44] Renno C, Petito F, Gatto A. Artificial neural network models for predicting the solar radiation as input of a concentrating photovoltaic system. Energy Convers Manag 2015;106:999–1012. doi:10.1016/j.enconman.2015.10.033.

[45] Armendariz-Lopez JF, Luna-Leon A, Gonzalez-Trevizo ME, Arena-Granados AP, Bojorquez-Morales G. Life cycle cost of photovoltaic technologies in commercial buildings in Baja California, Mexico. Renew Energy 2016;87:564–71. doi:10.1016/j.renene.2015.10.051.

[46] Adam AD, Apaydin G. Grid connected solar photovoltaic system as a tool for green house gas emission reduction in Turkey. Renew Sustain Energy Rev 2016;53:1086–91. doi:10.1016/j.rser.2015.09.023.

[47] Kulworawanichpong T, Mwambeleko JJ. Design and costing of a stand-alone solar photovoltaic system for a Tanzanian rural household. Sustain Energy Technol Assessments 2015;12:53–9. doi:10.1016/j.seta.2015.10.001.

[48] Quesada G, Guillon L, Rousse DR, Mehrtash M, Dutil Y, Paradis P-L. Tracking strategy for photovoltaic solar systems in high latitudes. Energy Convers Manag 2015;103:147–56. doi:10.1016/j.enconman.2015.06.041.

[49] Shivashankar S, Mekhilef S, Mokhlis H, Karimi M. Mitigating methods of power fluctuation of photovoltaic (PV) sources - A review. Renew Sustain Energy Rev 2016;59:1170–84. doi:10.1016/j.rser.2016.01.059.

[50] Pflaum P, Alamir M, Lamoudi MY. Battery sizing for PV power plants under regulations using randomized algorithms. Renew Energy 2017;113:596–607. doi:10.1016/j.renene.2017.05.091.

[51] de Oliveira e Silva G, Hendrick P. Lead–acid batteries coupled with photovoltaics for increased electricity self-sufficiency in households. Appl Energy 2016;178:856–67. doi:10.1016/j.apenergy.2016.06.003.

[52] Venu C, Riffonneau Y, Bacha S, Baghzouz Y. Battery Storage System sizing in distribution feeders with distributed photovoltaic systems. 2009 IEEE Bucharest PowerTech, IEEE; 2009, p. 1–5. doi:10.1109/PTC.2009.5282093.

[53] Chae YT, Kim J, Park H, Shin B. Building energy performance evaluation of building integrated photovoltaic (BIPV) window with semi-transparent solar cells. Appl Energy 2014;129:217–27. doi:10.1016/j.apenergy.2014.04.106.

[54] Luo X, Wang J, Dooner M, Clarke J. Overview of current development in electrical energy storage technologies and the application potential in power system operation. Appl Energy 2015;137:511–36. doi:10.1016/j.apenergy.2014.09.081.

[55] Hawkes a. D, Leach M a. On policy instruments for support of micro combined heat and power. Energy Policy 2008;36:2963–72. doi:10.1016/j.enpol.2008.04.011.

[56] Pellegrino S, Lanzini A, Leone P. Techno-economic and policy requirements for the market-entry of the fuel cell micro-CHP system in the residential sector. Appl Energy 2015;143:370–82. doi:10.1016/j.apenergy.2015.01.007.

[57] Pade L-L, Schröder ST. Fuel cell based micro-combined heat and power under different policy frameworks – An economic analysis. Energy Convers Manag 2013;66:295–303. doi:10.1016/j.enconman.2012.10.012.

[58] Athawale R, Felder FA. Incentives for Combined Heat and Power plants: How to increase societal benefits? Util Policy 2014;31:121–32. doi:10.1016/J.JUP.2014.10.005.

[59] Chou S-Y, Nguyen TAT, Yu TH-K, Phan NKP. Financial assessment of government subsidy policy on photovoltaic systems for industrial users: A case study in Taiwan. Energy Policy 2015;87:505–16. doi:10.1016/j.enpol.2015.09.039.

[60] Simpson G, Clifton J. Testing Diffusion of Innovations Theory with data: Financial incentives, early adopters, and distributed solar energy in Australia. Energy Res Soc Sci 2017;29:12–22. doi:10.1016/j.erss.2017.04.005.

[61] Bertsch V, Geldermann J, Lühn T. What drives the profitability of household PV investments, self-consumption and self-sufficiency? Appl Energy 2017;204:1–15. doi:10.1016/j.apenergy.2017.06.055.

[62] Fossati JP, Galarza A, Martín-Villate A, Fontán L. A method for optimal sizing energy storage systems for microgrids. Renew Energy 2015;77:539–49. doi:10.1016/j.renene.2014.12.039.

[63] Mehleri ED, Sarimveis H, Markatos NC, Papageorgiou LG. A mathematical programming approach for optimal design of distributed energy systems at the neighbourhood level. Energy 2012;44:96–104. doi:10.1016/j.energy.2012.02.009.

[64] Khaki M, Shahsavar A, Khanmohammadi S, Salmanzadeh M. Energy and exergy analysis and multi-objective optimization of an air based building integrated photovoltaic/thermal (BIPV/T) system. Sol Energy 2017;158:380–95. doi:10.1016/j.solener.2017.09.056.

[65] Mariaud A, Acha S, Ekins-Daukes N, Shah N, Markides CN. Integrated optimisation of photovoltaic and battery storage systems for UK commercial buildings. Appl Energy 2017;199:466–78. doi:10.1016/j.apenergy.2017.04.067.

[66] U.S. Department of Energy (DOE). Existing commercial reference buildings constructed in or after 1980 n.d. http://energy.gov/eere/buildings/existing-

commercial-reference-buildings-constructed-or-after-1980 (accessed April 11, 2017).

[67] Torcellini P, Deru M, Griffith B, Benne K, Halverson M WD et al. DOE Commercial Building Benchmark Models. NREL Conference Paper NREL/CP-550-43291, 2008 n.d. http://www.nrel.gov/docs/fy08osti/43291.pdf (accessed April 11, 2017).

[68] Cho H, Luck R, Eksioglu SD, Chamra LM. Cost-optimized real-time operation of CHP systems. Energy Build 2009;41:445–51. doi:10.1016/J.ENBUILD.2008.11.011.

[69] U.S. Environmental Protection Agency. Catalog of CHP Technologies. 2008.

[70] Mani S, Sokhansanj S, Tagore S, Turhollow a. F. Techno-economic analysis of using corn stover to supply heat and power to a corn ethanol plant - Part 2: Cost of heat and power generation systems. Biomass and Bioenergy 2010;34:356–64. doi:10.1016/j.biombioe.2009.11.007.

[71] Sanaye S, Katebi A. 4E analysis and multi objective optimization of a micro gas turbine and solid oxide fuel cell hybrid combined heat and power system. J Power Sources 2014;247:294–306. doi:10.1016/j.jpowsour.2013.08.065.

[72] U.S. Energy Information Administration (EIA). Average Retail Price of Electricity to Ultimate Customers by the End-Use Sector 2015. http://www.eia.gov/electricity/annual/html/epa_02_10.html (accessed August 25, 2015).

[73] U.S. Energy Information Administration (EIA). Natural Gas Prices 2015. http://www.eia.gov/dnav/ng/ng_pri_sum_a_EPG0_PCS_DMcf_a.htm (accessed August 25, 2015).

[74] U.S. Environmental Protection Agency (EPA). CHP Policies and incentives database 2015. http://www.epa.gov/chp/policies/database.html (accessed August 25, 2015).

[75] Cho H, Fumo N. Uncertainty Analysis for Dimensioning Solar Photovoltaic Arrays. Proc ASME 2012 6th Int Conf Energy Sustain 10th Fuel Cell Sci Eng Technol Conf 2012:1–5.

[76] Duffie JA, Beckman WA. Solar Engineering of Thermal Processes. 3rd ed. Wiley; 2006.

[77] Thevenard D, Haddad K. Ground reflectivity in the context of building energy simulation. Energy Build 2006;38:972–80. doi:10.1016/j.enbuild.2005.11.007.

[78] BEMBook. Ground Reflectance. Available <http//www.bembook.ibpsa.us/index.php?title=Ground_Reflectance> [Accessed 22 Dec 2015] n.d.

[79] U.S. Department of Energy (DOE). EnergyPlus Engineering Reference n.d. https://energyplus.net/sites/default/files/pdfs_v8.3.0/EngineeringReference.pdf (accessed March 22, 2017).

[80] NREL NREL. Dynamic Maps, GIS Data, & Analysis Tools n.d. http://www.nrel.gov/gis/solar.html (accessed March 22, 2017).

[81] Munsell M. Solar PV Pricing Continues to Fall During a Record-Breaking 2014. Available <http//www.greentechmedia.com/articles/read/solar-Pv-System-Prices-Continue-to-Fall-during-a-Record-Breaking-2014> [Accessed 22 Dec 2015] n.d.

[82] U.S.Energy Information Administration (EIA). ELECTRICITY DATA BROWSER 2017. https://www.eia.gov/electricity/data/browser/ (accessed August 1, 2017).

[83] Solar Energy Industries Association (SEIA). Solar Investment Tax Credit (ITC) n.d. https://www.seia.org/policy/finance-tax/solar-investment-tax-credit (accessed April 21, 2017).

[84] FPL. Net Metering 2016. https://www.fpl.com/clean-energy/net-metering/guidelines.html (accessed October 2, 2016).

[85] NC Clean Energy Technology Center. Florida Power and Light- Solar Rebate Program 2016. http://programs.dsireusa.org/system/program/detail/4870 (accessed February 5, 2018).

[86] Georgia Power. Advanced Solar Initiative 2016. http://www.georgiapower.com/about-energy/energy-sources/solar/advanced-solar-initiative.cshtml (accessed October 2, 2016).

[87] CleanEnergy Authority. Georgia Solar Rebates and Incentives Solar Buyback Program 2016. http://www.cleanenergyauthority.com/solar-rebates-and-incentives/georgia/ (accessed October 2, 2016).

[88] Hawaii State Energy Office. State of Hawaii and Federal Insentives n.d. http://energy.hawaii.gov/developer-investor/financing-and-incentives-for-renewable-energy-projects/state-of-hawaii-and-federal-incentives (accessed August 1, 2017).

[89] NVEnergy. RenewableGenerations n.d. http://www.nvenergy.com/renewablesenvironment/renewablegenerations/index.cfm (accessed October 2, 2016).

[90] CleanEnergy Authority. Nevada Solar Rebates and Incentives 2016. http://www.cleanenergyauthority.com/solar-rebates-and-incentives/nevada/ (accessed October 2, 2016).

[91] Green Mountain Power. Customer-Owned Generation and Distributed Resources 2016. http://www.greenmountainpower.com/customers/distributed-resources/ (accessed October 2, 2016).

[92] Green Mountain Power. GMP Solar FAQ 2016. http://www.greenmountainpower.com/innovative/solar/faqs/ (accessed October 2, 2016).

[93] U.S. Department of Energy (DOE). Commercial Prototype Building Models n.d. https://www.energycodes.gov/commercial-prototype-building-models (accessed October 2, 2016).

[94] Wilcox S, Marion W. Users Manual for TMY3 Data Sets 2008. https://www.nrel.gov/docs/fy08osti/43156.pdf (accessed June 4, 2018).

[95] de Simón-Martín M, Diez-Suárez AM, de Prado LÁ, González-Martínez A, de la Puente-Gil Á, Blanes-Peiró J. Development of a GIS tool for high precision PV degradation monitoring and supervision: Feasibility analysis in large and small PV plants. Sustain 2017;9:1–29. doi:10.3390/su9060965.

[96] Fu R, Chung D, Lowder T, Feldman D, Ardani K, Fu R, et al. U.S. Solar Photovoltaic System Cost Benchmark: Q1 2016. 2016.

[97] Mitsubishi Electric. MLU series Photovoltaic Modules n.d. http://www.mitsubishielectricsolar.com/images/uploads/documents/specs/MLU_spec_sheet_250W_255W.pdf (accessed March 22, 2017).

[98] Brusco G, Burgio A, Menniti D, Pinnarelli A, Sorrentino N. The economic viability of a feed-in tariff scheme that solely rewards self-consumption to promote the use of integrated photovoltaic battery systems. Appl Energy 2016;183:1075–85. doi:10.1016/j.apenergy.2016.09.004.

[99] Linssen J, Stenzel P, Fleer J. Techno-economic analysis of photovoltaic battery systems and the influence of different consumer load profiles. Appl Energy 2017;185:2019–25. doi:10.1016/j.apenergy.2015.11.088.

[100] Brekken TKA, Yokochi A, von Jouanne A, Yen ZZ, Hapke HM, Halamay DA. Optimal Energy Storage Sizing and Control for Wind Power Applications. IEEE Trans Sustain Energy 2010. doi:10.1109/TSTE.2010.2066294.

[101] Kerdphol T, Qudaih Y, Mitani Y. Optimum battery energy storage system using PSO considering dynamic demand response for microgrids. Int J Electr Power Energy Syst 2016;83:58–66. doi:10.1016/j.ijepes.2016.03.064.

[102] Han X, Zhang H, Yu X, Wang L. Economic evaluation of grid-connected micro-grid system with photovoltaic and energy storage under different investment and financing models. Appl Energy 2016;184:103–18. doi:10.1016/j.apenergy.2016.10.008.

[103] Schoenung SM, Hassenzahl W. Energy storage systems cost update: A study for the DOE energy storage system program. 2011. doi:SAND2011-2730.

[104] National Renewable Energy Laboratory (NREL). Distributed Generation Renewable Energy Estimate of Costs 2016. http://www.nrel.gov/analysis/tech_lcoe_re_cost_est.html (accessed August 1, 2017).

[105] United States Environmental Protection Agency. eGRID 2014v2 Summary Tables n.d. https://www.epa.gov/sites/production/files/2017-02/documents/egrid2014_summarytables_v2.pdf (accessed April 20, 2017).

[106] N.C. Clean Energy Technology Center. LADWP - Solar Incentive Program 2015. http://programs.dsireusa.org/system/program/detail/501 (accessed April 21, 2017).

[107] U.S. Department of Energy (DOE). LADWP - SOLAR INCENTIVE PROGRAM n.d. https://energy.gov/savings/ladwp-solar-incentive-program (accessed April 21, 2017).

[108] ENERGY.GOV. NY-SUN COMMERICAL/INDUSTRIAL INCENTIVE PROGRAM n.d. https://energy.gov/savings/ny-sun-commericalindustrial-incentive-program (accessed April 21, 2017).

[109] National Renewable Energy Laboratory (NREL). Issue Brief: A Survey of State Policies to Support Utility-Scale and Distributed-Energy Storage n.d. http://www.nrel.gov/docs/fy14osti/62726.pdf (accessed April 21, 2017).

[110] Stallings J, Keating Z, Gibbs S. Carbon Markets : Renewed Expectations. C Res Note 2015:1–7.

[111] Cho J, Jeong S, Kim Y. Commercial and research battery technologies for electrical energy storage applications. Prog Energy Combust Sci 2015;48:84–101. doi:10.1016/j.pecs.2015.01.002.

[112] Akter MN, Mahmud MA, Oo AMT. Comprehensive economic evaluations of a residential building with solar photovoltaic and battery energy storage systems: An Australian case study. Energy Build 2017;138:332–46. doi:10.1016/j.enbuild.2016.12.065.

[113] Yang F, Cho H, Zhang H, Zhang J. Thermoeconomic multi-objective optimization of a dual loop organic Rankine cycle (ORC) for CNG engine waste heat recovery. Appl Energy 2017;205:1100–18. doi:10.1016/J.APENERGY.2017.08.127.